Applied Soft Computing 113 (2021) 107955

Contents lists available at ScienceDirect

Applied Soft Computing

journal homepage: www.elsevier.com/locate/asoc

An entropy minimization based multilevel colour thresholding technique for analysis of breast thermograms using equilibrium slime mould algorithm

Manoj Kumar Naik [a], Rutuparna Panda [b,*], Ajith Abraham [c]

[a] Faculty of Engineering and Technology, Siksha O Anusandhan, Bhubaneswar, Odisha 751030, India
[b] Department of Electronics and Telecommunication Engineering, Veer Surendra Sai University of Technology, Burla, Odisha 768018, India
[c] Machine Intelligence Research Labs, Scientific Network for Innovation and Research Excellence, WA 98071-2259, USA

GRAPHICAL ABSTRACT

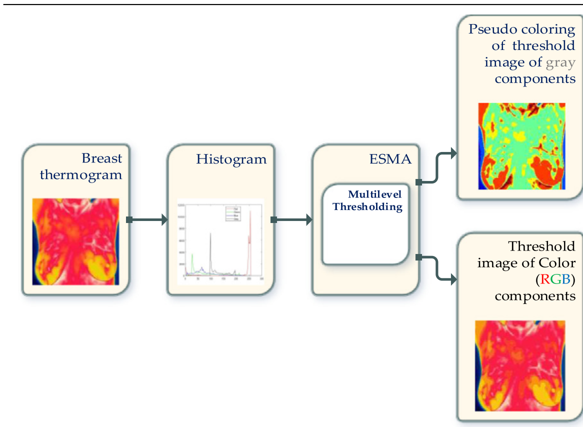

ARTICLE INFO

Article history:
Received 8 June 2020
Received in revised form 12 September 2021
Accepted 26 September 2021
Available online 6 October 2021

Keywords:
Multilevel thresholding
Entropy dependency
Optimization technique
Breast thermogram analysis
Infrared images

ABSTRACT

Breast cancer is one of the leading causes of death in women due to the abnormal growth of cells known as a tumour. Thermography is an imaging technique used to capture infrared radiation and generate a thermogram. The major advantages of thermography are contactless, radiation-free, painless, and real-time screening. The thermogram is used further in a pathological investigation. However, in the modern-day, machine intelligence technologies are used for the analysis of breast thermograms, which assist the expert in decision making. The machine intelligence technique requires a thresholding image during the preprocessing stage, which warrants an efficient thresholding method. Here, we investigate the multilevel thresholding objective function to minimize the information regarding the entropic dependence on various classes. A new Equilibrium Slime Mould Algorithm (ESMA) is proposed for colour image thresholding, an improvement of the Slime Mould Algorithm (SMA), by integrating the equilibrium practice in updating the slime mould positions from an equilibrium pool concept of Equilibrium Optimizer (EO). The ESMA performance is compared with well know optimization algorithms and ranked one based on Friedman's mean rank, when evaluated using 53 test problems. Further, the ESMA is used for the development of an entropy minimization based multilevel colour thresholding method for the analysis of breast thermograms. It is applied in two sets of experiments using grey components and the RGB components of breast thermograms. The encouraging results on the thermogram image analysis are presented. Even more interesting results are seen while evaluating our proposal in terms of different metrics—the peak signal to noise ratio (PSNR), the feature similarity

* Corresponding author.
E-mail addresses: naik.manoj.kumar@gmail.com (M.K. Naik), r_ppanda@yahoo.co.in (R. Panda), ajith.abraham@ieee.org (A. Abraham).

https://doi.org/10.1016/j.asoc.2021.107955
1568-4946/

(FSIM), and the structure similarity (SSIM). Statistical a nalysis provided reveals the suitability of the technique for the analysis of breast thermograms. The method may assist the medical practitioners, as an additional tool. The ESMA may be useful for solving different optimization problems in the world of engineering.

1. Introduction

Breast cancer is a leading cause of death in women [1,2], which starts in breast tissues leading to abnormal growth of cells around the breast. Therefore, the analysis of breast cancer images is a challenge for proper treatment planning. This, in turn, helps us to increase the survival rate [3]. The detection of breast cancer needs an imaging device [4] and an image processing technique to assist an accurate diagnostic [5]. The screening using medical imaging techniques helps in the cancer diagnostic process. Several medical imaging techniques used, during the last decade, to analyse breast cancer includes — mammography [6], dual-energy computed tomography (DE-CT) [7], ultrasound [8], magnetic Resonance Imaging (MRI) [9,10], single photon emission tomography (SPECT) [11,12], positron emission tomography (PET) [11,12] and thermography [13]. Mammography, a diagnostic imaging technique, uses low-dose x-ray gamma radiation to capture the breast tissues.

Mammography is widely used worldwide to diagnose breast cancer at an early stage, which is a painful and uncomfortable procedure. Mammography imaging has low sensitivity when a breast has dense tissues that can hide tumours under the tissue, which leads to high false-positive rates. As the imaging procedure uses X-ray gamma radiation, repeated use of it increases the chance of cancer in the future. The image using dual-energy computed tomography (DE-CT) [7] is better in image quality with higher contrast of tumours; also, it needs fewer images as compared to the CT. The DE-CT is used to discriminate and quantify the iodine, calcium, and fat contents near the breast cells when the highest concentration of calcium is found near the rapidly dividing cells, which leads to the formation of tumours. The ultrasound [8] uses the sound wave to capture the image of abnormal breast mass due to tumours, which helps to find the abnormality in finding in mammography or clinical trials. The ultrasound is very helpful for dense breast tissue, but due to a noisy environment, its performance is reduced. Magnetic Resonance Imaging (MRI) [9,10] is a highly sensitive imaging technique used for screening early breast cancer in women, which used high power magnets along with radio waves and a computer to capture the image. From the study [14], it is found that the MRI is over-utilized by low-risk women as compared to underutilize by high-risk women. The method requires a long acquisition time and gives rise to more false-positive rates. The single photon emission tomography (SPECT) [11,12] and positron emission tomography (PET) [11,12] are radionuclide imaging (RI) techniques. The SPECT captures the image using a gamma camera that uses a single γ-ray photon with different energy with the limitation of the line of response. The line of response in SPECT is difficult to determine as the origin of γ-ray photon. The PET uses positron-emitting radionuclides cyclotrons in more specific targets to measure *in vivo* cellular, molecular, and biochemical properties. The SPECT has the advantage of producing a high contrast image of the breast, with high sensitivity and quantitative capabilities. The screening methods based on the imaging techniques such as mammography [6], dual-energy computed tomography (DE-CT) [7], ultrasound [8], magnetic Resonance Imaging (MRI) [9,10], single photon emission tomography (SPECT) [11,12], positron emission tomography (PET) [11,12] used radiation. As these methods require physical contact with the machine, it is hurting, which is not desirable. There may be a coincidental future complication because these technologies are unprotected from the radiation. In contrary to the above methods, thermography [13] is a fast, non-contact, radiation-free, noninvasive, and simple procedure. It can be utilized in the breast tumour regions including tissues. The thermography uses an image that is the function of the temperature difference in the skin surface. Here, infrared frequencies are used, which is not harmful. The thermal image uses a greyscale, in which black represents the cold region (objects do not emit any radiation) and white represents the hot region (objects emit high radiation). The thermography uses a long infrared range wavelength ($9-14$ μm) to capture the thermal images. A higher infrared radiation is emitted around the breast tumour regions as compared to the normal regions [13].

Table 1
Parameter setting of the various optimization algorithms.

Algorithm	Parameters
ESMA	$N = 30$, $z = 0.03$
SMA	$N = 30$, $z = 0.03$
EO	$N = 30$, $a_1 = 2$, $a_2 = 1$ and $GP = 0.5$
HHO	$N = 30$, $\beta = 1.5$
GWO	$N = 30$, $a = [20]$
WDO	$N = 30$, RT coefficient $= 5$, constant in the update equation $= 0.5$, gravitational constant $= 0.2$, maximum allowed speed $= 0.3$ and Coriolis effect $= 0.4$
WOA	$N = 30$, $a = [0, 2]$, $b = 1$, and $l = [-1, 1]$
DE	$N = 30$, Crossover probability $C_r = 0.9$ and scaling factor $F = 0.5$,
CS	$N = 30$, Abandon probability $p_a = 0.25$, step size $\alpha = 1$, and $\lambda = 1.5$
PSO	$N = 30$, Inertia factor $= 0.3$, $c_1 = 2$, and $c_2 = 2$
FA	$N = 30$, $\alpha = 0.5$, $\beta = 0.2$, and $\gamma = 1$
L-SHADE	$N = 18D$, $H = 6$, $p = 0.11$ and Arc rate $= 2.6$
CMA-ES	$N = 4 + 3\log(D)$, $\mu = N/2$

Due to the advantages of thermography, it is used for breast thermogram analysis in young women, whose breast tissues are dense compared to the older women. The most common machine intelligence techniques used for breast thermogram analysis are — artificial neural network (ANN), fuzzy C means (FCM), symmetry check, spatial distributions, K-means clustering, and watershed segmentation [5,13,15]. The convolutional neural network (CNN) with Bayes algorithm [16] and the gradient vector flow [17] is used for the classification of normal breast vs. suspected breast tumour from a thermal segmented image as a complementary diagnostic, to speed up the tasks of pathology. The automatic colour segmentation of thermal images using the Gaussian mixture model with the expectation–maximization (EM) algorithm is proposed in [18]. However, in the above methods, the authors are silent about the segmentation method used, discuss only the post-processing steps like feature extraction, detection, etc. In this work, we focus on an easy method of segmentation using optimal multilevel colour thresholding using the soft computing approach.

Researchers employ nature-inspired algorithms to find the optimal threshold values for multilevel thresholding of the breast

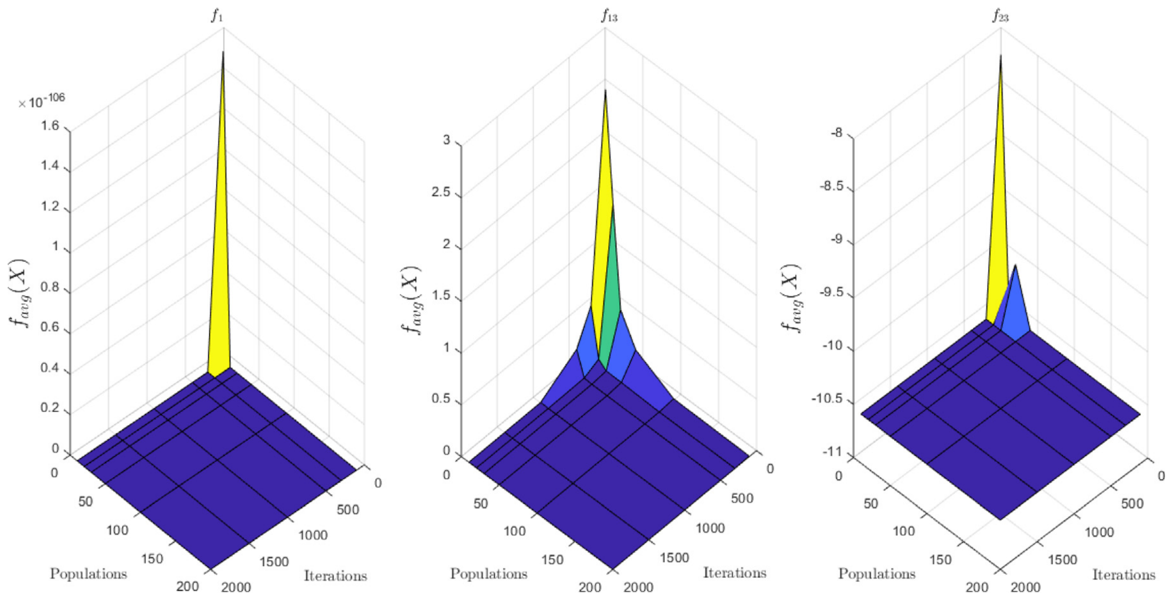

Fig. 1. The effect of population and iterations.

Table 2
Ranking of the results for $f_1 - f_{13}$ with varied values of z.

Test problems	$z = 0$	$z = 0.01$	$z = 0.02$	$z = 0.03$	$z = 0.04$	$z = 0.05$	$z = 0.06$	$z = 0.07$	0.08	$z = 0.09$	$z = 0.1$
f_1	0.000E+00	0.000E+00	0.000E+00	0.000E+00	0.000E+00	1.912E−297	7.255E−223	6.454E−179	1.050E−168	5.843E−144	1.099E−107
f_2	0.000E+00	0.000E+00	7.073E−288	2.336E−184	3.263E−149	4.519E−119	3.918E−111	1.376E−85	2.289E−79	1.651E−69	1.675E−68
f_3	0.000E+00	0.000E+00	0.000E+00	0.000E+00	0.000E+00	1.041E−284	1.281E−220	1.172E−181	3.984E−155	2.110E−131	6.814E−113
f_4	0.000E+00	0.000E+00	1.040E−321	6.640E−238	5.696E−172	3.576E−138	3.676E−105	1.102E−94	1.531E−81	1.657E−65	3.202E−48
f_5	2.871E+01	1.482E+01	5.401E+00	3.757E+00	2.116E+00	3.956E+00	2.375E+00	5.236E+00	1.333E+00	1.942E+00	1.579E+00
f_6	1.902E+00	1.349E−03	1.525E−03	2.018E−03	2.657E−03	3.988E−03	4.816E−03	7.630E−03	1.419E−02	1.925E−02	2.668E−02
f_7	7.448E−05	1.093E−04	9.901E−05	1.499E−04	1.600E−04	1.633E−04	1.626E−04	2.021E−04	2.185E−04	2.364E−04	1.524E−04
f_8	−8.219E+03	−1.257E+04	−1.257E+04	−1.257E+04	−1.257E+04	−1.257E+04	−1.257E+04	−1.257E+04	−1.257E+04	−1.257E+04	−1.257E+04
f_9	0.000E+00	0.000E+00	0.000E+00	0.000E+00	0.000E+00	0.000E+00	0.000E+00	0.000E+00	0.000E+00	0.000E+00	0.000E+00
f_{10}	8.882E−16	8.882E−16	8.882E−16	8.882E−16	8.882E−16	8.882E−16	8.882E−16	8.882E−16	8.882E−16	8.882E−16	8.882E−16
f_{11}	0.000E+00	0.000E+00	0.000E+00	0.000E+00	0.000E+00	0.000E+00	0.000E+00	0.000E+00	0.000E+00	0.000E+00	0.000E+00
f_{12}	4.634E−01	2.973E−02	5.354E−03	3.308E−03	2.747E−03	1.860E−03	9.684E−04	9.385E−04	8.512E−04	7.164E−04	6.431E−04
f_{13}	2.722E+00	2.943E−01	4.110E−03	3.603E−03	4.862E−03	2.488E−03	3.873E−03	3.633E−03	3.865E−03	3.586E−03	3.108E−03
Friedman's mean rank	6.385	4.923	4.692	**4.538**	5.462	5.923	6.538	7.154	6.769	6.923	6.692
Rank	6	3	2	**1**	4	5	7	11	9	10	8

Table 3
Result of scalable test problems f_{1-13}.

Test problem	Metric	ESMA	SMA	EO	HHO	GWO	WDO	WOA	DE	CS	PSO	FA	L-SHADE	CMA-ES
f_1	Avg	**0.000E+00**	1.191E−295	8.083E−41	1.119E−91	1.182E−07	5.707E−02	1.645E−18	2.689E+00	6.627E+00	5.184E−02	1.697E+00	1.100E−27	8.244E−11
	Std	**0.000E+00**	**0.000E+00**	2.732E−40	6.335E−91	3.511E−07	9.558E−02	2.591E−18	8.601E+00	6.738E−01	1.284E−02	1.602E+00	1.771E−27	4.272E−11
f_2	Avg	**2.336E−184**	2.853E−156	5.430E−24	5.293E−50	3.380E−05	7.794E−01	3.540E−11	4.090E−02	1.159E+01	1.033E+00	4.958E+00	2.948E−14	1.437E−05
	Std	**0.000E+00**	1.931E−155	5.354E−24	2.492E−49	3.573E−05	8.249E−01	3.022E−11	1.121E−01	7.468E−01	1.594E−01	2.329E+00	1.750E−14	4.577E−06
f_3	Avg	**0.000E+00**	1.055E−306	1.938E−09	1.884E−71	3.399E−01	3.536E−01	7.552E−05	5.748E+02	1.295E+02	5.082E−01	9.159E+00	1.863E−13	2.289E+00
	Std	**0.000E+00**	0.000E+00	4.082E−09	9.973E−71	4.297E−01	1.793E−01	1.980E−04	3.537E+02	8.175E+01	1.312E−01	3.866E+00	4.510E−13	3.064E+00
f_4	Avg	**6.640E−238**	7.849E−144	2.566E−10	7.796E−49	1.260E−01	3.352E−02	6.739E−05	2.437E+01	8.569E−01	1.443E−01	6.821E−01	2.746E−06	1.891E−04
	Std	**0.000E+00**	5.605E−143	4.361E−10	3.151E−48	9.560E−02	6.821E−02	5.824E−05	7.162E+00	4.382E−02	2.178E−02	1.548E−01	2.356E−06	6.397E−05
f_5	Avg	3.757E+00	7.813E+00	2.535E+01	**9.147E−03**	2.874E+01	3.810E+01	2.663E+01	2.714E+04	3.641E+02	3.403E+01	2.359E+02	1.413E+01	6.497E+01
	Std	8.436E+00	1.134E+01	1.955E−01	**1.130E−02**	3.842E−01	9.989E+00	1.010E+00	8.174E+04	4.273E+01	1.651E+00	2.133E+02	8.496E−01	1.678E+02
f_6	Avg	2.018E−03	6.126E−03	8.826E−06	1.816E−04	3.637E+00	2.502E−01	8.686E−01	3.033E+01	2.448E+01	5.478E−02	8.101E+00	**4.618E−27**	7.060E−11
	Std	8.364E−04	4.251E−03	6.470E−06	2.149E−04	6.940E−01	1.237E−01	3.958E−01	1.597E+02	1.870E+00	1.253E−02	1.835E+00	**2.204E−26**	3.665E−11
f_7	Avg	1.499E−04	1.747E−04	1.159E−03	**1.355E−04**	4.602E−03	1.519E−01	8.525E−03	6.801E−02	4.066E+01	1.245E−01	7.740E+00	1.335E−03	5.234E−03
	Std	**1.294E−04**	1.489E−04	5.690E−04	1.356E−04	2.940E−03	7.073E−02	5.007E−03	2.039E−02	1.028E+01	4.304E−02	1.348E+01	3.637E−04	1.961E−03
f_8	Avg	**−1.257E+04**	**−1.257E+04**	−8.970E+03	**−1.257E+04**	−3.942E+01	−9.292E+01	−7.936E+03	−7.212E+03	−3.896E+03	−1.657E+02	−5.361E+00	−3.264E+03	-inf
	Std	**1.575E−01**	3.355E−01	6.162E+02	8.296E−01	6.779E+00	9.888E−01	4.835E+02	1.089E+03	2.389E+02	3.292E+01	1.233E+00	4.153E+02	NaN
f_9	Avg	**0.000E+00**	**0.000E+00**	**0.000E+00**	**0.000E+00**	2.721E+01	6.904E+01	2.326E+01	1.614E+02	2.138E+02	1.844E+01	2.066E+02	6.429E+00	1.616E+02
	Std	**0.000E+00**	**0.000E+00**	**0.000E+00**	**0.000E+00**	3.459E+01	2.820E+01	1.296E+01	2.599E+01	1.648E+01	3.813E+00	1.828E+01	1.455E+00	9.411E+00
f_{10}	Avg	**8.882E−16**	**8.882E−16**	9.039E−15	**8.882E−16**	8.088E−05	1.535E−01	5.564E−10	1.615E+00	3.452E+00	2.819E−01	2.208E+00	4.199E−14	2.558E−06
	Std	**0.000E+00**	**0.000E+00**	2.868E−15	**0.000E+00**	1.671E−04	2.639E−01	5.270E−10	8.459E−01	1.052E−01	5.959E−02	8.470E−01	2.360E−14	6.983E−07
f_{11}	Avg	**0.000E+00**	**0.000E+00**	**0.000E+00**	**0.000E+00**	1.629E−09	3.150E−03	2.830E−17	4.061E−01	2.815E−01	3.430E−03	1.127E−01	**0.000E+00**	4.574E−10
	Std	**0.000E+00**	**0.000E+00**	**0.000E+00**	**0.000E+00**	4.091E−09	4.451E−03	4.887E−17	8.356E−01	3.516E−02	8.748E−04	8.810E−02	**0.000E+00**	2.279E−10
f_{12}	Avg	3.308E−03	2.989E−03	8.155E−07	7.176E−06	3.009E−01	3.593E−04	3.438E−02	1.513E+03	2.669E+00	7.880E−04	8.598E−01	**2.955E−16**	5.351E−12
	Std	4.855E−03	3.916E−03	9.837E−07	1.205E−05	8.632E−02	2.216E−04	1.929E−02	8.068E+03	3.535E−01	2.164E−04	2.248E−01	**1.542E−16**	2.828E−12
f_{13}	Avg	3.603E−03	6.515E−03	2.566E−02	9.872E−05	2.193E+00	6.626E−03	7.648E−01	8.988E+03	1.016E+00	2.030E−02	3.494E+00	**9.666E−15**	5.271E−11
	Std	5.389E−03	6.834E−03	4.235E−02	1.352E−04	3.191E−01	4.576E−03	2.480E−01	2.183E+04	1.139E−01	9.702E−03	3.801E−01	**5.930E−15**	3.320E−11

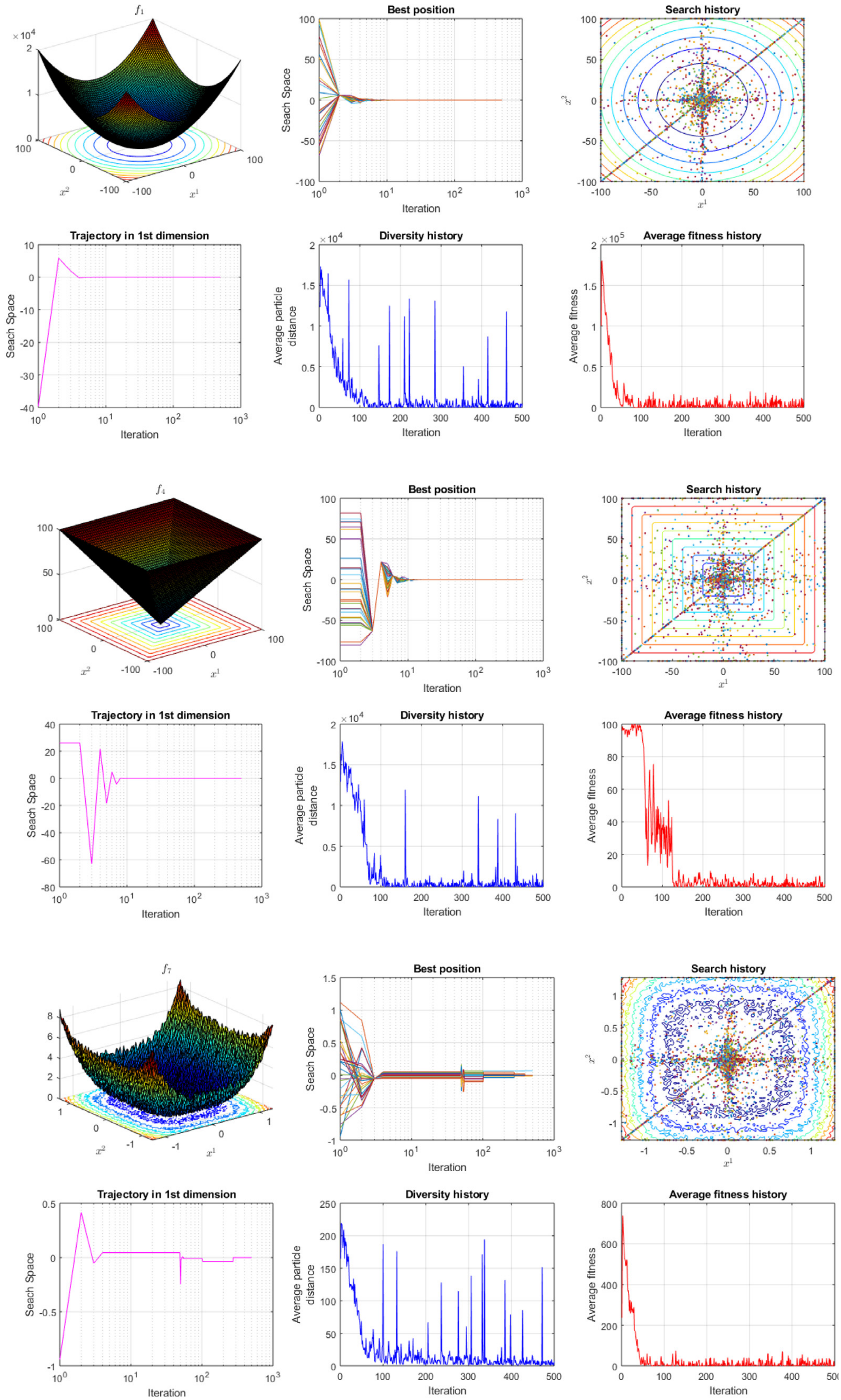

Fig. 2. Qualitative metrics for unimodal f_1, f_4, and f_7 test problems.

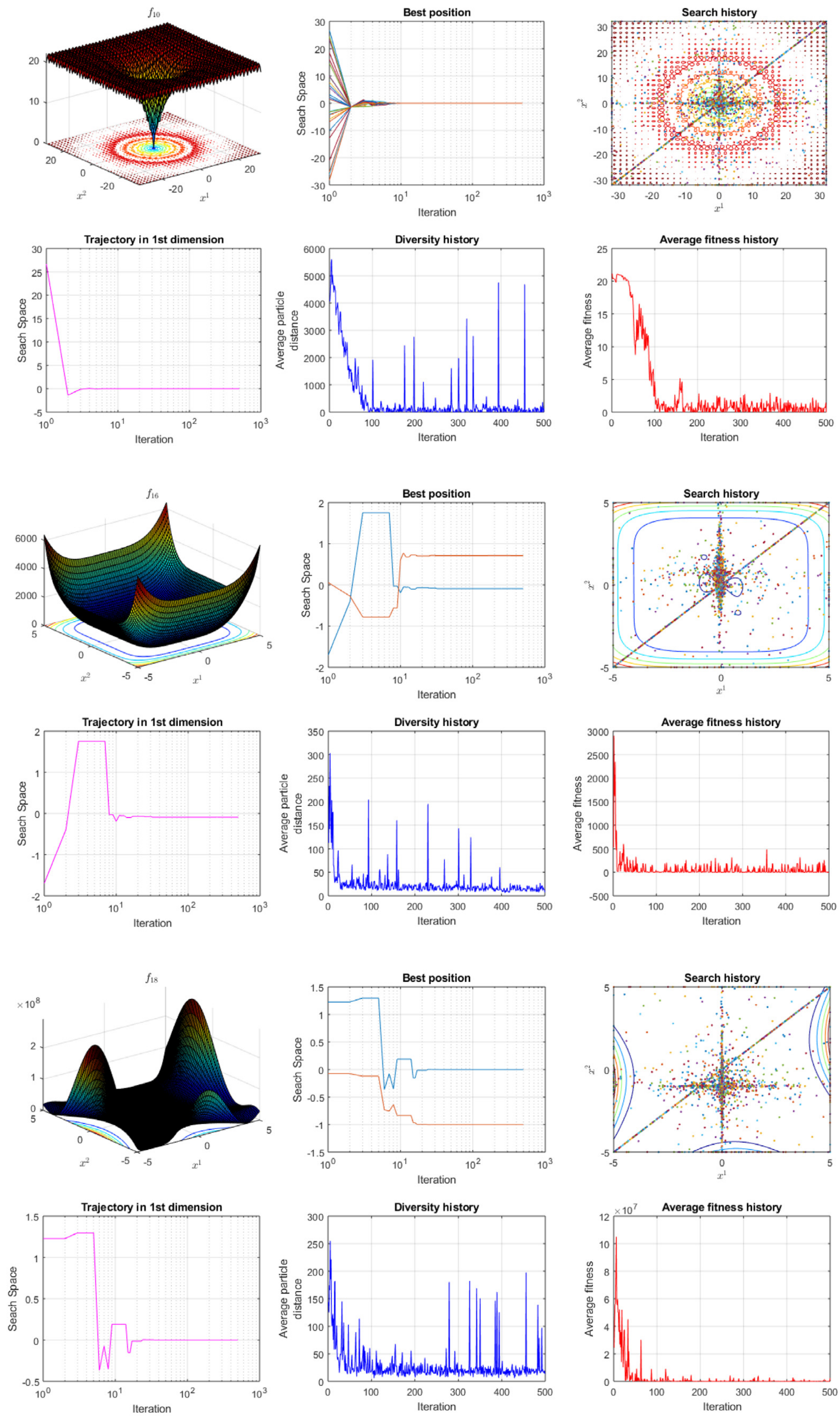

Fig. 3. Qualitative metrics for multimodal f_{10}, f_{16} and f_{18} test problems.

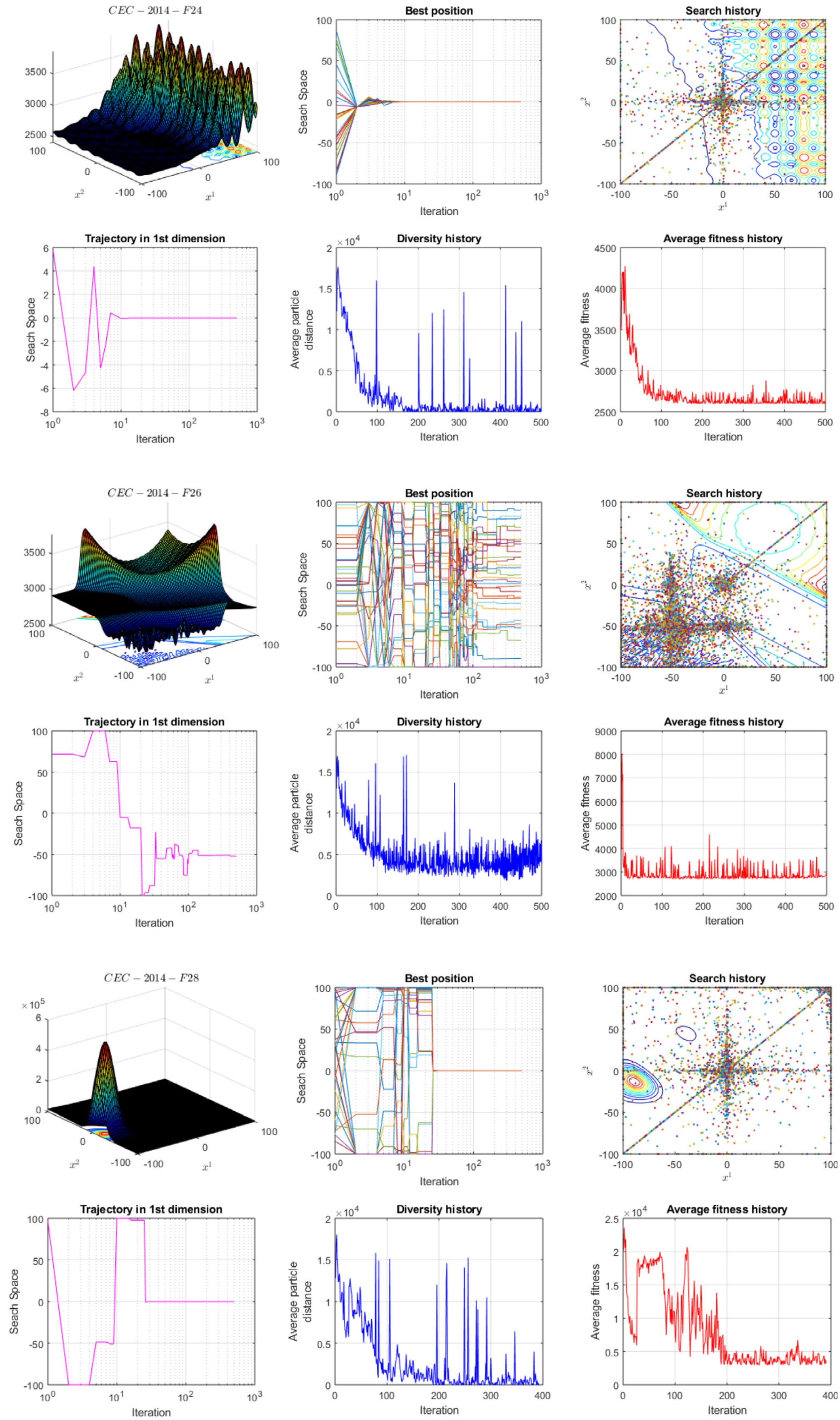

Fig. 4. Qualitative metrics for composition $CEC-2014-F24$, $CEC-2014-F26$, and $CEC-2014-F28$ test problems.

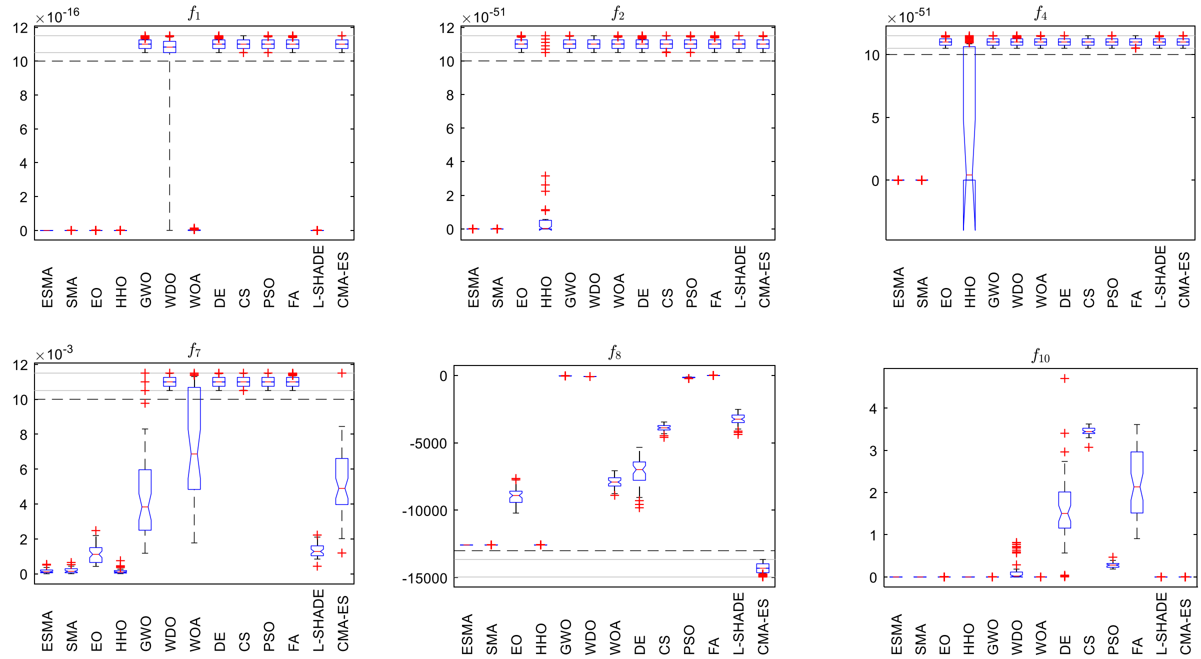

Fig. 5. Boxplot of six scalable unimodal and multimodal test problems.

Table 4
Result of non-scalable test problems f_{14-23}.

Test problem	Metric	ESMA	SMA	EO	HHO	GWO	WDO	WOA	DE	CS	PSO	FA	L-SHADE	CMA-ES
f_{14}	Avg	**0.9980**	**0.9980**	1.0369	1.6561	12.6705	12.6705	0.9980	1.0175	1.5656	12.6705	12.6705	8.6262	5.2521
	Std	**4.106E−13**	7.484E−13	2.778E−01	1.598E+00	1.715E−10	1.693E−11	1.255E−12	1.392E−01	8.513E−01	1.510E−12	1.453E−13	3.176E+00	3.574E+00
f_{15}	Avg	5.610E−04	5.577E−04	3.082E−03	3.899E−04	7.200E−04	4.509E−04	4.573E−04	9.254E−04	1.944E−03	3.717E−04	1.040E−03	**3.075E−04**	3.787E−04
	Std	2.183E−04	2.502E−04	6.962E−03	2.093E−04	6.538E−04	1.311E−04	2.479E−04	2.791E−03	9.357E−04	6.296E−05	1.221E−03	**3.025E−19**	7.391E−05
f_{16}	Avg	**−1.0316**	**−1.0316**	**−1.0316**	**−1.0316**	−1.0291	−1.0313	**−1.0316**	**−1.0316**	−1.0219	**−1.0316**	**−1.0316**	**−1.0316**	**−1.0316**
	Std	1.767E−09	2.342E−09	3.077E−16	1.032E−08	8.725E−03	3.064E−04	1.438E−10	**2.243E−16**	1.027E−02	1.330E−06	3.440E−16	2.608E−16	**2.243E−16**
f_{17}	Avg	**0.3979**	**0.3979**	**0.3979**	**0.3979**	1.0352	0.3981	**0.3979**	**0.3979**	0.4069	**0.3979**	23.8536	7.7924	4.8891
	Std	1.154E−07	1.239E−07	**3.924E−16**	5.132E−06	1.613E+00	1.581E−04	1.501E−08	**3.924E−16**	8.342E−03	5.816E−07	2.213E+00	3.444E−01	6.500E−01
f_{18}	Avg	**3.0000**	**3.0000**	**3.0000**	**3.0000**	4.6034	3.0230	**3.0000**	**3.0000**	4.2724	**3.0000**	7.2413	**3.0000**	**3.0000**
	Std	3.194E−11	1.407E−10	**1.669E−15**	4.786E−07	6.413E+00	2.510E−02	1.795E−08	3.976E−15	1.580E+00	3.683E−05	9.914E+00	2.224E−15	3.597E−15
f_{19}	Avg	**−3.8628**	**−3.8628**	**−3.8628**	−3.8603	−3.8547	−3.8540	−3.8583	**−3.8628**	−3.8485	−3.8569	−3.4638	**−3.8628**	**−3.8628**
	Std	3.053E−06	3.212E−07	**2.930E−15**	3.012E−03	1.061E−02	6.042E−03	3.942E−03	3.140E−15	1.144E−02	3.345E−03	7.909E−01	3.140E−15	3.140E−15
f_{20}	Avg	−3.2515	−3.2537	−3.2607	−3.1110	−2.6643	−3.1394	−2.8694	−3.2427	−2.9462	−3.0660	−3.2781	**−3.2946**	−3.2642
	Std	5.955E−02	6.004E−02	7.106E−02	7.513E−02	7.362E−01	9.930E−02	5.572E−01	5.660E−02	9.840E−02	2.656E−01	7.035E−02	**5.093E−02**	6.003E−02
f_{21}	Avg	**−10.1529**	**−10.1529**	−8.8130	−5.4333	−4.3097	−5.0340	−4.9733	−9.3198	−3.5169	−5.0548	−2.6794	−5.0558	−8.2993
	Std	2.196E−04	2.516E−04	2.493E+00	1.322E+00	1.623E+00	1.887E−02	5.845E−01	2.325E+00	9.006E−01	4.535E−04	1.129E+00	**5.627E−07**	3.209E+00
f_{22}	Avg	**−10.4026**	−10.4025	−8.8956	−5.3745	−4.7609	−5.0641	−5.0058	−10.2720	−3.6126	−5.0873	−2.6271	−5.0887	−10.4002
	Std	2.454E−04	2.733E−04	2.634E+00	1.175E+00	1.124E+00	2.006E−02	5.848E−01	9.352E−01	1.065E+00	2.950E−04	1.018E+00	1.252E−06	**8.970E−15**
f_{23}	Avg	**−10.5361**	−10.5360	−9.3553	−5.3068	−4.6394	−5.1061	−5.1285	−9.9832	−3.5023	−5.1281	−2.6394	−5.2571	−10.2217
	Std	**2.128E−04**	3.233E−04	2.616E+00	1.403E+00	1.345E+00	1.773E−02	5.160E−06	1.923E+00	7.299E−01	3.343E−04	9.615E−01	6.322E−01	1.590E+00

thermal images [19,20] and visual images [21,22]. This thresholded image is used further in the post-processing, for a better interpretation. The particle swarm optimization (PSO) is employed to find the optimal thresholds of the breast thermograms using Otsu's between class variance [23] thresholding techniques in [19]. The dragonfly algorithm (DA) is deployed to find optimal thresholds, using Otsu's between class variance [23] and Kapur's entropy [24], in [20] to generate the thresholded image that supports the decision making at the clinical level. Recently, the social group optimizer (SGO) is used with Kapur's entropy [24] to obtain the thresholded image of an infrared thermal image. Further, it is used in FCM clustering to find the abnormality in the symmetry of the left and right breast structure. The above study reveals that, during the preprocessing of the thermal image, a good thresholding technique is inevitable. The thresholded breast thermogram image is required to assist the pathological investigation, may be treated as a supplement to the mammography. Hence, more work is needed in these directions.

The time complexity of the multilevel thresholding problem increases with the increase in the number of threshold levels. Hence, there is a strong need to use the nature-inspired algorithm to reduce the time complexity. To do this, an optimizer with the ability to get an optimal solution or near-optimal solution is desirable, to compute the optimal threshold values in the multilevel thresholding. A bi-level thresholding approach, minimizing the entropic dependencies on the different classes, is discussed by Johannsen and Bille in [25]. Positive outcomes of this method are found from a comparison between many bi-level thresholding methods discussed in [26]. Interestingly, this idea is faster than the existing maximization of variance/entropy-based methods [18,20]. This could draw our attention to extend the idea for the development of a multilevel thresholding technique for the breast cancer thermogram images using the soft computing technique.

The earlier soft computing approaches are deterministic, which used the first-order derivative of the objective function equating it to zero to get the optimal solution. However, the modern-day soft computing approaches are better and stochastic, which are mostly nature-inspired optimizers. Nature-inspired optimization algorithms can be used in any type of optimization

Table 5
Result of CEC-2014 test problems.

Test problem	Metric	ESMA	SMA	EO	HHO	GWO	WDO	WOA	DE	CS	PSO	FA	L-SHADE	CMA-ES
CEC-2014-F1	Avg	**1.323E+07**	1.373E+07	1.341E+07	9.445E+07	1.400E+09	2.140E+09	4.372E+07	**8.598E+06**	1.398E+09	8.619E+06	2.787E+09	1.414E+09	3.321E+07
	Std	1.088E+07	7.992E+06	5.661E+06	4.059E+07	3.216E+08	6.374E+06	2.462E+07	**5.361E+06**	2.562E+08	1.011E+07	1.589E+07	2.124E+08	1.245E+07
CEC-2014-F2	Avg	**2.293E+04**	1.604E+05	1.565E+05	9.188E+08	7.657E+10	8.948E+10	4.681E+08	6.233E+07	8.135E+10	1.816E+08	1.016E+11	7.031E+10	1.997E+05
	Std	**1.308E+04**	8.587E+04	2.000E+05	5.165E+08	7.180E+09	1.716E+08	3.367E+08	2.765E+08	6.826E+09	5.289E+08	3.035E+08	5.963E+09	1.698E+05
CEC-2014-F3	Avg	1.687E+04	1.271E+04	2.271E+04	5.015E+04	8.673E+04	8.284E+04	2.601E+04	**2.497E+03**	9.432E+04	3.704E+04	2.032E+07	7.936E+04	2.571E+05
	Std	1.431E+04	1.208E+04	8.864E+03	7.997E+03	9.058E+02	1.464E+03	7.080E+03	**2.730E+03**	2.141E+04	4.685E+03	1.771E+06	4.900E+03	5.919E+04
CEC-2014-F4	Avg	5.402E+02	5.508E+02	5.216E+02	8.062E+02	1.195E+04	2.131E+04	6.005E+02	5.273E+02	1.703E+04	5.464E+02	2.531E+04	1.376E+04	**4.202E+02**
	Std	3.435E+01	5.344E+01	3.243E+01	1.297E+02	3.085E+03	7.185E+01	4.603E+01	4.031E+01	2.626E+03	4.717E+01	1.032E+02	1.958E+03	**7.424E−01**
CEC-2014-F5	Avg	5.210E+02	5.211E+02	5.210E+02	5.208E+02	5.207E+02	5.207E+02	5.208E+02	5.210E+02	5.211E+02	**5.201E+02**	5.213E+02	5.206E+02	5.210E+02
	Std	9.414E−02	6.347E−02	9.564E−02	1.205E−01	2.083E−01	8.471E−02	1.775E−01	4.348E−02	5.186E−02	**3.122E−02**	9.384E−02	1.250E−01	4.820E−02
CEC-2014-F6	Avg	6.191E+02	6.201E+02	6.110E+02	6.366E+02	6.480E+02	6.487E+02	6.232E+02	6.101E+02	6.429E+02	6.468E+02	6.510E+02	6.428E+02	**6.000E+02**
	Std	4.366E+00	3.520E+00	2.990E+00	3.559E+00	1.546E+00	6.516E−01	3.676E+00	5.512E+00	1.269E+00	1.150E+00	2.383E−01	1.023E+00	**5.296E−03**
CEC-2014-F7	Avg	7.011E+02	7.011E+02	7.002E+02	7.072E+02	1.434E+03	1.651E+03	7.053E+02	7.012E+02	1.492E+03	7.069E+02	1.760E+03	1.388E+03	**7.000E+02**
	Std	2.696E−02	4.274E−02	1.318E−01	4.168E+00	8.406E+01	1.575E+00	3.147E+00	2.902E+00	9.595E+01	1.423E+01	2.294E+00	7.288E+01	**9.041E−08**
CEC-2014-F8	Avg	**8.389E+02**	8.695E+02	8.664E+02	9.491E+02	1.207E+03	1.098E+03	9.185E+02	9.535E+02	1.164E+03	9.666E+02	1.311E+03	1.137E+03	9.608E+02
	Std	1.004E+01	1.906E+01	1.655E+01	1.635E+01	2.222E+01	**2.586E+00**	2.078E+01	3.743E+01	1.702E+01	9.789E+00	4.047E+00	1.162E+01	9.993E+00
CEC-2014-F9	Avg	1.034E+03	1.044E+03	**1.007E+03**	1.103E+03	1.224E+03	1.178E+03	1.098E+03	1.109E+03	1.292E+03	1.090E+03	1.360E+03	1.260E+03	1.067E+03
	Std	3.396E+01	3.315E+01	2.635E+01	2.294E+01	2.683E+01	5.954E+00	2.223E+01	1.728E+01	1.519E+01	6.080E+00	**4.608E+00**	1.205E+01	8.996E+00
CEC-2014-F10	Avg	**2.100E+03**	2.606E+03	3.057E+03	4.506E+03	9.223E+03	7.494E+03	3.665E+03	6.428E+03	8.700E+03	5.403E+03	1.133E+04	8.707E+03	8.046E+03
	Std	4.205E+02	4.534E+02	6.114E+02	7.365E+02	4.766E+02	**6.253E+01**	5.207E+02	9.820E+02	3.482E+02	2.134E+02	9.883E+01	3.626E+02	3.046E+02
CEC-2014-F11	Avg	**4.510E+03**	4.644E+03	5.023E+03	5.878E+03	9.859E+03	8.144E+03	5.072E+03	8.662E+03	9.156E+03	5.452E+03	1.333E+04	9.355E+03	8.298E+03
	Std	8.374E+02	6.558E+02	7.203E+02	7.652E+02	8.464E+02	1.393E+02	5.878E+02	3.542E+02	2.930E+02	2.929E+02	**1.027E+02**	3.374E+02	3.743E+02
CEC-2014-F12	Avg	**1.201E+03**	**1.201E+03**	1.202E+03	1.202E+03	1.202E+03	1.202E+03	**1.201E+03**	1.203E+03	1.203E+03	**1.201E+03**	1.206E+03	**1.201E+03**	1.203E+03
	Std	2.387E−01	2.891E−01	4.811E−01	5.460E−01	6.863E−01	7.909E−01	3.863E−01	4.604E−01	5.015E−01	4.160E−01	6.730E−01	**3.836E−02**	4.070E−01
CEC-2014-F13	Avg	1.301E+03	1.301E+03	**1.300E+03**	1.301E+03	1.308E+03	1.310E+03	1.301E+03	**1.300E+03**	1.309E+03	1.301E+03	1.311E+03	1.308E+03	**1.300E+03**
	Std	1.226E−01	1.292E−01	8.836E−02	2.066E−01	6.175E−01	**1.012E−02**	1.611E−01	9.126E−02	6.248E−01	1.277E−01	1.718E−02	4.882E−01	3.822E−02
CEC-2014-F14	Avg	1.401E+03	1.401E+03	1.400E+03	1.401E+03	1.653E+03	1.766E+03	1.401E+03	**1.400E+03**	1.698E+03	1.403E+03	1.806E+03	1.664E+03	**1.400E+03**
	Std	3.707E−01	3.678E−01	1.210E−01	2.181E+00	3.703E+01	4.740E−01	6.711E−01	1.655E−01	3.133E+01	6.012E+00	1.030E+00	2.052E+01	**7.991E−02**
CEC-2014-F15	Avg	1.513E+03	1.515E+03	**1.510E+03**	1.556E+03	2.525E+05	5.011E+05	1.547E+03	1.522E+03	4.699E+05	1.567E+03	9.717E+05	2.506E+05	1.514E+03
	Std	4.118E+00	4.780E+00	3.157E+00	1.552E+01	1.125E+05	5.952E+03	4.334E+01	5.172E+00	1.303E+05	1.061E+01	1.533E+04	7.488E+04	**7.954E−01**
CEC-2014-F16	Avg	**1.612E+03**	**1.612E+03**	1.612E+03	1.613E+03	1.614E+03	1.614E+03	1.613E+03	1.613E+03	1.614E+03	1.614E+03	1.614E+03	1.614E+03	1.613E+03
	Std	5.735E−01	5.366E−01	6.540E−01	3.504E−01	9.333E−02	3.848E−02	4.439E−01	2.652E−01	1.496E−01	**3.183E−02**	1.437E−01	1.219E−01	2.902E−01
CEC-2014-F17	Avg	2.541E+06	2.781E+06	1.167E+06	9.226E+06	2.570E+08	6.248E+08	1.943E+06	4.779E+05	6.800E+07	**1.525E+05**	9.244E+08	1.081E+08	1.875E+06
	Std	1.324E+06	1.561E+06	9.246E+05	6.806E+06	1.221E+08	4.799E+06	1.210E+06	4.804E+05	2.503E+07	**1.011E+05**	1.102E+07	3.826E+07	8.117E+05
CEC-2014-F18	Avg	1.692E+04	3.883E+04	5.188E+03	4.028E+05	5.764E+09	1.339E+10	8.311E+04	1.008E+04	3.487E+09	**5.161E+03**	1.514E+10	4.126E+09	1.846E+06
	Std	1.453E+04	4.178E+04	4.864E+03	5.824E+05	1.979E+09	4.291E+07	1.271E+05	1.512E+04	8.320E+08	**1.396E+03**	5.874E+07	1.143E+09	1.119E+06
CEC-2014-F19	Avg	1.922E+03	1.931E+03	1.914E+03	1.983E+03	2.328E+03	2.616E+03	1.925E+03	1.913E+03	2.419E+03	1.968E+03	2.774E+03	2.362E+03	**1.913E+03**
	Std	2.912E+01	3.348E+01	1.767E+01	3.846E+01	1.310E+02	4.650E+00	2.383E+01	1.533E+01	6.501E+01	2.111E+01	5.702E+00	4.576E+01	**8.722E−01**
CEC-2014-F20	Avg	3.868E+04	4.049E+04	2.193E+04	5.944E+04	3.517E+05	2.067E+09	3.019E+04	**7.649E+03**	5.980E+05	1.747E+04	2.998E+09	4.256E+05	7.339E+04
	Std	2.394E+04	2.373E+04	8.733E+03	3.388E+04	5.719E+04	3.347E+07	1.407E+04	5.743E+03	4.992E+05	**4.974E+03**	4.175E+07	2.643E+05	4.603E+04
CEC-2014-F21	Avg	7.742E+05	9.145E+05	5.403E+05	2.444E+06	1.420E+08	1.929E+09	5.958E+05	**4.816E+04**	2.496E+07	7.250E+04	2.628E+09	4.477E+07	1.149E+06
	Std	5.596E+05	7.388E+05	3.999E+05	2.904E+06	1.147E+08	1.654E+07	4.841E+05	**6.857E+04**	9.855E+06	7.545E+04	2.656E+07	1.970E+07	6.576E+05
CEC-2014-F22	Avg	2.893E+03	2.928E+03	2.607E+03	3.230E+03	1.502E+05	3.507E+06	2.899E+03	**2.562E+03**	4.338E+03	3.388E+03	5.394E+06	5.827E+03	2.772E+03
	Std	2.284E+02	2.213E+02	1.931E+02	3.168E+02	2.044E+05	5.724E+04	2.414E+02	2.479E+02	2.782E+02	3.546E+02	7.386E+04	1.689E+03	**1.251E+02**
CEC-2014-F23	Avg	**2.500E+03**	**2.500E+03**	2.615E+03	**2.500E+03**	**2.500E+03**	2.505E+03	**2.500E+03**	2.616E+03	2.567E+03	2.506E+03	2.529E+03	**2.500E+03**	2.629E+03
	Std	**0.000E+00**	**0.000E+00**	1.347E−01	**0.000E+00**	3.383E−03	5.218E+00	2.066E−08	9.806E−01	4.363E+00	8.288E−01	1.341E+01	1.844E−12	5.342E+00
CEC-2014-F24	Avg	**2.600E+03**	**2.600E+03**	**2.600E+03**	**2.600E+03**	2.602E+03	2.601E+03	**2.600E+03**	2.641E+03	2.607E+03	2.601E+03	2.604E+03	**2.600E+03**	2.646E+03
	Std	**0.000E+00**	**0.000E+00**	1.250E−02	8.225E−04	6.669E−01	2.834E−01	1.142E−01	2.502E+00	8.153E−01	1.680E−01	6.075E−01	5.444E−04	6.757E+00
CEC-2014-F25	Avg	**2.700E+03**	**2.700E+03**	2.701E+03	**2.700E+03**	**2.700E+03**	**2.700E+03**	**2.700E+03**	2.706E+03	2.701E+03	**2.700E+03**	2.700E+03	**2.700E+03**	2.708E+03
	Std	**0.000E+00**	**0.000E+00**	3.892E+00	**0.000E+00**	5.320E−05	7.100E−02	5.823E−10	1.539E+00	6.360E−02	1.212E−02	1.870E−01	5.716E−13	2.782E+00
CEC-2014-F26	Avg	2.703E+03	**2.701E+03**	2.728E+03	2.777E+03	2.800E+03	2.800E+03	**2.701E+03**	2.705E+03	2.710E+03	2.800E+03	2.800E+03	2.752E+03	2.706E+03
	Std	**1.389E+01**	1.627E−01	4.493E+01	4.262E+01	3.941E−04	6.482E−04	1.520E−01	1.956E+01	9.852E−01	4.446E−04	9.691E−03	3.327E+01	2.745E+01
CEC-2014-F27	Avg	**2.900E+03**	**2.900E+03**	3.293E+03	**2.900E+03**	**2.900E+03**	2.904E+03	**2.900E+03**	3.247E+03	3.194E+03	2.904E+03	2.979E+03	3.096E+03	3.540E+03
	Std	**0.000E+00**	6.087E−11	1.030E+02	**0.000E+00**	2.138E−03	5.433E+00	6.438E−09	9.001E+01	3.435E+01	9.106E−01	6.996E+01	3.292E+02	4.792E+02
CEC-2014-F28	Avg	**3.000E+03**	**3.000E+03**	3.827E+03	**3.000E+03**	**3.000E+03**	3.006E+03	**3.000E+03**	3.936E+03	3.317E+03	3.005E+03	3.105E+03	**3.000E+03**	3.223E+03
	Std	**0.000E+00**	9.289E−11	1.820E+02	**0.000E+00**	2.860E−03	6.651E+00	8.077E−09	2.735E+02	3.698E+01	1.143E+00	7.961E+01	1.811E−09	2.264E+01
CEC-2014-F29	Avg	2.939E+06	2.508E+06	1.696E+06	3.958E+06	7.146E+03	5.355E+06	**3.100E+03**	3.289E+06	7.554E+07	7.057E+06	3.796E+07	**3.100E+03**	3.130E+03
	Std	4.194E+06	4.126E+06	3.709E+06	1.182E+07	3.740E+03	6.123E+06	2.852E−02	4.929E+06	7.561E+06	8.059E+05	1.722E+07	**2.448E−05**	4.295E+00
CEC-2014-F30	Avg	1.138E+04	1.478E+04	1.132E+04	1.719E+05	3.506E+03	3.652E+05	1.883E+04	1.060E+04	1.752E+06	4.973E+05	2.541E+06	**3.200E+03**	4.589E+03
	Std	8.734E+03	9.762E+03	7.878E+03	2.901E+05	2.687E+02	3.954E+05	1.313E+04	9.318E+03	5.422E+05	6.685E+04	1.326E+06	**7.549E−04**	2.606E+02

Table 6
p-value of the Wilcoxon rank-sum test with a 5% significance of scalable benchmark functions f_{1-13} (p-values ≥ 0.05 are shown in boldface).

Test problem	SMA	EO	HHO	GWO	WDO	WOA	DE	CS	PSO	FA	L-SHADE	CMA-ES
f_1	**2.500E−01**	8.882E−16	8.882E−16	8.882E−16	8.882E−16	8.882E−16	8.882E−16	8.882E−16	8.882E−16	8.882E−16	8.882E−16	8.882E−16
f_2	1.212E−07	8.882E−16	8.882E−16	8.882E−16	8.882E−16	8.882E−16	8.882E−16	8.882E−16	8.882E−16	8.882E−16	8.882E−16	8.882E−16
f_3	**6.250E−02**	8.882E−16	8.882E−16	8.882E−16	8.882E−16	8.882E−16	8.882E−16	8.882E−16	8.882E−16	8.882E−16	8.882E−16	8.882E−16
f_4	4.619E−14	8.882E−16	8.882E−16	8.882E−16	8.882E−16	8.882E−16	8.882E−16	8.882E−16	8.882E−16	8.882E−16	8.882E−16	8.882E−16
f_5	**1.608E−01**	1.832E−08	1.179E−12	8.882E−16	8.882E−16	2.328E−09	8.882E−16	8.882E−16	8.882E−16	8.882E−16	1.832E−08	1.832E−08
f_6	2.328E−09	8.882E−16	4.619E−14	8.882E−16	8.882E−16	8.882E−16	1.967E−11	8.882E−16	8.882E−16	8.882E−16	8.882E−16	8.882E−16
f_7	**1.000E+00**	8.882E−16	**7.798E−01**	8.882E−16	8.882E−16	8.882E−16	8.882E−16	8.882E−16	8.882E−16	8.882E−16	8.882E−16	8.882E−16
f_8	6.210E−04	8.882E−16	**4.011E−01**	8.882E−16	8.882E−16	8.882E−16	8.882E−16	8.882E−16	8.882E−16	8.882E−16	8.882E−16	8.882E−16
f_9	**1.000E+00**	**1.000E+00**	**1.000E+00**	8.882E−16	3.553E−15	8.882E−16	8.882E−16	8.882E−16	8.882E−16	8.882E−16	8.882E−16	8.882E−16
f_{10}	**1.000E+00**	8.882E−16	**1.000E+00**	8.882E−16	8.882E−16	8.882E−16	8.882E−16	8.882E−16	8.882E−16	8.882E−16	8.882E−16	8.882E−16
f_{11}	**1.000E+00**	**1.000E+00**	**1.000E+00**	8.882E−16	5.684E−14	2.441E−04	8.882E−16	8.882E−16	8.882E−16	8.882E−16	**1.000E+00**	8.882E−16
f_{12}	**7.798E−01**	4.619E−14	1.179E−12	8.882E−16	4.601E−03	8.882E−16	8.882E−16	8.882E−16	9.191E−02	8.882E−16	8.882E−16	8.882E−16
f_{13}	1.097E−02	**4.011E−01**	1.179E−12	8.882E−16	5.704E−05	8.882E−16	8.882E−16	8.882E−16	1.179E−12	8.882E−16	8.882E−16	8.882E−16

Table 7
p-value of the Wilcoxon rank-sum test with a 5% significance of fixed dimension benchmark functions f_{14-23} (p-values $\geq$ 0.05 are shown in boldface).

Test problem	SMA	EO	HHO	GWO	WDO	WOA	DE	CS	PSO	FA	L-SHADE	CMA-ES
f_{14}	**1.000E+00**	4.619E−14	1.179E−12	8.882E−16	8.882E−16	4.601E−03	4.619E−14	8.882E−16	8.882E−16	8.882E−16	8.882E−16	8.882E−16
f_{15}	**7.798E−01**	1.474E−05	6.867E−07	**1.000E+00**	4.887E−02	1.769E−03	**5.758E−01**	4.619E−14	5.704E−05	**7.798E−01**	8.882E−16	5.704E−05
f_{16}	4.887E−02	8.882E−16	4.887E−02	8.882E−16	8.882E−16	5.704E−05	8.882E−16	8.882E−16	8.882E−16	8.882E−16	8.882E−16	8.882E−16
f_{17}	1.097E−02	8.882E−16	**4.011E−01**	8.882E−16	8.882E−16	1.967E−11	8.882E−16	8.882E−16	**2.624E−01**	8.882E−16	8.882E−16	4.887E−02
f_{18}	**9.191E−02**	8.882E−16	1.212E−07	8.882E−16	8.882E−16	4.619E−14	8.882E−16	8.882E−16	8.882E−16	3.389E−06	8.882E−16	8.882E−16
f_{19}	1.832E−08	8.882E−16	4.619E−14	8.882E−16	8.882E−16	**4.011E−01**	8.882E−16	8.882E−16	8.882E−16	**5.758E−01**	8.882E−16	8.882E−16
f_{20}	**1.000E+00**	6.210E−04	1.967E−11	1.967E−11	1.980E−04	2.328E−09	1.980E−04	8.882E−16	5.704E−05	4.601E−03	2.328E−09	6.210E−04
f_{21}	**7.798E−01**	1.980E−04	8.882E−16	8.882E−16	8.882E−16	8.882E−16	1.832E−08	8.882E−16	8.882E−16	8.882E−16	8.882E−16	6.210E−04
f_{22}	**9.191E−02**	6.210E−04	8.882E−16	8.882E−16	8.882E−16	8.882E−16	4.619E−14	8.882E−16	8.882E−16	8.882E−16	8.882E−16	8.882E−16
f_{23}	**1.000E+00**	3.389E−06	8.882E−16	8.882E−16	8.882E−16	8.882E−16	2.416E−10	8.882E−16	8.882E−16	8.882E−16	8.882E−16	1.179E−12

Table 8
p-value of the Wilcoxon rank-sum test with 5% significance of CEC-2014 test functions (p-values $\geq$ 0.05 are shown in boldface).

Test problem	SMA	EO	HHO	GWO	WDO	WOA	DE	CS	PSO	FA	L-SHADE	CMA-ES
CEC-2014-F1	**9.191E−02**	**4.011E−01**	8.882E−16	8.882E−16	8.882E−16	1.832E−08	4.887E−02	8.882E−16	9.191E−02	8.882E−16	8.882E−16	1.967E−11
CEC-2014-F2	8.882E−16	1.179E−12	8.882E−16	8.882E−16	8.882E−16	8.882E−16	2.416E−10	8.882E−16	8.882E−16	8.882E−16	8.882E−16	8.882E−16
CEC-2014-F3	**4.011E−01**	1.097E−02	2.416E−10	8.882E−16	8.882E−16	6.210E−04	4.619E−14	8.882E−16	1.212E−07	8.882E−16	8.882E−16	8.882E−16
CEC-2014-F4	**7.798E−01**	1.097E−02	8.882E−16	8.882E−16	8.882E−16	2.328E−09	2.409E−02	8.882E−16	4.011E−01	8.882E−16	8.882E−16	8.882E−16
CEC-2014-F5	**1.000E+00**	**1.608E−01**	2.416E−10	2.416E−10	4.619E−14	1.967E−11	**4.011E−01**	2.409E−02	8.882E−16	4.619E−14	4.619E−14	**1.608E−01**
CEC-2014-F6	**5.758E−01**	2.328E−09	8.882E−16	8.882E−16	8.882E−16	1.980E−04	2.328E−09	8.882E−16	8.882E−16	8.882E−16	8.882E−16	8.882E−16
CEC-2014-F7	3.389E−06	8.882E−16	8.882E−16	8.882E−16	8.882E−16	8.882E−16	1.980E−04	8.882E−16	**9.191E−02**	8.882E−16	8.882E−16	8.882E−16
CEC-2014-F8	1.179E−12	2.416E−10	8.882E−16	8.882E−16	8.882E−16	8.882E−16	8.882E−16	8.882E−16	8.882E−16	8.882E−16	8.882E−16	8.882E−16
CEC-2014-F9	**4.011E−01**	6.210E−04	2.416E−10	8.882E−16	8.882E−16	1.967E−11	4.619E−14	8.882E−16	2.416E−10	8.882E−16	8.882E−16	1.474E−05
CEC-2014-F10	1.769E−03	1.832E−08	4.619E−14	8.882E−16	8.882E−16	8.882E−16	8.882E−16	8.882E−16	8.882E−16	8.882E−16	8.882E−16	8.882E−16
CEC-2014-F11	**7.798E−01**	4.601E−03	2.328E−09	8.882E−16	8.882E−16	1.980E−04	8.882E−16	8.882E−16	6.867E−07	8.882E−16	8.882E−16	8.882E−16
CEC-2014-F12	**5.758E−01**	1.967E−11	8.882E−16	8.882E−16	4.619E−14	2.409E−02	8.882E−16	8.882E−16	1.769E−03	8.882E−16	2.328E−09	8.882E−16
CEC-2014-F13	**5.758E−01**	4.619E−14	6.867E−07	8.882E−16	8.882E−16	4.601E−03	6.867E−07	8.882E−16	1.097E−02	8.882E−16	8.882E−16	8.882E−16
CEC-2014-F14	**2.624E−01**	1.832E−08	1.474E−05	8.882E−16	8.882E−16	6.210E−04	1.097E−02	8.882E−16	4.887E−02	8.882E−16	8.882E−16	**2.624E−01**
CEC-2014-F15	**9.191E−02**	1.980E−04	8.882E−16	8.882E−16	8.882E−16	8.882E−16	2.416E−10	8.882E−16	8.882E−16	8.882E−16	8.882E−16	4.601E−03
CEC-2014-F16	**1.000E+00**	**4.011E−01**	6.867E−07	8.882E−16	8.882E−16	3.389E−06	4.619E−14	8.882E−16	8.882E−16	8.882E−16	8.882E−16	2.416E−10
CEC-2014-F17	**2.624E−01**	1.474E−05	2.328E−09	8.882E−16	8.882E−16	**9.191E−02**	4.619E−14	8.882E−16	8.882E−16	8.882E−16	8.882E−16	4.011E−01
CEC-2014-F18	4.887E−02	5.704E−05	8.882E−16	8.882E−16	8.882E−16	2.416E−10	5.704E−05	8.882E−16	6.210E−04	8.882E−16	8.882E−16	8.882E−16
CEC-2014-F19	1.097E−02	1.980E−04	2.416E−10	8.882E−16	8.882E−16	3.389E−06	6.210E−04	8.882E−16	1.832E−08	8.882E−16	8.882E−16	1.769E−03
CEC-2014-F20	**7.798E−01**	2.409E−02	1.980E−04	8.882E−16	8.882E−16	**2.624E−01**	4.619E−14	8.882E−16	1.980E−04	8.882E−16	8.882E−16	1.980E−04
CEC-2014-F21	**5.758E−01**	**5.758E−01**	4.601E−03	8.882E−16	8.882E−16	**2.624E−01**	8.882E−16	8.882E−16	4.619E−14	8.882E−16	8.882E−16	1.097E−02
CEC-2014-F22	**7.798E−01**	5.704E−05	1.474E−05	8.882E−16	8.882E−16	**2.624E−01**	1.212E−07	8.882E−16	1.212E−07	8.882E−16	8.882E−16	4.601E−03
CEC-2014-F23	**1.000E+00**	8.882E−16	**1.000E+00**	8.882E−16	8.882E−16	8.882E−16	8.882E−16	8.882E−16	8.882E−16	8.882E−16	8.882E−16	8.882E−16
CEC-2014-F24	**1.000E+00**	8.882E−16	2.274E−13	8.882E−16	8.882E−16	8.882E−16	8.882E−16	8.882E−16	8.882E−16	8.882E−16	8.882E−16	8.882E−16
CEC-2014-F25	**1.000E+00**	8.882E−16	**1.000E+00**	8.882E−16	8.882E−16	8.882E−16	8.882E−16	8.882E−16	8.882E−16	8.882E−16	8.882E−16	8.882E−16
CEC-2014-F26	**5.758E−01**	1.769E−03	9.021E−05	8.882E−16	8.882E−16	**7.798E−01**	1.980E−04	4.619E−14	8.882E−16	8.882E−16	4.619E−14	1.179E−12
CEC-2014-F27	**5.000E−01**	8.882E−16	**1.000E+00**	8.882E−16	8.882E−16	8.882E−16	8.882E−16	8.882E−16	8.882E−16	8.882E−16	8.882E−16	8.882E−16
CEC-2014-F28	**5.000E−01**	8.882E−16	**5.000E−01**	8.882E−16	8.882E−16	8.882E−16	8.882E−16	8.882E−16	8.882E−16	8.882E−16	8.882E−16	8.882E−16
CEC-2014-F29	**9.191E−02**	**7.798E−01**	5.418E−07	**2.624E−01**	**1.608E−01**	1.832E−08	**4.011E−01**	8.882E−16	2.409E−02	8.882E−16	1.832E−08	1.832E−08
CEC-2014-F30	1.097E−02	**5.758E−01**	**2.529E−01**	1.967E−11	1.212E−07	6.210E−04	**4.011E−01**	8.882E−16	8.882E−16	8.882E−16	1.967E−11	2.416E−10

Table 9
Friedman mean rank for test problems for 30 dimensions (The data are rounded up to 3 decimal points).

Test problems	Metric	Optimization algorithm												
		ESMA	SMA	EO	HHO	GWO	WDO	WOA	DE	CS	PSO	FA	L-SHADE	CMA-ES
Scalable test problems f_{1-13}	Mean rank	**2.654**	3.269	4.192	2.808	8.615	8.692	6.923	11.462	11.923	8.692	11.538	4.077	6.154
	Rank	**1**	3	5	2	8	9	7	11	13	10	12	4	6
Non-scalable test problems f_{14-23}	Mean rank	4.300	4.300	4.700	6.900	11.400	9.300	7.300	**4.000**	11.000	8.200	10.400	5.150	4.050
	Rank	3	4	5	7	13	10	8	**1**	12	9	11	6	2
CEC14 test problems F1 to F30	Mean rank	**3.400**	4.300	4.267	6.200	8.933	10.033	5.167	5.667	10.400	6.300	12.300	7.733	6.300
	Rank	**1**	3	2	6	10	11	4	5	12	7	13	9	8
Overall (f_{1-23} and F1 to F30)	Mean rank	**3.387**	4.047	4.330	5.500	9.321	9.566	6.000	6.774	10.887	7.245	11.755	6.349	5.840
	Rank	**1**	2	3	4	10	11	6	8	12	9	13	7	5

problem, because they are simple to implement, derivative-free, and can avoid local minima [27,28]. This encourages the researchers to use the derivative-free nature-inspired optimization algorithm instead of a conventional deterministic optimizer. The nature-inspired algorithms are mainly classified into three categories: evolution-based, physics-based, and swarm-based. The evolution-based optimization algorithms are inspired by the laws of natural evolution. The most prominent in the evolution-based category is the differential evolution (DE) [29]. However, more advanced high-performance optimization techniques are — successful history-based adaptive DE with linear population size reduction (L-SHADE) [30] and evolution strategy with covariance matrix adaptation (CMA-ES) [31]. The physics-based optimization algorithms, such as the wind driven optimization (WDO) [32] and recently developed Equilibrium optimizer (EO) [33], mimic the laws of the physical world. The swarm-based mimic the social behaviour or foraging mechanism or hunting mechanism of groups of an organism. Some of the famous and recently developed swarm-based optimizers are particle swarm optimization (PSO) [29], cuckoo search (CS) [34], Harris hawk's optimization (HHO) [35], grey wolf optimizer (GWO) [27], wind driven optimization (WDO) [32], and whale optimization algorithm (WOA) [28]. The overall performances of L-SHADE [30], CMA-ES [31], EO [33], HHO [35] and GWO [27] on general benchmark function evaluation are quite satisfactory. The DE [29] and CS [34] are good at multimodal benchmark functions for fixed dimensions, widely used in many applications. The PSO [29], WDO [32] and FA [34] have shown interesting results in the diversified fields.

Recently, the slime mould algorithm (SMA) [36] is proposed by taking inspiration from the foraging behaviour and morphological variation of slime mould *Physarum polycephalum.* An Equilibrium optimizer (EO) is also proposed recently in [33], based on the equilibrium states of control volume mass balance models. The searching pattern, as well as the results of SMA and EO, is quite impressive when compared with some state-of-the-art

Table 10
Average time (in a sec) of ESMA and other optimization algorithms.

Test problems	ESMA	SMA	EO	HHO	GWO	WDO	WOA	DE	CS	PSO	FA	L-SHADE	CMA-ES
f_1	1.880	1.934	0.218	0.209	0.072	0.152	0.153	0.266	0.330	0.051	0.099	9.938	4.818
f_2	2.125	1.931	0.195	0.221	0.107	0.160	0.151	0.291	0.345	0.065	0.091	10.152	4.928
f_3	2.233	2.202	0.474	0.959	0.407	0.429	0.419	0.843	0.619	0.329	0.372	11.909	6.453
f_4	1.926	1.959	0.189	0.281	0.077	0.156	0.148	0.283	0.341	0.053	0.081	9.544	5.002
f_5	1.967	1.976	0.221	0.397	0.115	0.186	0.178	0.361	0.381	0.085	0.119	9.903	5.071
f_6	1.947	1.933	0.190	0.311	0.077	0.153	0.146	0.283	0.339	0.053	0.085	10.177	4.885
f_7	2.096	2.083	0.336	0.599	0.243	0.316	0.292	0.576	0.487	0.228	0.227	19.657	5.614
f_8	2.002	1.971	0.246	0.438	0.108	0.196	0.199	0.359	0.385	0.100	0.113	10.531	5.469
f_9	1.962	1.954	0.199	0.349	0.091	0.175	0.170	0.330	0.369	0.074	0.103	12.008	4.917
f_{10}	1.955	1.957	0.206	0.360	0.091	0.177	0.172	0.325	0.379	0.080	0.110	9.938	4.831
f_{11}	2.010	2.019	0.235	0.418	0.114	0.196	0.200	0.382	0.407	0.092	0.123	9.910	5.093
f_{12}	2.430	2.378	0.613	1.331	0.497	0.581	0.579	1.144	0.771	0.471	0.504	13.911	7.001
f_{13}	2.405	2.468	0.641	1.395	0.489	0.576	0.580	1.157	0.772	0.475	0.505	14.095	7.052
f_{14}	1.513	1.459	1.022	2.383	0.903	0.974	0.948	1.955	1.016	0.888	0.911	1.072	3.474
f_{15}	0.732	0.691	0.166	0.276	0.071	0.124	0.118	0.254	0.188	0.059	0.075	0.861	0.053
f_{16}	0.659	0.614	0.158	0.272	0.067	0.123	0.112	0.255	0.174	0.052	0.071	0.471	1.598
f_{17}	0.648	0.605	0.153	0.226	0.057	0.113	0.102	0.226	0.163	0.043	0.062	0.815	0.040
f_{18}	0.638	0.603	0.145	0.230	0.055	0.110	0.101	0.226	0.172	0.038	0.061	0.447	1.544
f_{19}	0.786	0.684	0.173	0.292	0.099	0.146	0.132	0.291	0.209	0.071	0.108	0.676	1.899
f_{20}	0.943	0.856	0.181	0.303	0.087	0.144	0.136	0.288	0.211	0.069	0.087	1.316	2.482
f_{21}	0.801	0.761	0.199	0.361	0.104	0.165	0.153	0.335	0.226	0.090	0.112	0.931	2.245
f_{22}	0.817	0.855	0.245	0.402	0.127	0.181	0.195	0.367	0.245	0.108	0.128	0.977	2.342
f_{23}	0.839	0.790	0.245	0.473	0.153	0.213	0.203	0.428	0.273	0.133	0.154	1.006	2.491
CEC-2014-F1	2.274	2.058	0.313	0.619	0.193	0.279	0.266	0.532	0.466	0.173	0.208	13.793	5.904
CEC-2014-F2	2.239	2.065	0.344	0.479	0.139	0.229	0.216	0.437	0.408	0.121	0.151	12.756	5.538
CEC-2014-F3	2.228	1.986	0.264	0.524	0.138	0.230	0.213	0.434	0.408	0.120	0.152	12.098	5.568
CEC-2014-F4	2.255	1.989	0.277	0.478	0.135	0.225	0.213	0.425	0.407	0.119	0.151	12.646	5.521
CEC-2014-F5	2.248	2.020	0.285	0.616	0.152	0.248	0.237	0.484	0.451	0.142	0.175	11.484	5.985
CEC-2014-F6	4.198	3.859	2.008	5.413	1.773	1.968	2.000	4.096	2.223	1.860	1.862	28.183	14.123
CEC-2014-F7	2.338	2.049	0.294	0.571	0.162	0.250	0.258	0.497	0.454	0.145	0.182	14.118	5.905
CEC-2014-F8	2.289	2.009	0.254	0.504	0.123	0.208	0.207	0.495	0.408	0.105	0.141	10.266	5.445
CEC-2014-F9	2.261	2.035	0.287	0.569	0.152	0.238	0.233	0.484	0.429	0.134	0.166	13.668	5.782
CEC-2014-F10	2.330	2.138	0.334	0.701	0.200	0.287	0.281	0.582	0.478	0.187	0.214	12.025	6.084
CEC-2014-F11	2.330	2.148	0.370	0.783	0.231	0.329	0.319	0.647	0.512	0.215	0.246	11.175	6.286
CEC-2014-F12	2.622	2.390	0.689	1.514	0.495	0.592	0.583	1.179	0.770	0.485	0.512	13.376	7.554
CEC-2014-F13	2.337	2.036	0.268	0.519	0.137	0.227	0.216	0.445	0.410	0.123	0.154	13.941	5.653
CEC-2014-F14	2.271	2.024	0.272	0.521	0.145	0.237	0.222	0.453	0.418	0.128	0.159	13.268	6.147
CEC-2014-F15	2.292	2.043	0.310	0.562	0.167	0.250	0.244	0.484	0.444	0.154	0.199	14.172	5.759
CEC-2014-F16	2.291	2.081	0.296	0.613	0.159	0.249	0.245	0.506	0.436	0.143	0.175	11.904	5.976
CEC-2014-F17	2.342	2.098	0.329	0.669	0.192	0.282	0.290	0.586	0.473	0.177	0.208	13.128	6.437
CEC-2014-F18	2.300	2.106	0.293	0.578	0.156	0.242	0.237	0.484	0.431	0.139	0.168	11.568	6.017
CEC-2014-F19	2.687	2.501	0.657	1.371	0.454	0.586	0.611	1.226	0.826	0.485	0.515	15.928	7.895
CEC-2014-F20	2.272	2.203	0.307	0.621	0.163	0.258	0.252	0.503	0.456	0.148	0.179	12.220	6.075
CEC-2014-F21	2.251	2.201	0.333	0.639	0.191	0.288	0.280	0.562	0.491	0.175	0.209	14.698	6.148
CEC-2014-F22	2.299	2.259	0.370	0.728	0.216	0.311	0.317	0.618	0.513	0.200	0.236	14.068	6.272
CEC-2014-F23	2.866	2.696	0.823	1.925	0.699	0.791	0.773	1.545	0.976	0.666	0.701	16.352	8.316
CEC-2014-F24	2.614	2.537	0.620	1.399	0.482	0.578	0.578	1.188	0.793	0.465	0.502	13.451	7.388
CEC-2014-F25	2.713	2.674	0.707	1.599	0.560	0.659	0.656	1.320	0.875	0.548	0.601	15.149	7.968
CEC-2014-F26	4.806	4.708	2.681	6.319	2.366	2.647	2.691	5.449	2.892	2.480	2.536	34.628	18.125
CEC-2014-F27	4.632	4.611	2.653	6.213	2.383	2.578	2.581	5.172	2.911	2.451	2.479	36.148	18.445
CEC-2014-F28	2.963	2.873	0.969	2.160	0.810	0.873	0.888	1.796	1.106	0.828	0.803	16.952	9.135
CEC-2014-F29	3.075	2.954	1.024	2.166	0.801	0.929	0.929	1.946	1.196	0.815	0.854	17.499	10.149
CEC-2014-F30	2.751	2.587	0.700	1.572	0.540	0.651	0.648	1.303	0.856	0.531	0.562	14.683	8.139

algorithms. The searching pattern of SMA requires differential information of two random slime moulds with the best slime mould, which may tends to deviate the results from the optimal value. The searching pattern of EO depends on the equilibrium pools of the best candidate solutions. So, to supplement the features of the SMA by integrating the equilibrium pool, an equilibrium slime mould algorithm (ESMA) is proposed in this paper. The performance of the ESMA is evaluated using 23 test problems from [37,38] and 30 test problems from the IEEE CEC 2014 test suite [39]. The ESMA results are compared with the three groups of active optimization algorithms – (i) the well-known optimization algorithms: DE, CS, PSO, FA, WDO; (ii) the recently developed algorithms: SMA, EO, HHO, GWO, WOA; (iii) the high-performance optimization algorithms: CMA-ES and L-SHADE as they performed well in the test problems or diversified applications. Both quantitative and qualitative analysis is done in the result section. The statistical analysis of results using Wilcoxon's test and Friedman means rank test shows that the proposed ESMA ranked first. And the next five (second to sixth) ranked algorithms are SMA, EO, HHO, WOA, and DE.

The performance of the ESMA has motivated us to use it as an optimizer. The reason for the choice is to make the multilevel image thresholding method, for breast thermogram analysis, computationally efficient. The problem statement is formed for the multilevel thresholding technique, to minimize the objective functions. To experiment, 10 thermogram images in RGB coordinates are retrieved from the Database for Breast Research with Infrared Image [40]. Two experiments are performed on grey and RGB coordinates of thermogram images, to show the efficiency of the multilevel thresholding using colour coordinates. The performance of both experiments is compared with the top rank holder optimizers in our study. The quantitative results of both experiments are compared in terms of peak signal to noise ratio (PSNR) [41], the structure similarity (SSIM) [42], and the feature similarity (FSIM) [43]. It is observed that the multilevel

Table 11
A comparison of the average value of PSNR obtained for test image using ESMA, SMA, EO, HHO, WOA, and CMA-ES.

Test image	K	ESMA		SMA		EO		HHO		WOA		CMA-ES	
		RGB	Grey	RGB	Grey	RGB	Grey	RGB	Grey	RGB	Grey	RGB	Grey
Test1	2	23.2856	**24.2261**	22.8930	23.5447	22.6333	23.3350	22.8407	22.8802	22.9046	**24.2261**	23.2331	24.1052
	3	**24.8761**	24.6221	24.4601	24.6509	24.6342	24.6463	24.7153	24.2766	24.5584	24.6467	24.6286	24.5963
	4	**27.4404**	25.6851	27.1808	25.0101	26.8695	25.0646	26.4242	25.0518	27.2789	25.0681	27.1116	24.7857
	5	**29.2237**	27.5266	28.0661	26.4100	28.2667	27.1085	27.6329	26.4102	28.6148	26.6624	28.3341	26.7459
Test2	2	21.5603	17.9833	21.4308	18.2526	21.8513	18.5958	21.2686	**22.2940**	21.1819	17.5116	21.9069	17.6445
	3	22.7459	24.3127	22.6287	23.7160	22.8801	24.4282	22.5494	23.6189	23.2096	23.8358	22.5604	**24.3689**
	4	**24.8828**	24.5539	24.8485	24.0017	24.5962	23.9234	24.8427	24.2459	24.6820	24.5977	24.4832	24.5002
	5	**26.8817**	25.7843	26.2864	25.6745	26.2098	25.8259	26.4634	25.8386	27.0003	25.6574	26.5149	25.0269
Test3	2	23.0600	19.8095	22.7253	20.2393	22.7208	20.5297	22.7863	21.4278	**23.0661**	19.1138	23.0600	19.1113
	3	**25.3872**	25.0358	24.9004	24.5812	24.8721	24.7427	24.7922	24.6421	25.0281	25.1338	25.0895	24.7495
	4	**26.8815**	28.3684	26.7799	27.3365	26.7772	27.2524	26.1879	26.6625	26.8299	27.4373	26.7752	27.8292
	5	**28.6434**	28.4991	28.1732	27.5080	28.2569	28.0506	27.9164	27.5371	28.6504	28.4373	28.1249	27.7081
Test4	2	**22.5445**	19.9797	22.3732	20.0129	22.1482	20.0429	22.2199	20.3999	22.0266	19.9792	**22.5445**	20.0188
	3	24.4428	24.6113	24.3263	24.6804	24.3223	24.8035	24.2959	24.7387	24.1879	24.3122	24.7178	**24.9282**
	4	**26.4851**	25.7235	25.7523	25.7509	26.3523	25.7799	26.3042	25.1243	25.9290	25.7153	26.3589	25.9391
	5	27.7357	**28.2691**	27.4200	27.0513	27.6395	27.5601	27.2169	27.7927	27.8225	27.5484	27.2906	27.4853
Test5	2	**23.8515**	20.2270	23.8280	20.2167	23.7772	20.2085	22.9043	21.3366	23.7255	20.2270	**23.8515**	20.2219
	3	25.6171	25.7194	25.0522	25.8270	24.9031	25.8601	24.9362	24.9016	25.1668	25.7161	24.9547	**25.8822**
	4	**27.9285**	27.2002	26.7993	26.6625	26.8897	27.0266	26.3281	26.7603	27.3879	26.8529	26.2929	27.0510
	5	**28.5904**	28.2492	27.8813	27.7162	28.5282	27.5524	27.7198	26.4918	28.2625	28.0247	28.1391	28.3377
Test6	2	21.1587	**22.3496**	20.8484	22.3008	20.8383	22.3046	21.2888	22.3264	21.0260	**22.3496**	21.0197	22.3492
	3	25.1695	**25.9842**	24.0243	25.5210	24.3336	25.3417	24.8983	24.8310	24.6146	25.9071	24.4238	**25.9842**
	4	**26.7138**	26.3081	26.1343	25.6654	26.1958	26.0168	25.8824	25.7594	26.3628	26.5081	26.6128	25.9948
	5	**28.0929**	27.9866	27.2813	26.2375	27.0527	27.2690	27.4639	26.1634	27.3872	27.1062	27.1675	27.4261
Test7	2	21.1763	18.6419	**21.2486**	18.5799	21.2611	18.5856	21.0304	19.3253	21.1632	18.6419	21.2453	18.6135
	3	**23.6955**	23.4246	22.9500	21.6204	23.5764	21.9395	23.3558	22.0091	23.1084	21.9911	23.0647	22.2488
	4	25.2914	**25.7846**	25.0939	25.2234	25.1724	25.0340	24.6472	24.9130	25.1396	25.7921	25.2331	25.4347
	5	27.6459	**27.6612**	26.8174	27.4025	27.1346	26.8605	26.6492	26.5856	27.5904	27.6733	27.0156	27.1586
Test8	2	**25.2835**	21.6188	24.3735	21.6381	25.0676	21.6227	23.2707	22.0478	24.8803	21.6232	25.1366	21.6298
	3	**26.5163**	25.8222	26.0804	25.0887	25.7059	25.4611	25.6530	24.9650	26.3592	26.0364	25.9518	26.0739
	4	**27.5308**	27.1904	27.0063	26.8207	27.0869	26.8387	26.3394	26.8741	27.2856	27.0510	27.3092	26.9008
	5	**28.6593**	28.5394	28.3694	28.7770	28.4870	28.6538	28.0886	27.8327	28.9028	28.8201	28.4873	28.1393
Test9	2	22.6659	23.0331	22.7500	21.5712	22.5556	22.5406	23.0551	22.5241	22.8229	22.6691	22.6801	**23.6351**
	3	25.4169	24.7282	24.8198	24.6471	24.5622	24.6326	24.2458	23.9904	**25.4482**	24.6175	24.8628	24.6294
	4	**27.2413**	25.5730	26.3862	25.8820	26.7776	25.6956	26.3168	25.4857	26.7887	25.4061	26.8323	25.4406
	5	**28.3599**	27.6521	27.8975	27.0931	27.6879	26.9816	27.1203	26.7461	28.1915	26.5925	27.7396	27.3049
Test10	2	**21.9270**	17.9469	21.8374	17.8857	21.8271	17.8946	21.1357	18.2129	21.7803	17.9469	**21.9270**	17.9314
	3	22.9374	**24.7069**	23.2893	24.4136	23.0637	24.0074	23.3401	23.4239	22.9347	24.7040	23.3184	24.3659
	4	25.9976	**26.3827**	25.4619	25.5997	25.1368	25.5956	24.7187	25.3707	25.9436	25.7208	25.7033	25.5975
	5	27.1337	**27.8536**	26.4981	26.5613	26.6767	27.2300	25.9207	26.1377	27.1703	27.0657	26.4809	27.1620
Friedman mean rank		9.8500	7.8000	6.3750	4.6000	6.4500	5.4250	5.2250	3.9000	8.2250	6.4125	7.4250	6.3125
Rank		1	3	7	11	5	9	10	12	2	6	4	8

thresholding using RGB coordinates, by employing ESMA, yields better results.

The main contributions of this paper are as follows:

I. An equilibrium slime mould algorithm (ESMA) is proposed by integrating the equilibrium pool from the equilibrium optimizer (EO) in the search pattern of the slime mould algorithm (SMA). The qualitative and quantitative performance of the ESMA is evaluated using 53 test problems, including 30 test problems from the IEEE CEC 2014 test suite. The results are compared with state-of-the-art optimizers.
II. An objective function for the multilevel thresholding problem is investigated, which is based on the minimization of the entropic dependencies among the different classes in an image.
III. The proposed ESMA is employed to find the optimal threshold values, for multilevel thresholding of the breast thermogram images.

The rest of the paper is organized as follows. In Section 2, the proposed ESMA is discussed. Mathematical modelling and its performance analysis are also carried out in this section. An objective function to minimize the entropic dependencies among different classes, as a problem statement of the multilevel thresholding, is presented in Section 3 for readers. Section 4 presents the performance of the grey and colour thresholding of thermogram images using entropy minimization based objective function. The concluding remarks and the future work are highlighted in Section 5.

2. The proposed equilibrium slime mould algorithm (ESMA)

In this section, a new hybridized optimization algorithm coined as an equilibrium slime mould algorithm (ESMA) is introduced. The searchability of the slime mould algorithm (SMA) [36] is enhanced by hybridizing the integrity feature of the equilibrium pool described in the equilibrium optimizer (EO) [33]. We need to mention here that, the equilibrium pool helps in exploring the best solutions from the search space. The mathematical foundation of the ESMA and its performance evaluations are explicitly discussed in the following sub-sections.

2.1. Basic algorithms

In this subsection, we briefly discussed the two key algorithms SMA and EO, on which our proposed ESMA is coined.

Table 12
A comparison of the average value of FSIM obtained for test image using ESMA, SMA, EO, HHO, WOA, and CMA-ES.

Test image	K	ESMA		SMA		EO		HHO		WOA		CMA-ES	
		RGB	Grey	RGB	Grey	RGB	Grey	RGB	Grey	RGB	Grey	RGB	Grey
Test1	2	**0.7497**	0.6833	0.7399	0.6802	0.7285	0.6804	0.7354	0.6811	0.7429	0.6833	0.7371	0.6815
	3	**0.7642**	0.6997	0.7541	0.7039	0.7547	0.7038	0.7620	0.7031	0.7579	0.6998	0.7606	0.7004
	4	**0.8263**	0.7235	0.8178	0.7143	0.8069	0.7177	0.8136	0.7277	0.8219	0.7098	0.8234	0.7130
	5	**0.8851**	0.7642	0.8491	0.7475	0.8501	0.7620	0.8327	0.7509	0.8661	0.7425	0.8638	0.7382
Test2	2	**0.7535**	0.7051	0.7537	0.7041	0.7416	0.7082	0.7485	0.7315	0.7412	0.7011	0.7453	0.7029
	3	0.7594	0.7521	0.7562	0.7420	0.7541	0.7485	0.7539	0.7374	0.7588	0.7494	**0.7609**	0.7468
	4	**0.7718**	0.7535	0.7812	0.7421	0.7712	0.7424	0.7932	0.7444	0.7691	0.7546	0.7676	0.7539
	5	**0.8263**	0.7619	0.8138	0.7596	0.8051	0.7577	0.8198	0.7665	0.8192	0.7648	0.8140	0.7648
Test3	2	**0.7809**	0.6859	0.7702	0.6880	0.7719	0.6916	0.7679	0.6929	0.7793	0.6827	0.7797	0.6827
	3	0.8028	0.7306	0.7938	0.7207	0.7950	0.7208	0.7911	0.7214	**0.8041**	0.7326	0.7989	0.7316
	4	**0.8360**	0.7894	0.8181	0.7685	0.8186	0.7665	0.8245	0.7602	0.8345	0.7727	0.8183	0.7772
	5	**0.8610**	0.7862	0.8458	0.7727	0.8489	0.7801	0.8545	0.7764	0.8581	0.7873	0.8528	0.7900
Test4	2	0.7535	0.7097	0.7506	0.7093	0.7490	0.7101	0.7514	0.7100	0.7484	0.7097	**0.7539**	0.7097
	3	**0.7818**	0.7463	0.7796	0.7472	0.7791	0.7484	0.7827	0.7458	0.7799	0.7437	0.7808	0.7422
	4	**0.8248**	0.7503	0.8160	0.7537	0.8223	0.7520	0.8200	0.7518	0.8107	0.7516	0.8192	0.7528
	5	**0.8465**	0.7917	0.8388	0.7762	0.8409	0.7802	0.8372	0.7965	0.8446	0.7789	0.8346	0.7831
Test5	2	0.7918	0.7694	0.7940	0.7690	0.7944	0.7684	0.7900	0.7696	0.7923	0.7694	**0.7954**	0.7694
	3	**0.8139**	0.7858	0.8055	0.7834	0.8030	0.7838	0.8085	0.7809	0.8065	0.7857	0.8013	0.7857
	4	**0.8433**	0.7934	0.8289	0.7871	0.8266	0.7911	0.8249	0.7945	0.8386	0.7903	0.8300	0.7877
	5	0.8468	0.8024	0.8449	0.7956	0.8442	0.7940	0.8482	0.7897	0.8457	0.8012	**0.8495**	0.7979
Test6	2	0.7622	0.7462	0.7624	0.7464	0.7617	0.7458	**0.7671**	0.7444	0.7624	0.7462	0.7619	0.7462
	3	**0.8028**	0.7759	0.7932	0.7730	0.7918	0.7713	0.8023	0.7702	0.8014	0.7756	0.7980	0.7717
	4	0.8175	0.7736	0.8202	0.7688	0.8192	0.7726	0.8173	0.7703	0.8174	0.7743	**0.8205**	0.7751
	5	0.8417	0.7842	0.8368	0.7732	0.8397	0.7821	0.8330	0.7775	0.8386	0.7802	**0.8418**	0.7801
Test7	2	0.7917	0.7674	0.7912	0.7622	0.7904	0.7626	0.7913	0.7604	0.7914	0.7674	**0.7921**	0.7672
	3	**0.7952**	0.7867	0.7898	0.7776	0.7963	0.7787	0.8001	0.7764	0.7939	0.7819	0.7934	0.7815
	4	0.8131	0.7946	0.8037	0.7906	0.8096	0.7909	**0.8152**	0.7907	0.8065	0.7957	0.8051	0.7955
	5	**0.8405**	0.8194	0.8322	0.8090	0.8275	0.8020	0.8368	0.8091	0.8404	0.8157	0.8380	0.8127
Test8	2	**0.8250**	0.7608	0.8083	0.7584	0.8218	0.7579	0.8031	0.7613	0.8187	0.7606	0.8246	0.7607
	3	**0.8362**	0.7901	0.8257	0.7837	0.8262	0.7879	0.8323	0.7805	0.8355	0.7913	0.8267	0.7873
	4	**0.8544**	0.7965	0.8400	0.7922	0.8445	0.7923	0.8381	0.7922	0.8480	0.7958	0.8478	0.7972
	5	**0.8706**	0.8142	0.8617	0.8081	0.8565	0.8089	0.8625	0.8101	0.8690	0.8181	0.8624	0.8152
Test9	2	0.7503	0.7173	0.7498	0.7090	0.7407	0.7152	**0.7600**	0.7151	0.7541	0.7160	0.7485	0.7182
	3	**0.7964**	0.7399	0.7791	0.7364	0.7763	0.7371	0.7726	0.7315	0.7970	0.7382	0.7824	0.7391
	4	**0.8261**	0.7518	0.8073	0.7535	0.8091	0.7499	0.8065	0.7488	0.8160	0.7449	0.8196	0.7550
	5	**0.8372**	0.7773	0.8296	0.7675	0.8276	0.7693	0.8278	0.7706	0.8371	0.7626	0.8281	0.7753
Test10	2	0.7665	0.7312	0.7640	0.7291	0.7640	0.7296	0.7530	0.7318	0.7642	0.7312	**0.7670**	0.7312
	3	0.7700	0.7641	0.7721	0.7582	0.7708	0.7559	**0.7816**	0.7525	0.7703	0.7639	0.7708	0.7632
	4	**0.8202**	0.7777	0.8022	0.7686	0.7970	0.7658	0.8070	0.7694	0.8162	0.7746	0.8142	0.7730
	5	0.8239	0.7887	0.8159	0.7778	0.8187	0.7871	0.8216	0.7760	**0.8289**	0.7827	0.8065	0.7901
Friedman mean rank		**11.1500**	4.7000	8.6000	2.3625	8.4000	3.0500	9.2250	3.0125	9.9125	3.8625	9.7125	4.0125
Rank		**1**	7	5	12	6	10	4	11	2	9	3	8

2.1.1. Slime mould algorithm

The slime mould algorithm (SMA) [36] is based on the behaviour and morphological variations of the slime mould *Physarum polycephalum* during foraging. The slime mould approaches the food according to the odour in the air, which imitates the contraction mode. The slime mould used a biological oscillator which depends on the concentration of food, which means higher food concentration (fitness) leads to stronger waves generated by bio-oscillator and faster the cytoplasm flows. The bio-oscillator simulates the positive and negative feedback among vein width, food concentration, and slime mould. Based on the oscillation behaviour and way of approaching the foods during foraging by slime mould is mathematically modelled as SMA in [36]. Slime mould does not have any brain or neurons. Still, it is very intelligent and capable to solve many computationally difficult problems. It possesses a dynamic structure that helps to maintain a more stable balance between the global and local exploration drifts. Most importantly, it can optimize the form of its network extracting more and more pieces of information. The SMA has shown remarkable performance on benchmark function optimization. It is used to solve various real-world optimization tasks in engineering and industry better than its counterparts.

2.1.2. Equilibrium optimizer

The equilibrium optimizer (EO) [33] is mathematically modelled by taking inspiration from dynamic mass balance models in a control volume to estimate both dynamic and equilibrium states. Each particle in EO acts as a search agent that randomly updates its positions to best-so-far solutions known as the equilibrium candidates. The equilibrium candidate is a particle randomly chosen from the equilibrium pool, which contains the best four-particle concentration along with the average concentration among them. The EO uses the generation rate to a trade-off between exploration and exploitation to avoid the local minima. So, each particle uses the updating rule composed of the current positions, equilibrium candidate positions, generation rate along memory saving mechanism to reach the equilibrium states (optimal solutions) in the EO [33]. It contains special features like — high exploration and high exploitation. It is self-sufficient to randomly change the solutions. It can update its concentrations randomly to retrieve the best fit solution candidates. An inbuilt mechanism (generation rate) helps it to reinforce its exploration ability in the initial search and exploitation capability in the final search. The EO has shown quite impressive results on the benchmark function optimization when compared with the state-of-art algorithms.

Table 13
A comparison of the average value of SSIM obtained for test image using ESMA, SMA, EO, HHO, WOA, and CMA-ES.

Test image	K	ESMA		SMA		EO		HHO		WOA		CMA-ES	
		RGB	Grey	RGB	Grey	RGB	Grey	RGB	Grey	RGB	Grey	RGB	Grey
Test1	2	**0.9758**	0.7245	0.9724	0.7108	0.9728	0.7085	0.9716	0.7025	0.9724	0.7245	0.9723	0.7129
	3	**0.9839**	0.7365	0.9822	0.7403	0.9831	0.7399	0.9825	0.7331	0.9828	0.7371	0.9832	0.7374
	4	**0.9905**	0.7588	0.9900	0.7462	0.9894	0.7474	0.9877	0.7508	0.9902	0.7453	0.9900	0.7498
	5	**0.9931**	0.7965	0.9914	0.7747	0.9919	0.7891	0.9907	0.7803	0.9923	0.7757	0.9921	0.7720
Test2	2	**0.9673**	0.6814	0.9650	0.6815	0.9651	0.6889	0.9589	0.7359	0.9637	0.6738	0.9650	0.6771
	3	0.9729	0.7658	0.9715	0.7580	0.9724	0.7667	0.9717	0.7507	0.9748	0.7609	**0.9764**	0.7563
	4	**0.9838**	0.7683	0.9836	0.7596	0.9826	0.7601	0.9832	0.7621	0.9831	0.7693	0.9832	0.7687
	5	0.9892	0.7769	0.9881	0.7762	0.9877	0.7714	0.9872	0.7820	**0.9894**	0.7802	0.9881	0.7792
Test3	2	0.9701	0.6605	0.9684	0.6656	0.9679	0.6712	0.9692	0.6857	0.9709	0.6490	**0.9722**	0.6490
	3	**0.9828**	0.7540	0.9810	0.7403	0.9809	0.7426	0.9810	0.7411	0.9812	0.7564	0.9804	0.7552
	4	**0.9881**	0.8147	0.9877	0.7902	0.9878	0.7877	0.9853	0.7801	0.9879	0.7968	0.9876	0.8013
	5	**0.9919**	0.8075	0.9910	0.7917	0.9912	0.7995	0.9904	0.7946	0.9917	0.8090	0.9914	0.8121
Test4	2	0.9613	0.6746	0.9608	0.6742	0.9566	0.6755	0.9554	0.6795	0.9538	0.6746	**0.9647**	0.6746
	3	0.9713	0.7606	0.9715	0.7626	0.9716	0.7662	0.9727	0.7633	0.9699	0.7552	**0.9734**	0.7522
	4	**0.9831**	0.7874	0.9777	0.7892	0.9820	0.7876	0.9805	0.7740	0.9783	0.7859	0.9815	0.7881
	5	0.9857	0.8308	**0.9858**	0.8090	0.9848	0.8158	0.9856	0.8243	0.9857	0.8179	0.9846	0.8228
Test5	2	0.9769	0.7723	0.9773	0.7719	0.9769	0.7710	0.9673	0.7756	0.9770	0.7723	**0.9779**	0.7723
	3	**0.9848**	0.8093	0.9830	0.8094	0.9828	0.8120	0.9822	0.8051	0.9842	0.8091	0.9823	0.8101
	4	**0.9905**	0.8243	0.9885	0.8157	0.9888	0.8218	0.9857	0.8222	0.9896	0.8227	0.9877	0.8173
	5	**0.9922**	0.8352	0.9907	0.8255	0.9921	0.8249	0.9904	0.8171	0.9915	0.8314	0.9919	0.8317
Test6	2	**0.9453**	0.7501	0.9414	0.7495	0.9413	0.7484	0.9447	0.7468	0.9436	0.7501	0.9452	0.7501
	3	0.9699	0.7915	0.9666	0.7856	0.9687	0.7834	**0.9723**	0.7803	0.9684	0.7914	0.9702	0.7855
	4	**0.9789**	0.7943	0.9759	0.7842	0.9760	0.7909	0.9745	0.7869	0.9775	0.7953	0.9775	0.7951
	5	**0.9832**	0.8081	0.9802	0.7929	0.9795	0.8031	0.9822	0.7930	0.9809	0.8027	0.9808	0.8010
Test7	2	0.9419	0.7777	**0.9454**	0.7709	0.9452	0.7715	0.9411	0.7691	0.9418	0.7777	0.9429	0.7774
	3	**0.9796**	0.8105	0.9758	0.8032	0.9793	0.8042	0.9752	0.8053	0.9775	0.8075	0.9795	0.8075
	4	**0.9855**	0.8381	0.9846	0.8338	**0.9855**	0.8342	0.9830	0.8245	0.9853	0.8380	0.9846	0.8384
	5	**0.9912**	0.8581	0.9893	0.8473	0.9900	0.8412	0.9865	0.8426	0.9906	0.8568	0.9893	0.8525
Test8	2	**0.9739**	0.7611	0.9719	0.7587	0.9728	0.7582	0.9650	0.7648	0.9731	0.7609	0.9738	0.7610
	3	**0.9834**	0.8089	0.9819	0.7988	0.9802	0.8045	0.9778	0.7970	0.9827	0.8105	0.9815	0.8047
	4	**0.9864**	0.8270	0.9852	0.8214	0.9853	0.8199	0.9813	0.8188	0.9862	0.8260	0.9862	0.8264
	5	0.9897	0.8427	0.9886	0.8393	0.9894	0.8384	0.9872	0.8341	**0.9900**	0.8464	**0.9900**	0.8430
Test9	2	0.9654	0.7308	**0.9660**	0.7090	0.9652	0.7240	0.9659	0.7239	0.9656	0.7261	0.9657	0.7333
	3	**0.9802**	0.7623	0.9788	0.7569	0.9777	0.7572	0.9746	0.7470	0.9801	0.7590	0.9782	0.7600
	4	**0.9866**	0.7765	0.9842	0.7798	0.9857	0.7765	0.9837	0.7724	0.9855	0.7732	0.9859	0.7797
	5	**0.9904**	0.8069	0.9892	0.7933	0.9881	0.7943	0.9863	0.7944	0.9898	0.7899	0.9891	0.8032
Test10	2	**0.9690**	0.7266	0.9680	0.7233	0.9680	0.7237	0.9561	0.7273	0.9667	0.7266	**0.9690**	0.7266
	3	0.9716	0.7839	**0.9759**	0.7800	0.9711	0.7777	0.9718	0.7728	0.9721	0.7839	0.9740	0.7837
	4	**0.9847**	0.8016	0.9827	0.7919	0.9810	0.7882	0.9792	0.7904	0.9836	0.7993	0.9839	0.7973
	5	**0.9885**	0.8167	0.9866	0.8029	0.9861	0.8115	0.9848	0.7945	0.9880	0.8085	0.9840	0.8171
Friedman mean rank		**11.2250**	4.7500	9.1000	2.5250	8.9875	3.0375	7.9250	2.6750	9.8625	3.9125	9.9000	4.1000
Rank		**1**	7	4	12	5	10	6	11	3	9	2	8

2.2. Mathematical foundation of ESMA

The foraging behaviour of the slime mould provides us with a rich source of inspiration for the development of efficient optimization techniques. The mathematical modelling of the foraging strategy is precisely explained below.

The slime mould uses the odour in the air to reach the food. Let us assume that there are N slime mould whose position vector is described as $X = \left[\vec{X}_1, \vec{X}_2, \ldots, \vec{X}_N\right]'$. The initial position vector of ith slime mould is initialized randomly as follows:

$$\vec{X}_i\left(t = 1\right) = r_1 \cdot \left(UB - LB\right) + LB, \quad i = 1, 2, \ldots, N. \tag{1}$$

The UB and LB are the upper and lower boundary of search space, t is the current iteration.

The position of ith slime mould X_i $(j = 1, 2, \ldots, N)$ at the new iteration $(t + 1)$ is modelled in SMA [36] as:

$$\vec{X}_i\left(t+1\right) = \begin{cases} r_1 \cdot \left(UB - LB\right) + LB & r_1 < z \\ \vec{X}_{Gbest} + \overrightarrow{step}_a \cdot \left(\vec{W} \cdot \vec{X}_A - \vec{X}_B\right) & r_2 < p_i\left(t\right) \text{ and } r_1 \geq z \\ \overrightarrow{step}_b \cdot \vec{X}_i\left(t\right) & r_2 \geq p_i\left(t\right) \text{ and } r_1 \geq z \end{cases} \tag{2}$$

The r_1 and r_2 are random values in [0, 1]. The $\vec{X}_{Gbest}$ is the global best fitness value among iteration 1 to t. The $\vec{X}_A$ and $\vec{X}_B$ are two randomly selected individuals for N slime mould at iteration t. The z is the probability used to eliminate and disperse the slime mould which is fixed at 0.03 in [36].

The $\vec{W}$ represents the weighting factor of slime mould at iteration t, which is calculated from the local fitness value. Let us sort the fitness values in ascending order (minimization problem):

$$\left[sortf, sortIndex\right] = sort\left(f\right), \quad \text{where } f = \left\{f_1, f_2, \ldots, f_N\right\}. \tag{3}$$

Then, $\vec{W}$ is formulated as

$$\vec{W}\left(sortIndex\left(j\right)\right) = \begin{cases} 1 + r_3 \cdot \log\left(\dfrac{f_{Lbest} - sortf\left(j\right)}{f_{Lbest} - f_{Lworst}} + 1\right) & 1 \leq j \leq \dfrac{N}{2} \\ 1 - r_3 \cdot \log\left(\dfrac{f_{Lbest} - sortf\left(j\right)}{f_{Lbest} - f_{Lworst}} + 1\right) & \dfrac{N}{2} < j \leq N, \end{cases} \tag{4}$$

where r_3 is a random number in the range [0, 1]. The f_{Lbest} and f_{Lworst} are the local best and the worst fitness in the current iterations which are determined as:

$$f_{Lbest} = sortf(1), \tag{5}$$

Table 14
Optimal threshold values of grey component for test image using ESMA, SMA, EO, HHO, WOA, and CMA-ES.

Image	K	Optimal threshold values					
		ESMA	SMA	EO	HHO	WOA	CMA-ES
Test1	2	63, 149	89, 147	92, 149	92, 147	92, 149	92, 136
	3	77, 134, 201	83, 139, 196	63, 149, 196	89, 140, 199	63, 149, 196	84, 149, 196
	4	68, 108, 151,201	81, 129, 182, 199	92, 107, 155, 201	63, 120, 169, 199	84, 127, 179, 201	92, 107, 155, 201
	5	22, 64, 118, 155, 196	42, 85, 115, 156, 206	24, 83, 107, 151, 196	28, 78, 108, 152, 196	63, 92, 107, 154, 196	42, 89, 107, 151, 201
Test2	2	77, 147	84, 148	86, 148	86, 148	86, 206	86, 206
	3	77, 146, 206	69, 148, 206	77, 148, 206	75, 147, 216	77, 148, 206	86, 148, 206
	4	90, 107, 145, 220	38, 94, 146, 206	54, 86, 148, 206	42, 77, 144, 199	54, 89, 148, 206	54, 89, 148, 206
	5	53, 86, 126, 155, 215	11, 53, 120, 168, 204	11, 86, 123, 166, 206	52, 90, 112, 150, 206	54, 86, 126, 177, 215	11, 86, 123, 166, 206
Test3	2	91, 130	92, 199	92, 130	88, 134	92, 199	92, 199
	3	88, 134, 199	75, 125, 201	87, 130, 199	82, 139, 199	87, 130, 199	91, 130, 199
	4	85, 125, 161, 214	93, 122, 161,199	87, 125, 154, 199	92, 124, 153, 203	92, 125, 159, 199	87, 125, 157, 199
	5	78, 105, 137, 157, 205	94, 111, 125, 157, 199	87, 117, 152, 181, 209	91, 118, 152, 184, 205	93, 124, 152, 181, 199	88, 125, 152, 183, 214
Test4	2	86, 152	74, 197	86, 205	82, 197	91, 205	91, 205
	3	62, 125, 205	77, 136, 199	80, 136, 205	67, 136, 197	80, 152, 205	74, 152, 205
	4	82, 125, 165, 198	92, 125, 168, 198	80, 126, 182, 205	81, 126, 181, 198	26, 74, 152, 205	64, 126, 182, 205
	5	26, 80, 122, 152, 205	28, 76, 122, 165, 220	26, 64, 110, 152, 204	28, 58, 113, 150, 205	26, 79, 125, 152, 205	26, 86, 128, 182, 205
Test5	2	88, 128	90, 197	84, 197	93, 195	84, 197	84, 197
	3	90, 139, 197	84, 144, 197	84, 128, 197	77, 138, 197	80, 128, 197	80, 128, 197
	4	70, 122, 152, 206	90, 111, 150, 204	84, 110, 153, 197	94, 119, 151, 197	84, 110, 153, 197	84, 128, 180, 197
	5	69, 120, 148, 184, 204	86, 119, 153, 177, 203	84, 120, 153, 182, 197	67, 107, 150, 179, 206	32, 87, 120, 153, 197	80, 110, 151, 182, 206
Test6	2	86, 153	83, 178	86, 178	81, 178	86, 178	86, 178
	3	86, 129, 178	88, 131, 181	81, 128, 178	81, 133, 179	74, 128, 178	74, 128, 178
	4	83, 126, 153, 178	77, 126, 151, 200	28, 74, 128, 178	75, 126, 151, 196	86, 111, 151, 199	67, 111, 153, 199
	5	29, 63, 127, 161, 199	28, 62, 110, 150, 179	28, 74, 111, 153, 199	28, 72, 114, 153, 195	28, 81, 128, 178, 235	28, 67, 111, 151, 199
Test7	2	91, 151	91, 198	91, 198	91, 198	91, 198	91. 198
	3	27, 76, 151	28, 83, 198	80, 151, 198	81, 149, 198	79, 151, 198	79, 151, 198
	4	25, 91, 121, 151	27, 80, 146, 205	28, 80, 151, 198	25, 76, 149, 207	28,80, 151, 198	28, 85, 151, 198
	5	22, 84, 117, 159, 201	28, 72, 109, 152, 216	28, 79, 110, 151, 198	27, 79, 132, 168, 198	28, 79, 110, 151, 198	28, 71, 107, 151, 198
Test8	2	88, 127	69, 199	88, 201	75,199	76, 201	76, 201
	3	54, 127, 182	75, 126, 201	76, 127, 201	53, 126, 182	69, 127, 201	76, 127, 201
	4	26, 92, 127, 160	26, 94, 128, 178	87, 127, 152, 201	26, 76, 124, 180	26, 69, 127, 201	76, 127, 152, 201
	5	27, 91, 128, 161, 197	28, 93, 125, 167, 201	26, 88, 112, 152, 201	22, 76, 120, 152, 199	26, 68, 127, 155, 201	26, 75, 112, 152, 201
Test9	2	73, 150	79, 151	91, 153	79, 150	78, 153	78, 153
	3	73, 136, 200	93, 130, 197	78, 130, 200	79, 133, 204	78, 130, 200	73, 130, 200
	4	88, 121, 153, 198	89, 128, 165, 204	73, 105, 153, 200	61, 131, 164, 199	68, 130, 164, 200	63, 89, 130, 198
	5	23, 72, 124, 153, 200	21, 77, 125, 164, 193	23, 78, 130, 164, 200	22, 79, 128, 161, 201	23, 78, 130, 164, 204	25, 73, 130, 164, 200
Test10	2	93, 150	85, 200	77, 198	87, 198	77, 198	77, 198
	3	71, 143, 198	68, 154, 198	74, 150, 198	72, 150, 197	71, 150, 198	73, 150, 198
	4	66, 122, 164, 203	84, 122,165, 212	65, 122, 165, 198	27, 74, 152, 198	71, 122, 165, 198	77, 122, 165, 198
	5	64, 119, 152, 179, 203	23, 61, 129, 166, 209	27, 81, 127, 165, 198	25, 84, 126, 164, 198	27, 74, 122, 165, 198	27, 74, 122, 166, 198

and

$$f_{Lworst} = sortf(N). \tag{6}$$

The p_i is the probability to decide the ith slime mould trajectory with the help of other slime moulds; and the highest concentrated slime mould when $r_2 < p_i(t)$ or just navigate itself to reach the higher-order concentration when $r_2 \geq p_i(t)$. Then the p_i is formulated as:

$$p_i = \tanh \left| f(X_i) - f_{Gbest} \right|, \tag{7}$$

where $i = 1, 2, \ldots, N$, $f(X_i)$ represents the fitness value of ith slime mould in positions X_i and f_{Gbest} is the global best fitness value from the initial iteration ($t = 1$) to current iteration (t).

The $\overrightarrow{step_a}$ is a step size that depends on uniform distribution within the range $[-a, a]$ and $\overrightarrow{step_b}$ is a step size that depends on uniform distribution within the range $[-b, b]$. The a and b depend on the current iteration t and the maximum iteration T, which are modelled as:

$$a = arctanh\left(-\left(\frac{t}{T}\right) + 1\right), \tag{8}$$

and

$$b = 1 - \frac{t}{T}. \tag{9}$$

Although the SMA has shown promising results as discussed in [36], there is a scope of improvement in the search process which is evident in Eq. (2). Note that the slime mould trajectory can be modified with the help of the random slime mould. As $\overrightarrow{X_A}$ and $\overrightarrow{X_B}$ are two randomly selected individuals for N slime mould, the optimization may fall in the local minima, which limits the search process. So, we have coined the equilibrium slime mould algorithm (ESMA), that replaces $\overrightarrow{X_A}$ by a position vector from an equilibrium pool, which consists of four best-so-far position vectors and considers the average position of them, taking inspiration from the equilibrium optimizer (EO) [33]. Interestingly, this replacement makes the algorithm efficient enough to explore better. It can achieve optimal solutions.

Let us define the individual elements of the equilibrium pool as:

$$\begin{aligned}
\vec{X}_{eq(1)} &= X\left(sortIndex\left(1\right)\right) \\
\vec{X}_{eq(2)} &= X\left(sortIndex\left(2\right)\right) \\
\vec{X}_{eq(2)} &= X\left(sortIndex\left(2\right)\right) \\
\vec{X}_{eq(3)} &= X\left(sortIndex\left(3\right)\right) \\
\vec{X}_{ave} &= \frac{\vec{X}_{eq(1)} + \vec{X}_{eq(2)} + \vec{X}_{eq(3)} + \vec{X}_{eq(4)}}{4}
\end{aligned} \tag{10}$$

Table 15
Optimal threshold values of RGB components for test image using ESMA, SMA, EO, HHO, WOA, and CMA-ES.

Image	K	Optimal threshold values					
Test1		ESMA			SMA		
		R	G	B	R	G	B
	2	40, 133	83, 171	30, 83	52, 177	84, 171	81, 155
	3	55, 136, 174	66, 126, 177	39, 81, 137	40, 133, 174	20, 50, 129	31, 79, 149
	4	27, 113, 177, 212	20, 49, 105, 175	31, 75, 106, 150	34, 108, 151, 212	21, 46, 94, 177	37, 84,121, 160
	5	15, 72, 119, 176, 213	20, 47, 78, 123, 177	30, 52, 84, 116, 161	38, 100, 133, 161, 210	16, 45, 95, 149, 190	27, 53, 85, 122, 157
		EO			HHO		
		R	G	B	R	G	B
	2	40, 177	78, 171	83, 161	40, 176	78, 171	84,155
	3	40, 119, 212	20, 78, 171	30, 83, 155	18, 100, 170	20, 68, 143	31, 79, 150
	4	19, 80, 147, 213	20, 66, 117, 177	30, 83, 116, 161	19, 79, 170, 221	47, 89, 123, 180	20, 83, 114, 169
	5	34, 72, 129, 169, 235	16, 35, 66, 130, 185	30, 55, 82, 118, 155	23, 57, 100, 119, 200	43, 84, 126, 187, 217	34, 52, 91, 130, 161
		WOA			CMA-ES		
		R	G	B	R	G	B
	2	40, 177	66, 171	83, 161	40, 177	78, 171	83, 161
	3	40, 100, 177	66, 111, 177	30, 83, 155	19, 119, 213	47, 123, 185	30, 83, 161
	4	40, 100, 154, 213	20, 47, 111, 171	30, 83, 122, 161	19, 67, 136, 212	20, 47, 111, 171	30, 83, 116, 161
	5	16, 40, 119, 176, 213	20, 44, 80, 123, 185	30, 52, 83, 121, 161	23, 71, 119, 170, 213	20, 46, 83, 123, 177	14, 52, 83, 122, 161
Test2		ESMA			SMA		
		R	G	B	R	G	B
	2	99, 211	87, 185	73, 153	103, 200	117, 185	73, 149
	3	37, 95, 211	3, 99, 185	33, 76, 151	48, 94, 205	3, 100, 182	34, 103, 153
	4	16, 69, 95, 203	63, 128, 187, 220	37, 75, 121, 167	17, 64, 100, 201	3, 61, 123, 149	46, 79, 123, 149
	5	21, 101, 156, 187, 216	14, 67, 118, 192, 220	29, 51, 77, 111, 179	73, 99, 144, 204, 240	3, 48, 95, 164, 222	32, 87, 125, 144, 192
		EO			HHO		
		R	G	B	R	G	B
	2	91, 211	99, 185	76, 151	62, 211	119, 185	76, 153
	3	37, 95, 211	3, 99, 185	33, 76, 151	37, 91, 214	3, 99, 185	26, 83, 149
	4	17, 69, 95, 211	3, 45, 119, 185	33, 76, 128, 153	23, 93, 156	14, 66, 107, 185	27, 83, 127, 151
	5	17, 53, 95, 156, 211	3, 63, 122, 185, 220	13, 49, 76, 128, 153	48, 103, 170, 206, 238	19, 59, 110, 181, 225	24, 88, 129, 155, 198
		WOA			CMA-ES		
		R	G	B	R	G	B
	2	37, 211	99, 185	76, 151	91, 211	99, 185	76, 151
	3	26, 95, 206	3, 92, 184	22, 81, 156	37, 95, 211	3, 99, 185	33, 76, 151
	4	37, 95, 140, 211	14, 105, 185, 220	33, 76, 128, 179	37, 69, 156, 221	3, 85, 171, 220	27, 74, 128, 157
	5	30, 99, 156, 204, 238	3, 45, 115, 177, 220	33, 77, 123, 153, 179	17, 53, 92, 180, 234	20, 67, 118, 169, 222	30, 84, 121, 151, 179
Test3		ESMA			SMA		
		R	G	B	R	G	B
	2	69, 179	74, 145	82, 178	79, 207	76, 150	82, 178
	3	30, 96, 194	67, 122, 177	51, 102, 193	29, 107, 172	55, 118, 179	52, 104, 193
	4	31, 130, 179, 220	36, 72, 133, 182	49, 84, 131, 187	29, 84, 112, 191	47, 89, 131, 179	30, 81, 123, 174
	5	47, 91, 130, 181, 205	43, 75, 107, 145, 173	37, 78, 101, 141, 187	30, 64, 108, 183, 226	44, 76, 110, 142, 180	32, 80, 120, 161, 199
		EO			HHO		
		R	G	B	R	G	B
	2	69, 140	78, 145	82, 181	78, 159	74, 146	82, 183
	3	47, 128, 183	70, 118, 178	46, 102, 181	47, 96, 179	76, 143, 204	49, 101, 178
	4	30, 69, 138, 205	43, 78, 118, 177	32, 82, 142, 187	30, 91, 138, 201	41, 78, 118, 179	50, 106, 140, 193
	5	30, 79, 140, 159, 205	35, 78, 118, 177, 224	32, 77, 102, 142, 183	13, 47, 138, 187, 225	46, 79, 107, 153, 224	41, 76, 121, 158, 193
		WOA			CMA-ES		
		R	G	B	R	G	B
	2	69, 140	78, 145	82, 181	69, 183	78, 145	82, 183
	3	56, 107, 205	74, 118, 178	46, 102, 187	30, 79, 150	70, 122, 177	52, 102, 181
	4	47, 84, 140, 205	43, 78, 118, 177	32, 84, 142, 187	16, 79, 146, 187	70, 110, 138, 178	37, 85, 122, 174
	5	16, 56, 107, 173, 225	46, 78, 131, 178, 224	46, 82, 117, 142, 193	42, 96, 128, 158, 216	34, 75, 103, 145, 178	48, 83, 105, 141, 183

(*continued on next page*)

The equilibrium pool $\vec{X}_{eq,pool}$ is constructed using these five-position vectors.

$$\vec{X}_{eq,pool} = \left\{\vec{X}_{eq(1)}, \vec{X}_{eq(2)}, \vec{X}_{eq(3)}, \vec{X}_{eq(4)}, \vec{X}_{ave}\right\} \tag{11}$$

The position vector of ith slime mould $X_i\,(j = 1, 2, \ldots, N)$ at the new iteration $(t+1)$ is modelled in ESMA as:

$$\vec{X}_i\,(t+1) = r_1 \cdot (UB - LB) + LB, \ \text{when } r_1 < z \tag{12a}$$

Table 15 (*continued*).

Image	K	Optimal threshold values					
Test4		ESMA			SMA		
		R	G	B	R	G	B
	2	83, 195	20, 105	83, 176	67, 218	20, 106	81, 176
	3	58, 94, 173	55, 112, 178	51, 103, 153	39, 137, 201	20, 65, 184	50, 104, 160
	4	40, 104, 135, 170	16, 51, 111, 184	31, 73, 100, 183	29, 107, 135, 195	19, 50, 124, 184	52, 108, 153, 191
	5	51, 82, 132, 167, 219	17, 53, 122, 173, 216	47, 73, 103, 140, 188	34, 67, 132, 200, 228	2, 51, 87, 148, 184	29, 78, 105, 147, 181
		EO			HHO		
		R	G	B	R	G	B
	2	82, 173	20, 112	83, 176	67, 192	2, 112	83, 153
	3	12, 82, 173	20, 74, 178	48, 103, 176	47, 135, 218	20, 66, 177	51, 100, 187
	4	17, 83, 135, 192	20, 70, 121, 184	48, 103, 153, 187	13, 99, 132, 181	20, 65, 112, 181	44, 81, 104, 183
	5	12, 99, 135, 173, 218	20, 70, 121, 178, 218	34, 81, 105, 153, 187	39, 99, 137, 17, 225	21, 46, 74, 124, 218	42, 68, 106, 143, 187
		WOA			CMA-ES		
		R	G	B	R	G	B
	2	67, 173	2, 112	83, 176	67, 173	20, 106	83, 176
	3	39, 76, 173	20, 74, 178	48, 103, 176	53, 135, 192	21, 75, 185	40, 103, 183
	4	39, 83, 137, 218	20, 70, 121, 184	48, 103, 153, 187	47, 83, 135, 192	20, 64, 125, 181	51, 98, 153, 190
	5	12, 104, 137, 173, 201	20, 70, 128, 184, 218	40, 73, 104, 153, 187	19, 67, 83, 169, 224	52, 82, 105, 141, 194	52, 82, 105, 141, 194
Test5		ESMA			SMA		
		R	G	B	R	G	B
	2	41, 169	93, 172	80, 185	41, 168	83, 177	86, 192
	3	44, 114, 184	76, 127, 181	54, 106, 197	41, 85, 161	72, 125, 181	51, 108, 197
	4	41, 87, 168, 217	47, 77, 121, 177	45, 84, 137, 192	41, 126, 151, 200	44, 70, 118, 177	34, 98, 136, 185
	5	26, 68, 95, 161, 200	47, 78, 117, 151, 179	46, 85, 120, 163, 192	41, 65, 98, 159, 203	45, 74, 121, 171, 216	16, 50, 99, 136, 192
		EO			HHO		
		R	G	B	R	G	B
	2	41, 178	76, 177	84, 197	44, 178	89, 177	95, 197
	3	44, 105, 200	69, 127, 177	51, 104, 197	18, 87, 172	81, 121, 172	60, 104, 192
	4	15, 109, 161, 200	67, 109, 171, 218	49, 89, 134, 199	54, 87, 114, 197	86, 146, 177, 218	42, 85, 122, 197
	5	32, 80, 122, 172, 217	47, 76, 125, 180, 212	47, 81, 114, 160, 197	55, 105, 142, 196, 217	63, 98, 123, 180, 218	48, 83, 116, 136, 186
		WOA			CMA-ES		
		R	G	B	R	G	B
	2	41, 178	76, 177	84, 197	44, 178	93, 177	85, 197
	3	41, 95, 200	69, 127, 177	51, 114, 197	33, 121, 200	89, 173, 212	47, 117, 197
	4	18, 44, 95, 200	47, 76, 121, 177	45, 84, 137, 197	30, 95, 126, 189	64, 125, 163, 212	44, 81, 129, 197
	5	23, 65, 99, 168, 221	10, 47, 76, 121, 177	45, 81, 104, 137, 197	22, 99, 117, 168, 200	41, 75, 129, 172, 214	53, 90, 132, 160, 199
Test6		ESMA			SMA		
		R	G	B	R	G	B
	2	34, 171	2, 149	75, 145	26, 182	2, 149	82, 141
	3	22, 127, 227	2, 72, 152	73, 116, 150	47, 98, 169	2, 80, 153	11, 103, 153
	4	34, 98, 149, 227	2, 71, 102, 181	50, 81, 115, 155	39, 127, 147, 189	2, 70, 107, 179	11, 50, 106, 158
	5	55, 111, 127, 148, 196	2, 35, 74, 112, 174	11, 73, 103, 125, 159	19, 73, 127, 153, 216	2, 36, 76, 124, 179	34, 73, 108, 154, 197
		EO			HHO		
		R	G	B	R	G	B
	2	49, 182	2, 149	75, 156	49, 144	80, 153	82, 156
	3	49, 127, 201	2, 76, 149	75, 116, 156	49, 148, 189	54, 108, 149	31, 82, 141
	4	24, 98, 148, 202	2, 69, 108, 174	31, 82, 116, 156	42, 106, 131, 183	52, 108, 153, 175	27, 56, 115, 150
	5	26, 100, 148, 171, 202	2, 36, 69, 108, 174	56, 83, 116, 156, 196	42, 89, 149, 171, 223	30, 80, 110, 147, 184	68, 115, 143, 165, 197
		WOA			CMA-ES		
		R	G	B	R	G	B
	2	49, 182	2, 149	75, 156	49, 182	2, 149	82, 156
	3	29, 100, 182	2, 76, 149	75, 116, 156	46, 99, 171	2, 74, 153	11, 106, 155
	4	19, 49, 100, 182	2, 69, 108, 174	23, 75, 116, 156	29, 98, 131, 192	2, 64, 114, 185	31, 73, 115, 153
	5	19, 100, 144, 171, 227	2, 36, 69, 108,174	31, 75, 115, 156, 196	29, 100, 144, 176, 230	2, 71, 105, 150, 184	11, 67, 107, 143, 165

(*continued on next page*)

$$\vec{X}_i(t+1) = \vec{X}_{Gbest} + \overrightarrow{step}_a \cdot \left(\vec{W} \cdot \vec{X}_{eq} - \vec{X}_B\right),$$
$$\text{when } r_2 < p_i(t) \text{ and } r_1 \geq z \quad (12b)$$

$$\vec{X}_i(t+1) = \overrightarrow{step}_b \cdot \vec{X}_i(t), \text{ when } r_2 \geq p_i(t) \text{ and } r_1 \geq z \quad (12c)$$

Note that $\vec{X}_{eq}$ is a random position vector from the equilibrium pool, which helps in a better trade-off between exploration–exploitation behaviour of the ESMA with the help of the weighting factor $\vec{W}$ and random slime mould $\vec{X}_B$ form the search space. The $'z'$ helps in exploration to ensure ESMA from the beginning to end of the search process for escaping the local minima, which is experimentally determined and set as 0.03.

It is noteworthy to mention here that the ESMA updates the position vector in the next iteration with the help of the global

Table 15 (*continued*).

Image	*K*	Optimal threshold values					
Test7		ESMA			SMA		
		R	G	B	R	G	B
	2	68, 159	21, 119	75, 179	19, 159	21, 121	73, 179
	3	40, 102, 210	21, 78, 146	36, 106, 164	40, 125, 201	21, 85, 179	52, 105, 179
	4	68, 95, 161, 236	16, 57, 119, 170	33, 96, 164, 195	19, 65, 153, 224	18, 71, 129, 184	75, 115, 143, 186
	5	40, 81, 129, 201, 238	18, 66, 118, 179, 222	7, 33, 73, 105, 179	19, 30, 101, 168, 230	18, 35, 77, 121, 185	37, 75, 94, 146, 175
		EO			HHO		
		R	G	B	R	G	B
	2	65, 201	21, 118	105, 179	65, 201	21, 121	103, 166
	3	40, 112, 201	21, 114, 179	52, 105, 179	40, 129, 228	21, 83, 178	52, 101, 166
	4	19, 81, 143, 201	21, 66, 118, 179	33, 73, 105, 179	45, 95, 168, 200	20, 37, 103, 146	29, 75, 107, 168
	5	15, 65, 95, 159, 228	18, 66, 118, 179, 222	35, 73, 105, 158, 197	11, 30, 75, 138, 238	37, 77, 97, 123, 179	33, 73, 115, 144, 158
		WOA			CMA-ES		
		R	G	B	R	G	B
	2	40, 201	21, 118	105, 179	68, 201	21, 114	105, 179
	3	40, 112, 201	21, 114, 179	33, 105, 179	33, 113, 201	18, 100, 179	73, 116, 173
	4	19, 65, 159, 201	21, 66, 118, 179	52, 105, 152, 195	19, 48, 156, 200	16, 69, 124, 178	32, 75, 112, 181
	5	15, 55, 112, 148, 236	18, 77, 127, 180, 222	27, 73, 107, 142, 179	29, 65, 95, 137, 237	21, 36, 71, 117, 179	46, 79, 113, 150, 200
Test8		ESMA			SMA		
		R	G	B	R	G	B
	2	51, 175	69, 152	82, 152	51, 157	71, 149	84, 155
	3	51, 100, 206	21, 75, 155	46, 103, 152	36, 143, 220	20, 84, 152	48, 102, 155
	4	55, 94, 170, 224	19, 59, 106, 155	47, 84, 121, 169	11, 100, 144, 211	17, 72, 124, 189	52, 84, 123, 173
	5	21, 51, 100, 138, 226	18, 34, 71, 113, 154	21, 51, 83, 119, 155	38, 95, 138, 166, 212	19, 53, 70, 109, 190	47, 82, 118, 155, 182
		EO			HHO		
		R	G	B	R	G	B
	2	51, 193	71, 154	83, 155	28, 193	75, 154	83, 152
	3	40, 100, 193	20, 71, 154	83, 119, 155	16, 112, 193	21, 72, 167	83, 152, 196
	4	30, 100, 157, 220	20, 71, 113, 154	46, 83, 119, 155	9, 51, 138, 190	18, 75, 110, 185	46, 84, 117, 153
	5	16, 51, 112, 175, 224	20, 34, 71, 121, 185	46, 83, 121, 155, 187	16, 60, 85, 180, 220	18, 41, 72, 113, 167	27, 82, 123, 138, 187
		WOA			CMA-ES		
		R	G	B	R	G	B
	2	51, 157	71, 154	83, 155	51, 157	71, 154	83, 152
	3	47, 100, 193	20, 71, 154	46, 83, 155	21, 105, 193	21, 75, 150	50, 83, 148
	4	55, 100, 157, 193	20, 71, 113, 167	25, 83, 119, 155	51, 112, 157, 209	21, 74, 152, 196	49, 83, 121, 196
	5	17, 64, 119, 159, 193	21, 66, 116, 162, 193	46, 84, 117, 150, 190	33, 68, 100, 138, 214	22, 61, 117, 147, 196	53, 84, 107, 142, 178
Test9		ESMA			SMA		
		R	G	B	R	G	B
	2	41, 216	72, 148	84, 154	41, 220	72, 148	84, 152
	3	54, 124, 207	18, 69, 148	53, 101, 158	26, 151, 217	18, 76, 145	44, 82, 162
	4	32, 117, 153, 220	21, 70, 131, 181	40, 82, 121, 162	53, 107, 136, 217	18, 67, 114, 171	49, 73, 127, 173
	5	13, 80, 134,182, 226	18, 68, 102, 147, 188	46, 77, 106, 130, 170	11, 76, 137, 179, 216	13, 59, 117, 181, 207	45, 74, 103, 134, 173
		EO			HHO		
		R	G	B	R	G	B
	2	41, 185	72, 148	84, 165	82, 134	72, 148	84, 150
	3	41, 120, 220	20, 72, 148	74, 127, 165	47, 120, 213	18, 76, 147	36, 82, 150
	4	29, 105, 151, 217	20, 72, 121, 178	36, 81, 127, 165	22, 82, 134, 182	34, 76, 121, 178	50, 73, 103, 165
	5	33, 64, 120, 153, 217	20, 72, 111, 148, 183	36, 74, 103, 150, 186	34, 68, 99, 147, 202	20, 69, 115, 173, 221	35, 81, 129, 156, 181
		WOA			CMA-ES		
		R	G	B	R	G	B
	2	64, 185	72, 148	84, 165	48, 185	72, 148	83, 165
	3	41, 107, 185	20, 72, 148	74, 127, 165	41, 137, 196	21, 64, 148	36, 81, 142
	4	33, 99, 153, 207	20, 77, 121, 178	36, 81, 117, 165	41, 82, 117, 190	21, 57, 112, 180	48, 84, 131, 171
	5	20, 68, 107, 162, 220	20, 69, 121, 169, 213	39, 74, 101, 142, 186	41, 82, 136, 164, 206	20, 77, 111, 143, 182	48, 82, 113, 158, 191

(*continued on next page*)

best position, local best position from a best-so-far equilibrium pool, and a random vector, which leads to a decent trade-off between the exploration and the exploitation.

2.3. Pseudocode of the ESMA

In the start, suitably choose the problem dimension D, the number of slime mould N in the search space with an upper boundary UB and a lower boundary LB, maximum iterations T, the probability of elimination and dispersed z; and a fitness function

Table 15 (*continued*).

Image	K	Optimal threshold values					
Test10		ESMA			SMA		
		R	G	B	R	G	B
	2	75, 180	81, 179	72, 168	60, 172	21, 115	72, 143
	3	13, 79, 170	69, 115, 179	75, 115, 183	17, 75, 172	22, 83, 151	58, 152, 212
	4	74, 123, 184, 237	21, 66, 136, 178	27, 84, 136, 209	30, 60, 150, 239	16, 71, 118, 179	48, 105, 162, 212
	5	59, 98, 165, 200, 239	22,64, 111, 152, 175	29, 70, 115, 159, 206	13, 75, 109, 132, 209	20, 73, 103, 153, 181	23, 74, 105, 144, 209
		EO			HHO		
		R	G	B	R	G	B
	2	60, 172	21, 126	75, 153	59, 172	22, 119	75, 152
	3	60, 110, 172	21, 118, 179	73, 153, 212	64, 123, 182	19, 72, 146	61, 160, 212
	4	13, 75, 146, 206	21, 70, 126, 179	31, 75, 153, 212	86, 123, 148, 237	70, 114, 178, 223	30, 72, 143, 212
	5	21, 75, 110, 164, 206	2, 51, 102, 146, 179	32, 75, 117, 160, 212	30, 60, 114, 165, 239	22, 65, 145, 183, 218	30, 75, 102, 147, 183
		WOA			CMA-ES		
		R	G	B	R	G	B
	2	13, 172	70, 179	75, 153	64, 172	21, 118	71, 153
	3	60, 106, 148	21, 73, 179	29, 75, 153	45, 123, 165	21, 91, 179	71, 168, 212
	4	13, 79, 146, 206	21, 70, 126, 179	29, 75, 147, 212	64, 109, 172, 201	18, 69, 124, 189	72, 103, 149, 212
	5	38, 64, 106, 148, 206	21, 51, 98, 145, 179	32, 72, 102, 153, 212	60, 75, 148, 172, 213	19, 71, 114, 171, 221	48, 73, 102, 144, 209

f to evaluate the fitness value for a given problem statement. The pseudocode of the suggested ESMA is given below.

Begin
Inputs: N, D, T, UB, LB, and z.
Initialization: $X_i = \{x_i^1, x_i^2, \cdots, x_i^D\}$ for $i = 1,2,\cdots,N$ at a random position within the search boundary $[LB, UB]$ using Eq. (1) for a D dimension at initial iteration $t = 1$ to form $X = [\vec{X}_1, \vec{X}_2, \cdots, \vec{X}_i, \cdots \vec{X}_N]'$.
while $(\boldsymbol{t \le T})$
→ Evaluate the fitness $f(X)$ of N slime mould.
→ Sort the fitness value in ascending order (for minimization problem) using Eq. (3) and determine the f_{Lbest} using Eq. (5), f_{Lworst} using Eq. (6) and construct the $\vec{X}_{eq,pool}$ using Eq. (11).
→ Determine the weighting factor $\vec{W}$ using Eq. (4).
→ Update the $\vec{X}_{Gbest}$.
→ Determine the a using Eq. (8) and b using Eq. (9).
For $i = 1$: number of slime mould (N)
→ Generate a random value r_1.
If $(r_1 < z)$
○ Update the position vector $\vec{X}_i(t+1) = r_1 \cdot (UB - LB) + LB$.
Else If $(r_1 \ge z)$
○ Update the probability p_i, $\overrightarrow{step}_a$ and $\overrightarrow{step}_b$.
○ Randomly chose one position vector $\vec{X}_{eq}$ from the equilibrium pool.
○ Generate a random value r_2.
If $(r_2 < p_i)$
▪ Select a random position $\vec{X}_B$ a vector from X.
▪ Update the position vector $\vec{X}_i(t+1) = \vec{X}_{Gbest} + \overrightarrow{step}_a \cdot (\vec{W} \cdot \vec{X}_{eq} - \vec{X}_B)$.
Else If $(r_2 \ge p_i)$
▪ Update the position vector $\vec{X}_i(t+1) = \overrightarrow{step}_b \cdot \vec{X}_i(t)$.
End If
End If
End For
→ $t = t + 1$.
End While
Output: $\vec{X}_{Gbest}$
End

2.4. Computational complexity analysis of ESMA

The computational complexity of an optimization algorithm inputs parameters to the running time of an optimization algorithm. The Big-O notation is commonly used to represent the computational complexity. The complexity of ESMA mainly depends on the number of slime mould (N), a dimension of the problem (D), maximum iterations (T), cost of the fitness evaluation (C). The computational complexity of ESMA depends on initialization, fitness evaluation, sorting of fitness value, construction of equilibrium pool, weight update, and position update. The computational complexity of the initialization is $O(N \times D)$, the computational complexity of fitness evaluation is $O(N \times C)$, the computational complexity of sorting is $O(N \log N)$, the computational complexity of construction of equilibrium pool is $O(1)$, the computational complexity of weight update is $O(N \times D)$, and the computational complexity of position update is $O(N \times D)$. Therefore, the total computational complexity of ESMA is $O\big(N \times D + T\,(N \times C + N \log N + 1 + 2\,(N \times D))\big)$.

2.5. Simulation results of ESMA

2.5.1. Test problems, simulation setup, and compared optimization algorithms

The effectiveness of the proposed ESMA is investigated with the help of the well-known 23 test problems from the literature [37,38] and 30 test problems from the IEEE CEC 2014 test suite [39]. The first group consists of 7 scalable unimodal test functions $(f_1 - f_7)$, which have a single optimum solution and sightsee the exploitative capability of the optimization algorithms. The second group consists of 6 scalable multimodal test functions $(f_8 - f_{13})$. The third group consists of 10 fixed multimodal test functions $(f_{14} - f_{23})$ that has multiple minima and evoke the exploration capability of the optimization algorithms. The fourth group consists of 30 advanced test functions $(CEC - 2014 - F1$ to $CEC - 2014 - F30)$ which covers unimodal, multimodal, hybrid, and composition functions, they mimic the complexity of many local optima with dissimilar shapes of the functions in different regions in a challenging test problem.

The performance and results of the proposed ESMA are compared with the recent and well-established optimization algorithms — SMA [36], EO [33], HHO [35], GWO [27], WDO [32], WOA [28], DE [29], CS [34], PSO [29], FA [34], L-SHADE [30] and CMA-ES [31]. These algorithms are compared in terms of the average fitness value (‘**Avg**’) and the standard deviation (‘**Std**’) among 51 independent runs. The number of search agents N is set as 30 except L-SHADE and CMA-ES optimizer, to maintain the consistency of the results. The N of the L-SHADE and CMA-ES depends on the dimension of the problem, which are reported in Table 1. The maximum number of iterations is set to 500 for all optimization algorithms, for better illustration of the convergence analysis and maintains the consistency of the obtained results. All the algorithms are implemented in MATLAB on the Intel core

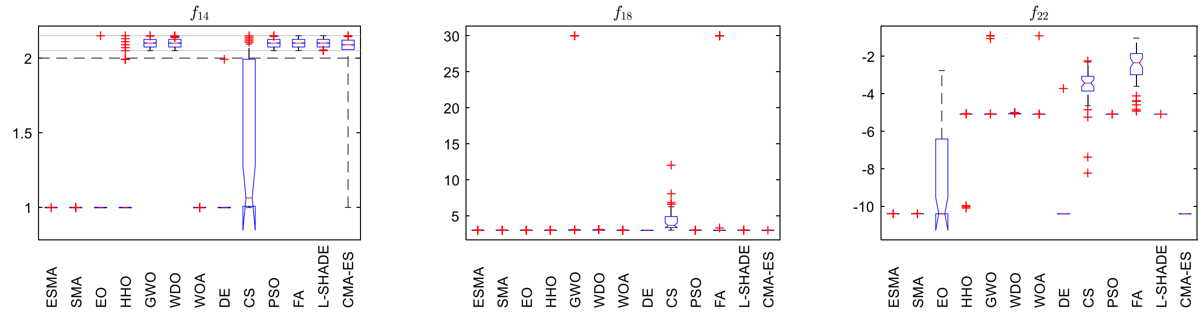

Fig. 6. Boxplot of three fixed multimodal test problem f_{14}, f_{18} and f_{22}.

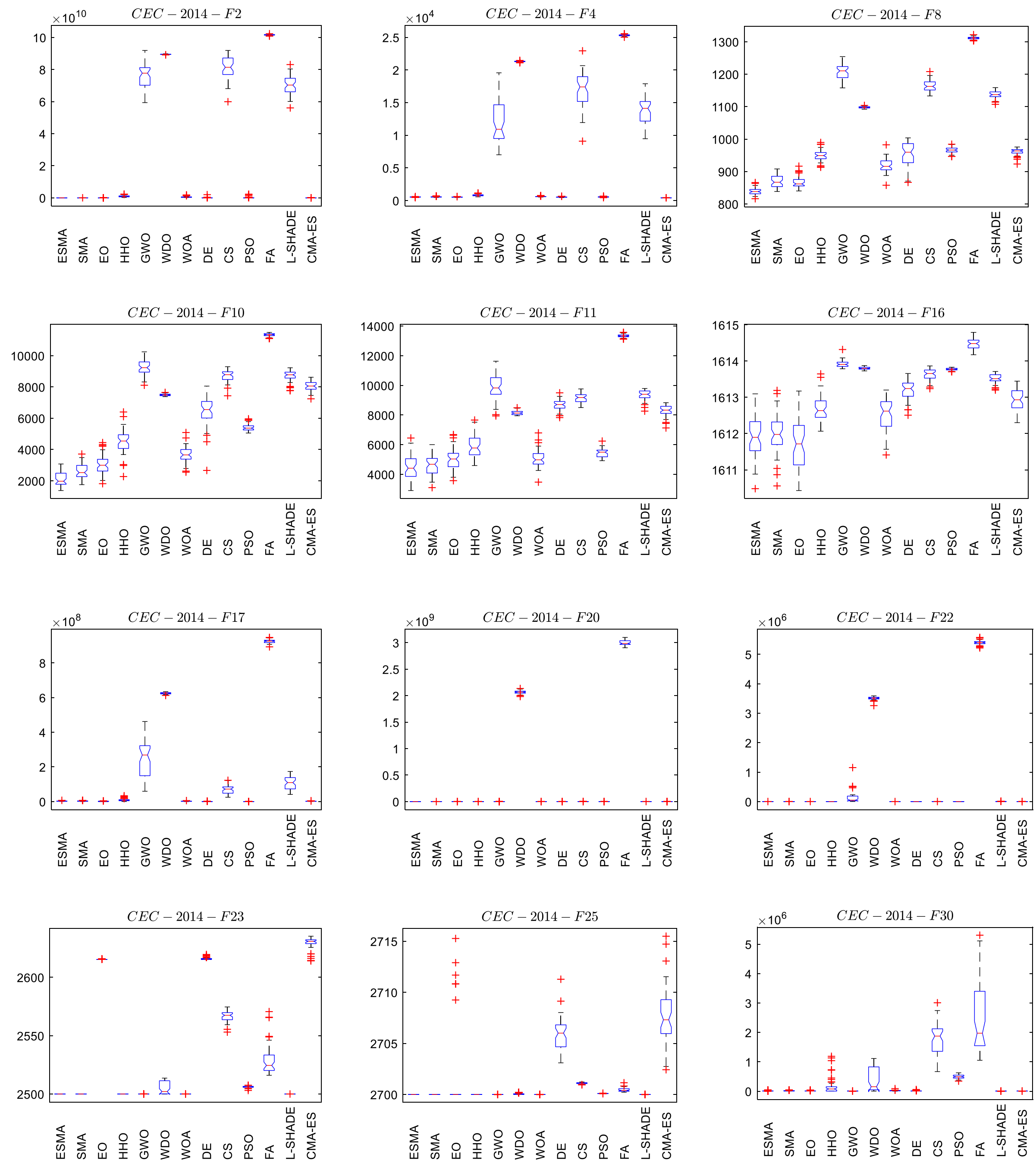

Fig. 7. Boxplot of twelve CEC 2014 test problems.

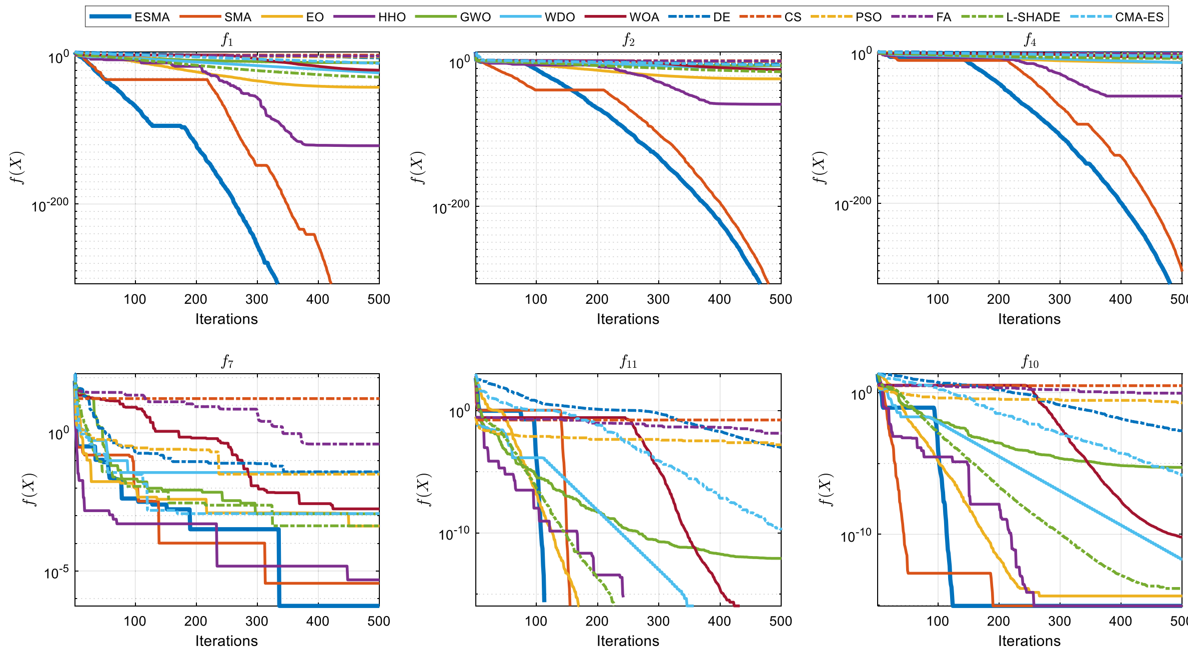

Fig. 8. Convergence curve of six scalable unimodal and multimodal test problem.

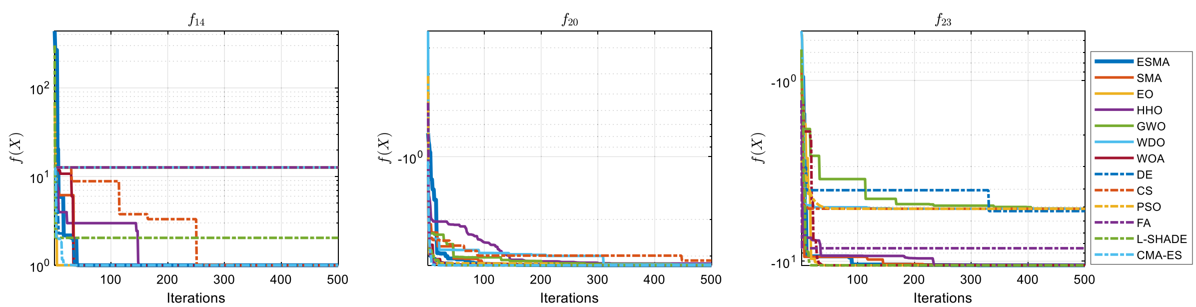

Fig. 9. Convergence curve of three fixed multimodal test problem.

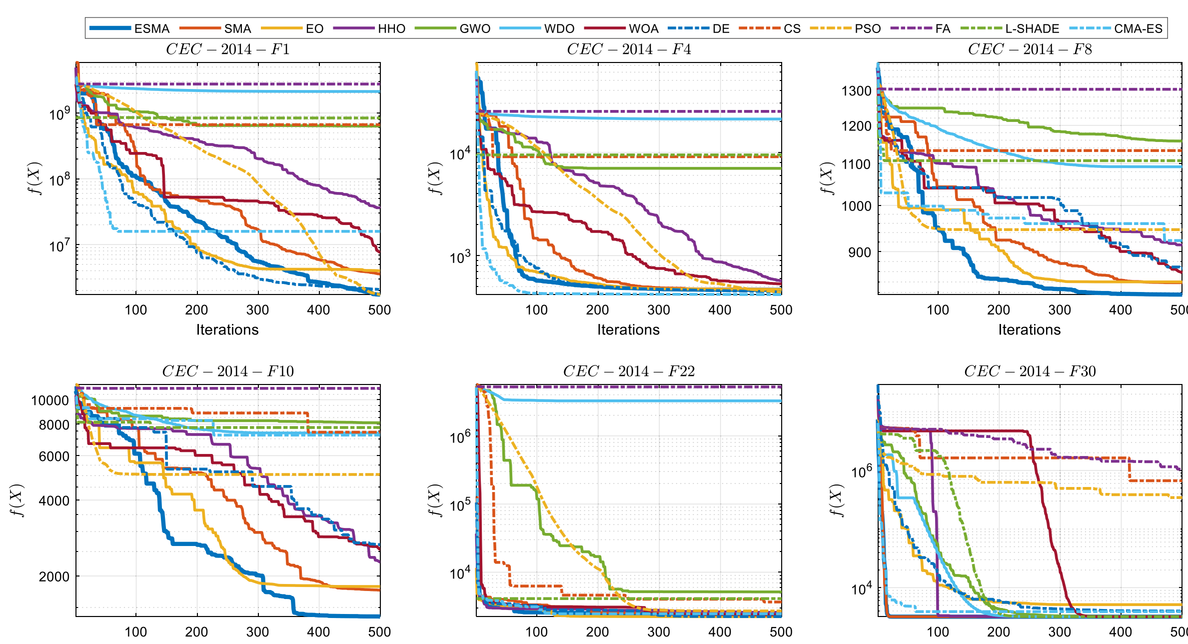

Fig. 10. The convergence curve of six test problems from the CEC 2014 test suite.

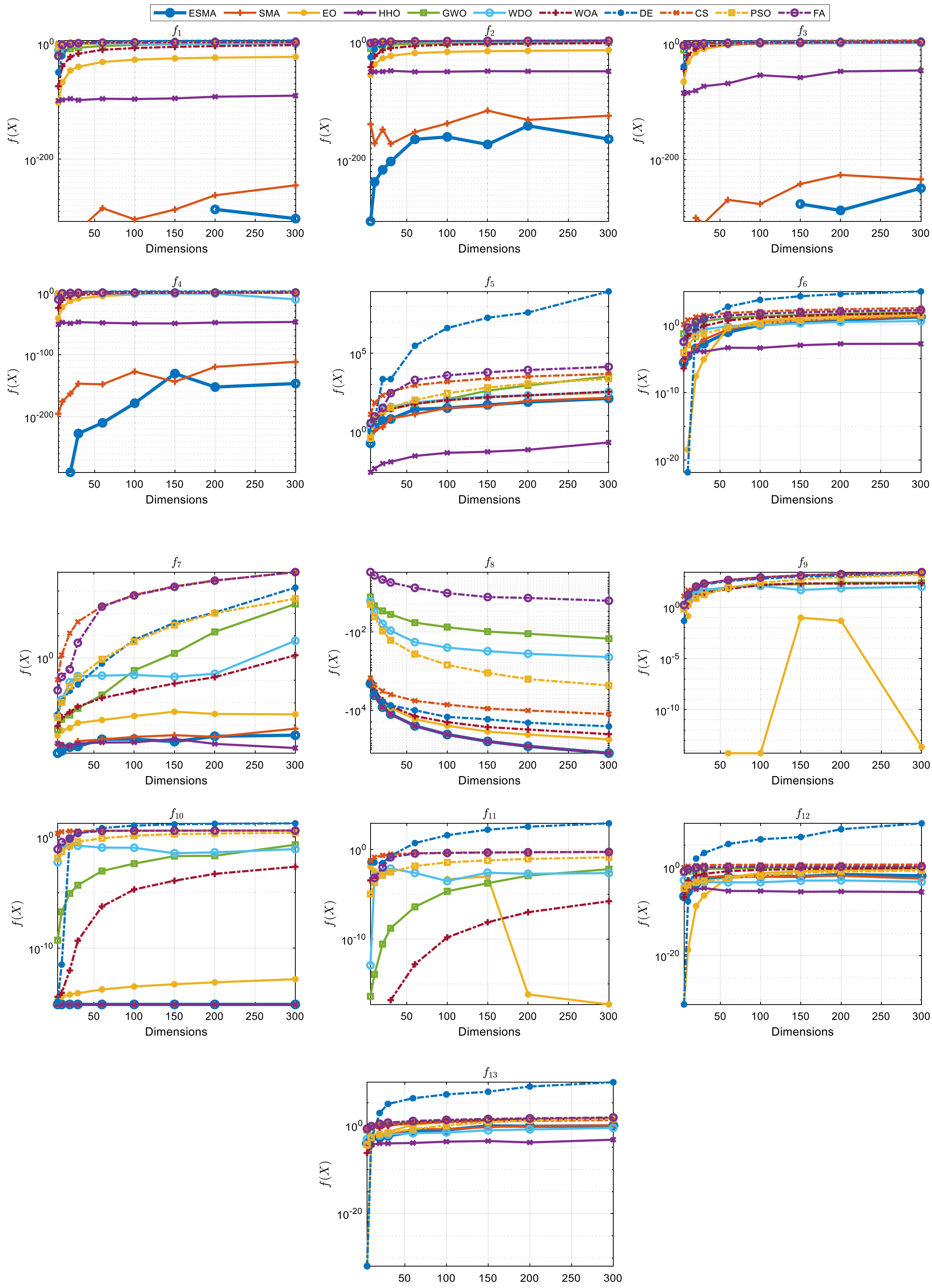

Fig. 11. Scalability results of ESMA versus other optimization algorithms.

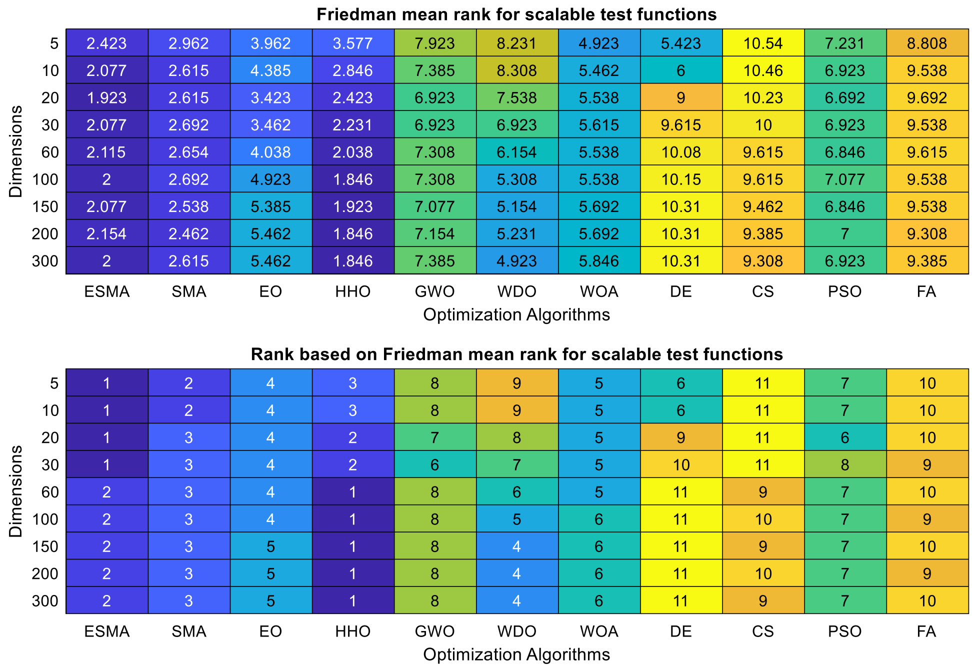

Fig. 12. Friedman's mean rank of ESMA versus other optimization algorithms.

i-3 (6th iteration) processor with 8GB RAM under Windows 10 environment. The experimental parameter z of ESMA is experimentally determined by parameter sensitivity analysis reported in Section 3.4.2. However for all other optimization algorithm the experimental parameters are chosen same as reported by original work SMA [36], EO [33], HHO [35], GWO [27], WDO [32], WOA [28], DE [29], CS [34], PSO [29], FA [34], L-SHADE [30] and CMA-ES [31]. The experimental parameters used for the performance comparison are reported in Table 1.

2.5.2. Parameter sensitivity analysis

The parameter sensitivity analysis is conducted to observe the impact of key parameters on the performance of the optimization algorithm. The parameter z, number of slime mould N and maximum number of iterations T are chosen for the evaluation of impact. Let chose the parameter z from a set of 11 values $[0, 0.01, 0.02, 0.03, 0.04, 0.05, 0.06, 0.07, 0.08, 0.09, 0.1]$ at an interval of 0.01 to observe the impact of z on the performance of ESMA. The results of different values of z with the $N = 30$ and $T = 500$ for test problems $f_1 - f_{13}$ presented in Table 2. From Table 2, it is observed that when $z = 0.03$, the ESMA performance achieved the well-balanced optimal solution based on Friedman's mean rank and ranked one. Based on this we have taken $z = 0.03$ as the parameter setting of ESMA, which is reported in Table 1.

The population and iterations are the other two important factors for any optimization algorithm, as they are directly proportional to the computational complexity. So, suitably choosing the number of population and the maximum number of iterations is essential. For the experiments, the population size N is taken as 10, 20, 30, 50, 100, and 200 and the maximum number of iterations T is taken as 100, 300, 500, 1000, 1500, and 2000. To study the influence of N and T, we have taken one test problem from each category such as f_1 as unimodal test problem, f_{13} as multimodal test problem and f_{23} as a multimodal test problem with fixed dimensions. The effect of N and T are visualized in Fig. 1, which shows that ESMA has shown consistency in performance when one chooses $N > 20$ and $T > 300$. This directs us to use $N = 30$ and $T = 500$ in our study.

2.5.3. Qualitative results of ESMA

The qualitative performance of the ESMA on some unimodal test problems is presented in Fig. 2, multimodal test problems are presented in Fig. 3, and composition test problems are presented in Fig. 4. The qualitative analysis includes best position, search history, a trajectory in 1st dimension, and average fitness history to demonstrate the search pattern of the slime mould during the initial iteration ($t = 1$) to maximum iteration ($t = T$).

The search history diagrams in Figs. 2–4 present the first two variable x^1 and x^2 of $X_i = \left\{x_i^1, x_i^2, \ldots, x_i^D\right\}$ for $i = 1, 2, \ldots, N$ during the $t = 1$ to T iterations in a two-dimensional plot. For the test problem f_1, f_4, f_7 and f_{10}, where optimal value is $\vec{0}$, it can be visible from Figs. 2–4, a higher concentration of points is available nearer to the optimal solutions that are nearer to 0. For other test problems with non-zero optimal values, the ESMA also tracks the position to its optimal solution specified by the test functions.

The best position diagrams in Figs. 2–4 present the trajectory of the $\vec{X}_{Gbest}$ during the 500 iterations. It can be visualized from Figs. 2–4, in most test problems (f_1, f_4, f_7, f_{10}, $CEC - 2014 - F24$ and $CEC - 2014 - F28$), during the initial iteration the position of slime mould diversified completely within the search space, and after 10 to 20 iterations tries to reach an optimal position. This reveals that the ESMA has a quick convergence.

The trajectory in the 1st dimension diagrams of Figs. 2–4 describe the trajectory of the x^1 of 1st slime mould positions X_1 for the iterations $t = 1$ to T. It can be visible from Figs. 2–4 that, the test problems with optimal solutions is $\vec{0}$ like f_1, f_4, f_7, f_{10}, $CEC - 2014 - F24$ and $CEC - 2014 - F28$, the 1st-dimensional position starts with a dispersed position in the search space, but during the iterations, it converges near to the optimal solutions ($\vec{0}$). Similarly, other test problems trajectory tries to reach optimal solutions. The trajectory and the best position diagrams demonstrate that the ESMA has maintained a good trade-off between the exploration and the exploitation, to reach the optimal solutions.

Diversity [44] is a metric based on the Euclidean distance between the position $X_i = \left(x_i^1, x_i^2, \ldots, x_i^D\right)$ for ith slime mould of D dimensional problem and is used to measure the exploration and the exploitation capability of an optimization algorithm. The

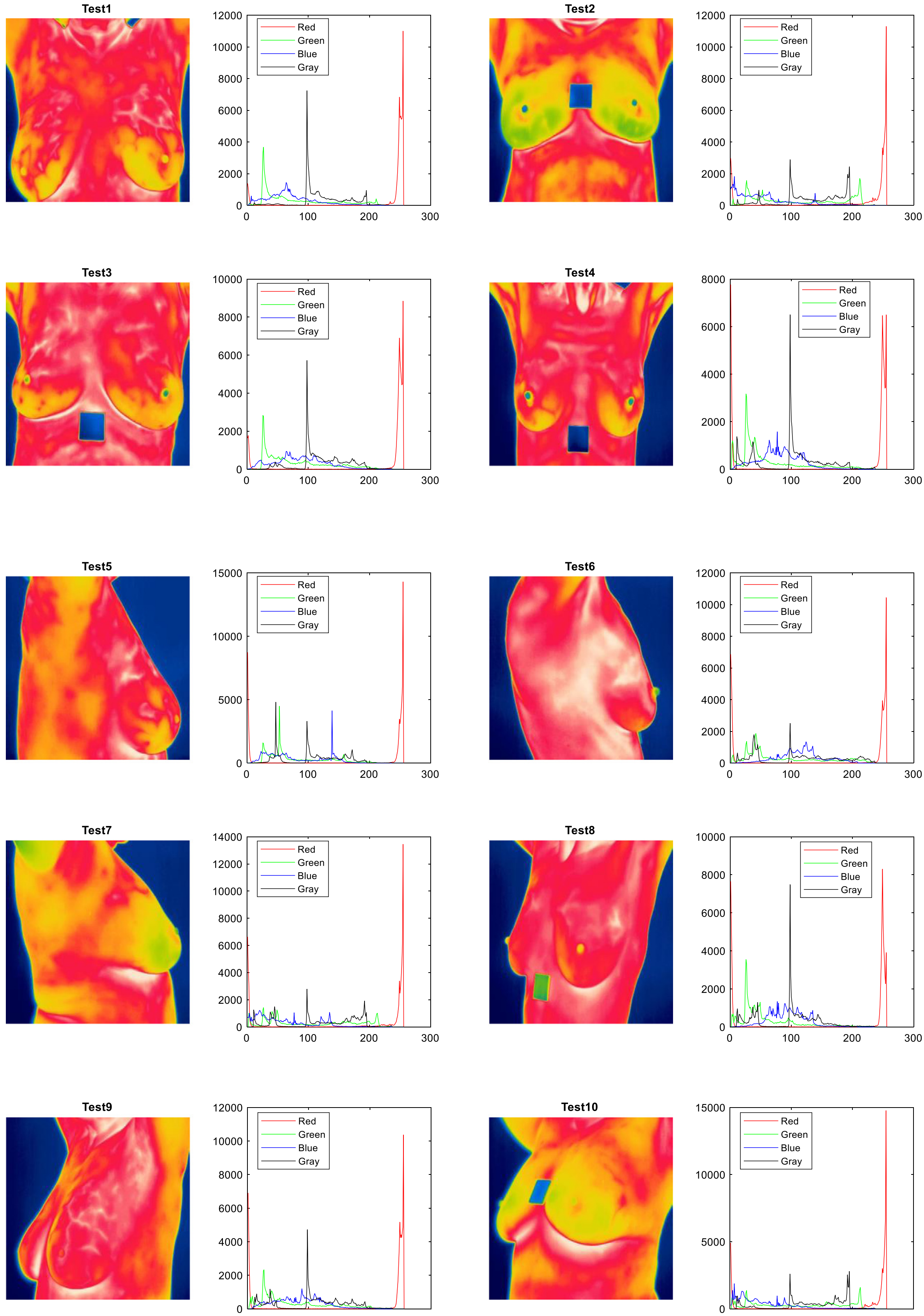

Fig. 13. Test images and their corresponding histogram.

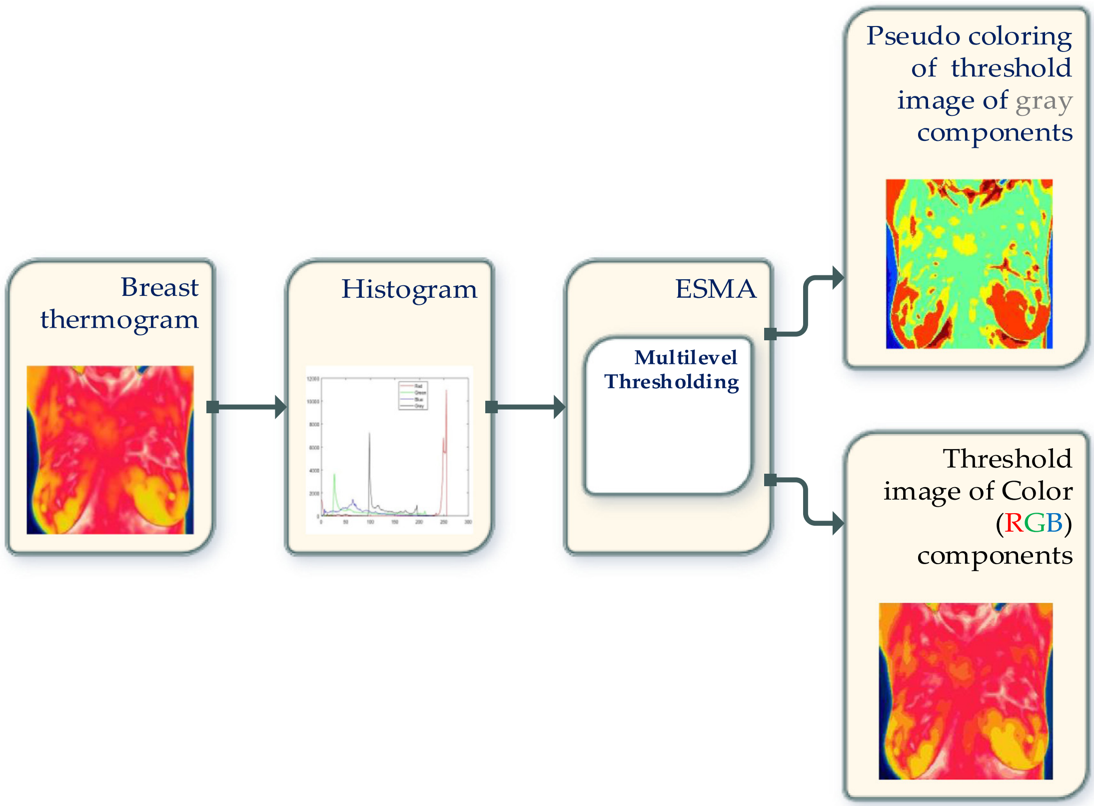

Fig. 14. Block diagram of multilevel thresholding using ESMA.

diversity is described for N slime mould as:

$$diversity\,(t) = \sum_{i=1}^{N}\left(\sum_{j=1}^{N}\sqrt{\sum_{k=1}^{d}\left(x_j^k\,(t) - x_i^k\,(t)\right)^2}\right). \tag{13}$$

From the diversity history of Figs. 2–4, it is observed that the diversity decreases with an increase in the iterations, from a very high value to a low value (≈ 0), which reveals that the ESMA has a better trade-off between the exploration and the exploitation. We observe some spikes during the iterations; this demonstrates that the exploration (due to the equilibrium pool) helps the ESMA to escape from the local optima.

The average fitness history diagrams presented in Figs. 2–4 show a collaborative behaviour of N slime mould during the iterations ($t = 1$ to T). It is observed from Figs. 2–4 that, a decreasing trend in the fitness value shows slime mould collaboratively updates the fitness values, as the iteration goes on.

2.5.4. ESMA results and comparisons on test problems

The results are evaluated using 51 independent runs with 15 000 function evaluations on 30 dimensions of test problems. The results of scalable unimodal and multimodal test problems ($f_1 - f_{13}$) are presented in Table 3, fixed dimensional multimodal test problems ($f_{14} - f_{23}$) are presented in Table 4 and advanced CEC 2014 test problems ($CEC - 2014 - F1$ to $CEC - 2014 - F30$) are presented in Table 5. For a better understanding of the distribution of results obtained from 51 independent runs of optimization algorithms for a test problem, a boxplot for comparison is presented in Figs. 5–7.

Table 3 presents the results of scalable test problems ($f_1 - f_{13}$), from which it is observed that the ESMA has shown superiority (results) on scalable functions on 30 dimensions, when compared with other optimization techniques, on most test problems. The ESMA shows superiority on test problems $f_1 - f_4$, and similar results on test problems $f_8 - f_{11}$ with SMA, EO, and HHO. However, the ESMA shows 2nd best values for the test problems f_5 and f_7, and 3rd best values for the test problems f_6, f_{12} and f_{13}. Fig. 5 shows the box plot of six scalable test problems f_1, f_2, f_4, f_7, f_8 and f_{10} (The rest of the seven scalable test problem box plots are shown in Fig. A.1 of Appendix A). It is seen that the ESMA has consistency in obtaining the optimal results, which is statistically observed from 'Std' of Table 3.

Table 4 presents the results of non-scalable fixed dimensional multimodal test problems ($f_{14} - f_{23}$), from which it is observed that the ESMA's performance is quite impressive although tight competitions from SMA, EO, DE, L-SHADE, and CMA-ES. From the boxplot of three test problems f_{14}, f_{18} and f_{22} in Fig. 6 (The rest seven non-scalable fixed dimensional multimodal test problems box plots are shown in Fig. A.2 of Appendix A), it is observed that the ESMA, SMA, L-SHADE, and CMA-ES are most consistent, over other optimization algorithms.

Table 5 presents the results of 30 test problems from the CEC 2014 test suite. From the results in Table 5, it is very difficult to tell that one algorithm is good for every test problem. So, for this set of test problems, the ESMA has a tight competition with the SMA and EO. From 12 test problem box plots presented in Fig. 7 (The rest eighteen test problem box plots are presented in Figs. A.3–A.5 of Appendix A), it is observed that the ESMA exhibits consistent results over other competitor optimization algorithms.

2.5.5. Comparison of convergence curves

The convergence curve helps for a better understanding of how the optimization algorithm trade-off between the exploration and exploitation to reach the global optimal solutions. The convergence curve is one of the qualitative performance metrics of an optimization algorithm, which is expressed as the fitness

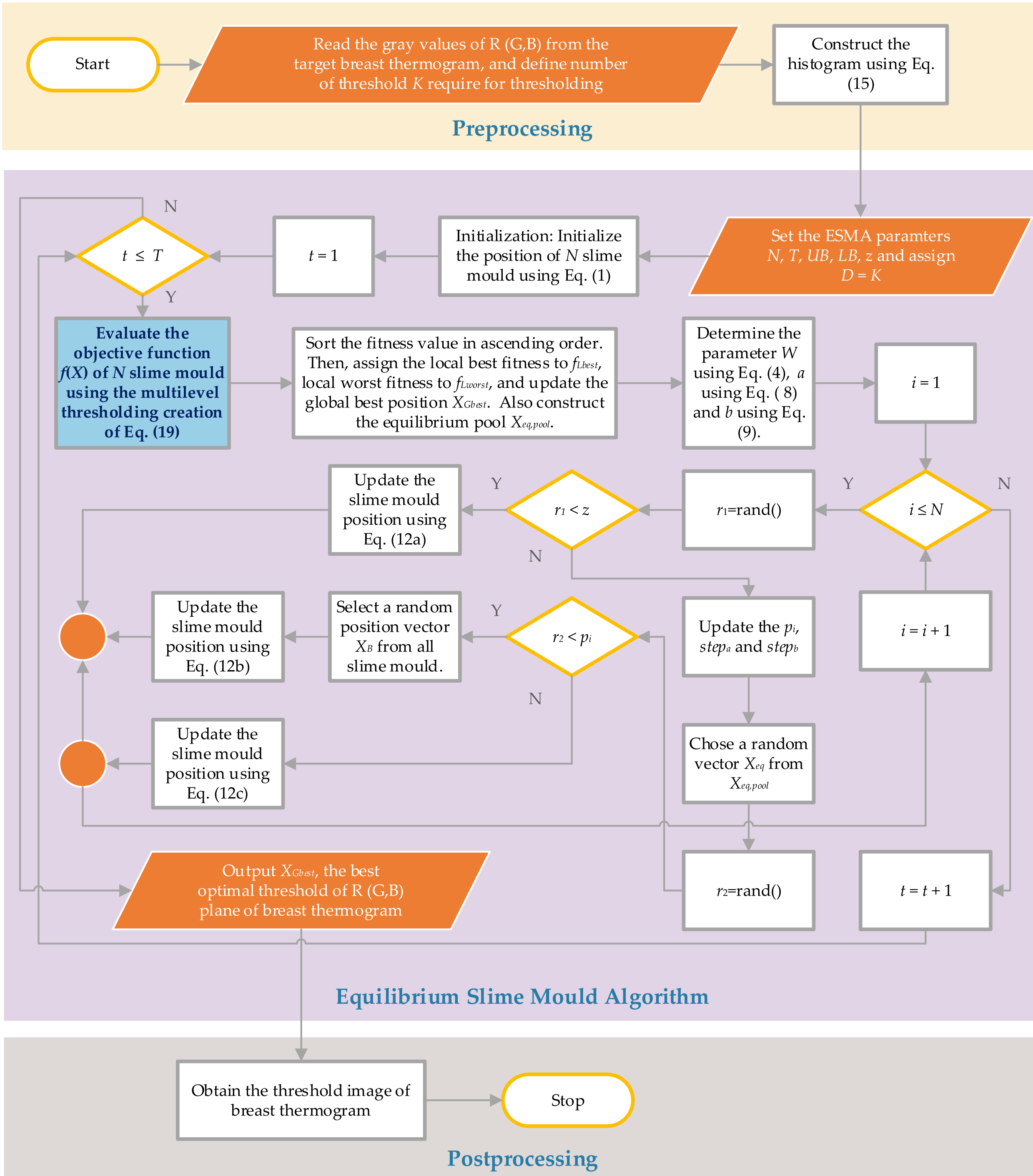

Fig. 15. Flowchart of colour multilevel thresholding using ESMA.

values vs. iterations. The unimodal test problems are used to describe exploration behaviour. The convergence curve of the ESMA for unimodal test problems $f_1, f_2\ f_4, f_7$ and $CEC-2014-F1$ shows rapid convergence throughout the iterations process which can be observed from Figs. 8 and 10. The multimodal test problems are designed to test the exploitive behaviour. The convergence curve of the ESMA for multimodal test problems with varied dimensions f_{10}, f_{11}, $CEC-2014-F4$, $CEC-2014-F8$, and $CEC-2014-F10$ express the slowest convergence in most of the iteration processes due to exploitation, which can be observed from Figs. 8 and 10. However, the exploitation capability of ESMA is more prominent when we observed the convergence curve of multimodal test problems with fixed dimensions f_{14}, f_{20} and f_{23} from Fig. 9. In these test problems, after the 50th iterations, the ESMA enter to exploitation phase to avoid the local optimal solution to reach the global optimal solution. As the hybrid and composite test problems are also used to describe the exploitative capability of the optimization algorithm. So, as the $CEC-2014-F22$ is a hybrid function composed of the multimodal test function, which shows the convergence curve as of multimodal test function can be visualized from Fig. 10. The composite test problem $CEC-2014-F30$ is a combination of unimodal and multimodal function, so the convergence curve of this function from Fig. 10 shows a rapid convergence during initial iterations

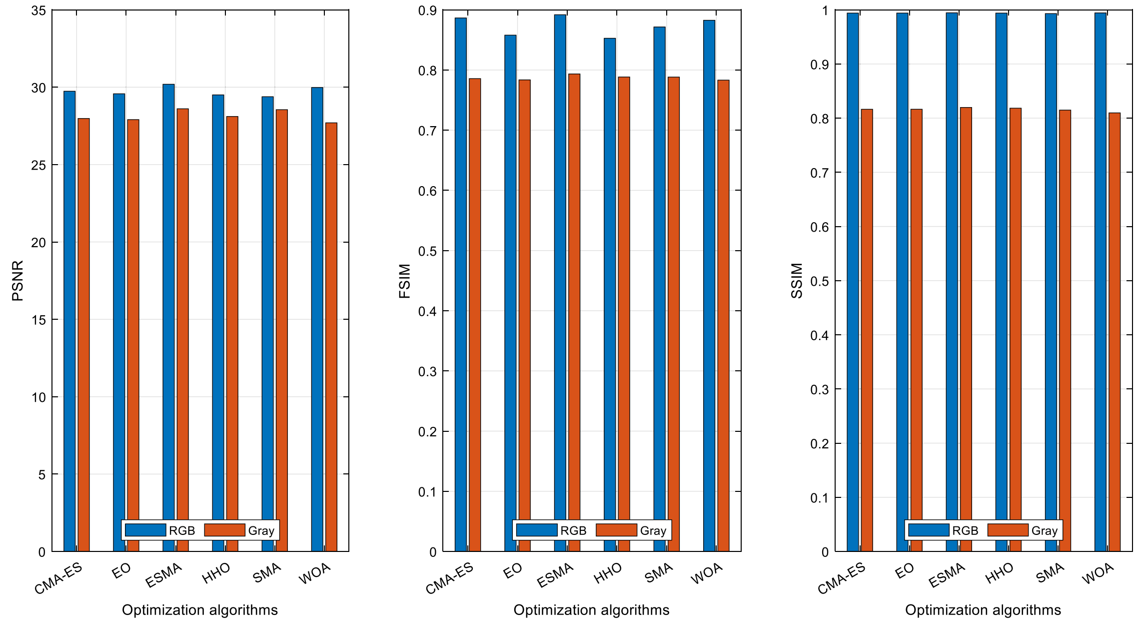

Fig. 16. A comparison of PSNR, FSIM, and SSIM between thresholding using RGB and Grey coordinates for test image Test1.

due to exploration however the later part of its convergence experiences the slower convergence due to exploitation.

A comparative convergence is performed between ESMA, SMA, EO, HHO, GWO, WDO, WOA, DE, CS, PSO, FA, L-SHADE, and CMA-ES to visualize how far the convergence of ESMA vary from another optimization algorithm. For all optimization algorithms, which are evaluated with 15 000 function evaluations, the convergence speed vs. iterations can be regarded as a qualitative metric. The convergence curve of six scalable unimodal and multimodal test problems is presented in Fig. 8, three non-scalable fixed dimensional multimodal test problems are presented in Fig. 9, and six test problems from the CEC 2014 test suite are presented in Fig. 10. From Fig. 8, it is shown that the ESMA converges faster in scalable unimodal and multimodal test problems as compared with other optimization algorithms. The convergence curve of non-scalable fixed dimensional multimodal test problems behaves in a similar manner, which is seen in Fig. 9. From the convergence curves presented in Fig. 10 on CEC 2014 test problems, the ESMA has shown quite an impressive convergence over other optimization algorithms, although a close tracking with the SMA and the EO.

2.5.6. Scalability analysis of ESMA

This section presents a scalability analysis of how the dimensions affect the results of the ESMA. The scalable test problems ($f_1 - f_{13}$) are taken for the experiments with 5, 10, 20, 30, 60, 100, 150, 200, and 300 dimensions for $N = 30$ with $T = 500$. The results of ESMA is compared with the SMA, EO, HHO, GWO, WDO, WOA, DE, CS, PSO, and FA, however, we have excluded L-SHADE and CMA-ES due to differences with larger search agents N ($N = 18D$ for L-SHADE and $N = 4 + 3\log(D)$ for CMA-ES) requirements in these two algorithms. The scalability results are illustrated in Fig. 11. The ESMA outperformed in all dimensions in the test problems f_1, f_2, f_3 and f_4, which is illustrated in Fig. 11. The ESMA, SMA, and HHO behaved in the same way on the test problems $f_8 - f_{11}$. Whereas, in the test functions f_5, f_6, f_7, f_{12} and f_{13}, its results are comparable with the HHO and WDO. For a better understanding, a Friedman mean rank test is conducted on the average values of various optimization algorithms for scalable test problems $f_1 - f_{13}$. The Friedman means rank is illustrated in Fig. 12, which clearly shows that, for the low dimension problem ($D < 60$), the ESMA ranked first, and for the high dimensional problem ($D \geq 60$), the ESMA ranked second over the various state-of-the-art algorithms.

2.5.7. Statistical analysis of ESMA

In this section, we present an illustration of the statistical results based on the non-parametric Wilcoxon rank-sum test at $\alpha = 0.05$ and Friedman mean rank test. The p-value of the scalable unimodal and multimodal test problems are presented in Table 6. For non-scalable fixed dimensional multimodal test problems, these p-values are presented in Table 7; and for CEC 2014 test functions, these are presented in Table 8. From the p-values, it is detected that the ESMA provides statistically meaningful results for EO, HHO, GWO, WDO, DE, CS, PSO, FA, L-SHADE, and CMA-ES. However, it also shows a significant improvement over the SMA. The Friedman mean-rank of the test problems are presented in Table 9. From Table 9, it is seen that for all categories like scalable ($f_1 - f_{13}$), non-scalable ($f_{14} - f_{23}$) and CEC 2014 test problems, the ESMA scored the first rank in both the individual/overall categories.

2.5.8. Computational timing analysis

In this section of experiments, the computational timing analysis of ESMA is compared with other 12 optimization algorithms such as SMA, EO, HHO, GWO, WDO, WOA, DE, CS, PSO, FA, L-SHADE, CMA-ES. The analysis is done on average time (in a sec) during 51 independent runs for fixed iterations $T = 500$ for all 53 test problems ($f_1 - f_{23}$ and $CEC - 2014 - F1\,to\,CEC - 2014 - F30$). The computational timing analysis is presented in Table 10, which shows that ESMA is quite expensive as compared to many algorithms due to the oscillation factor during the search process. However, ESMA still performed better timing than L-SHADE and CMA-ES, and a 6% marginally improvement of timing than SMA due to incorporating the equilibrium pool in SMA.

2.6. Discussion on simulation results of the ESMA

The qualitative, quantitative, and statistical results are discussed in the previous section. Nevertheless, the ESMA has shown superiority results among thirteen scalable unimodal and multimodal test problems $f_1 - f_{13}$, ten non-scalable fixed dimensional

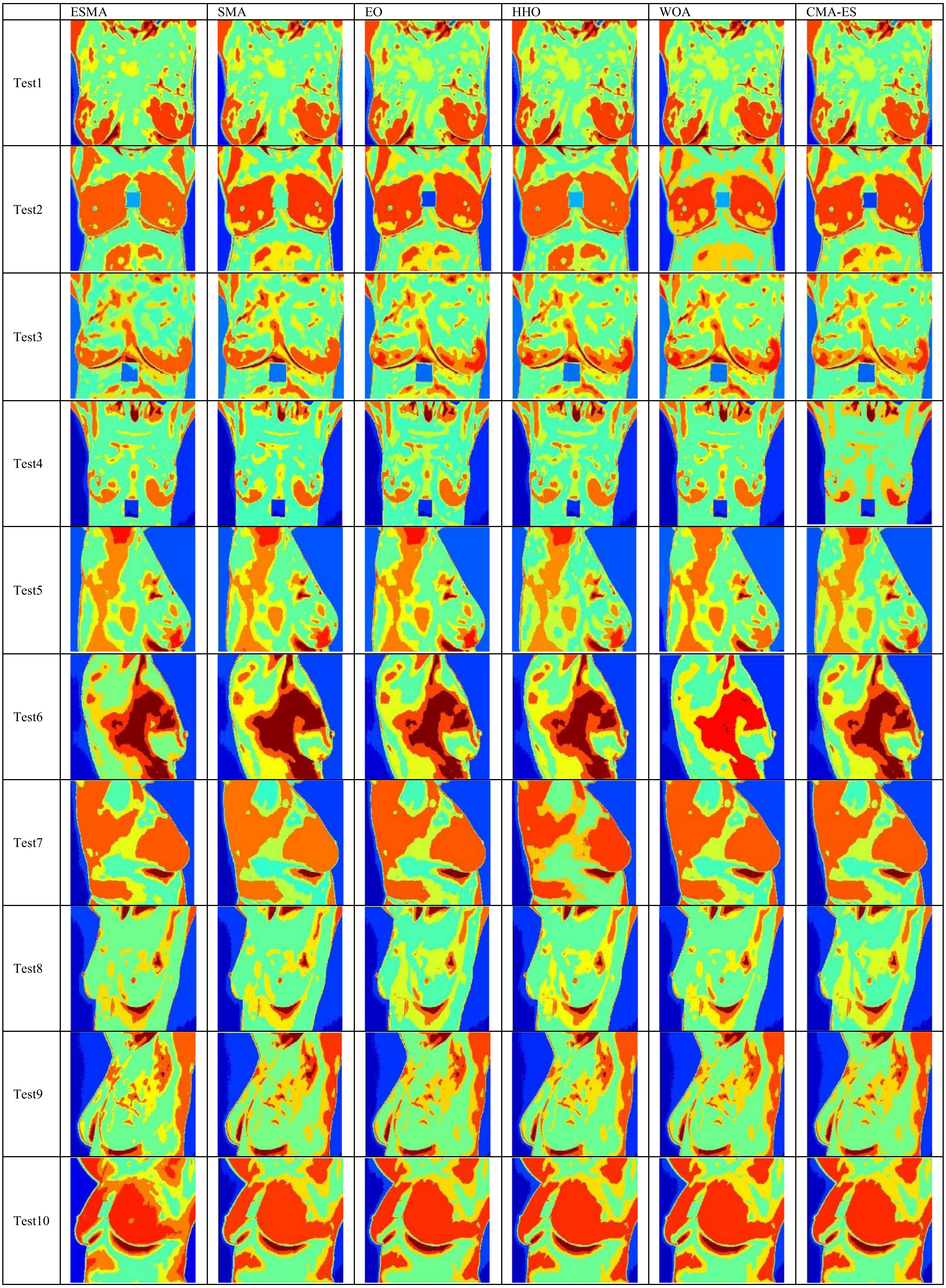

Fig. 17. Thresholded images obtained for grey component of test images using ESMA, SMA, EO, HHO, WOA, and CMA-ES with K = 5.

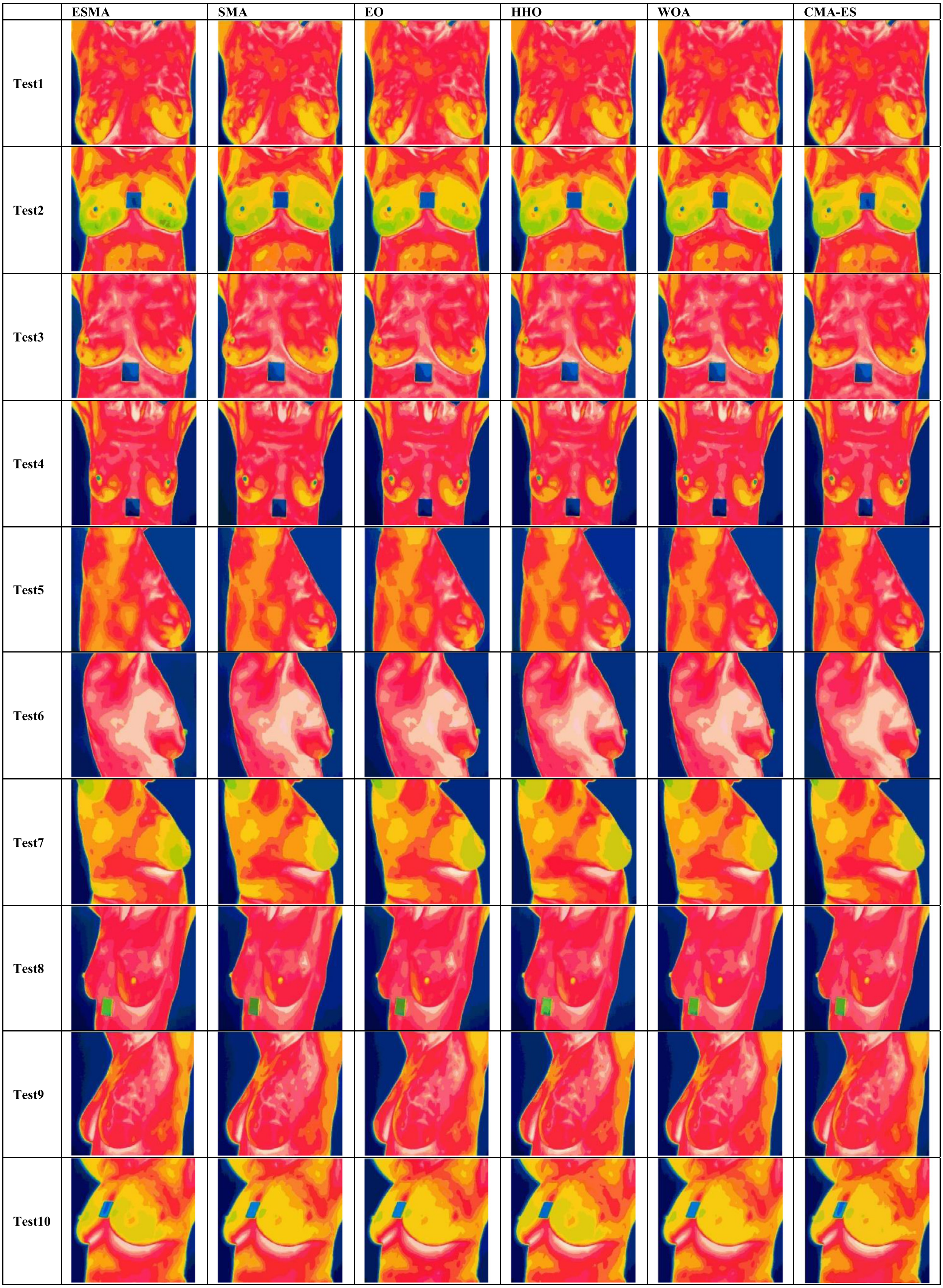

Fig. 18. Thresholded images obtained for RGB components of test images using ESMA, SMA, EO, HHO, WOA, and CMA-ES with $K = 5$.

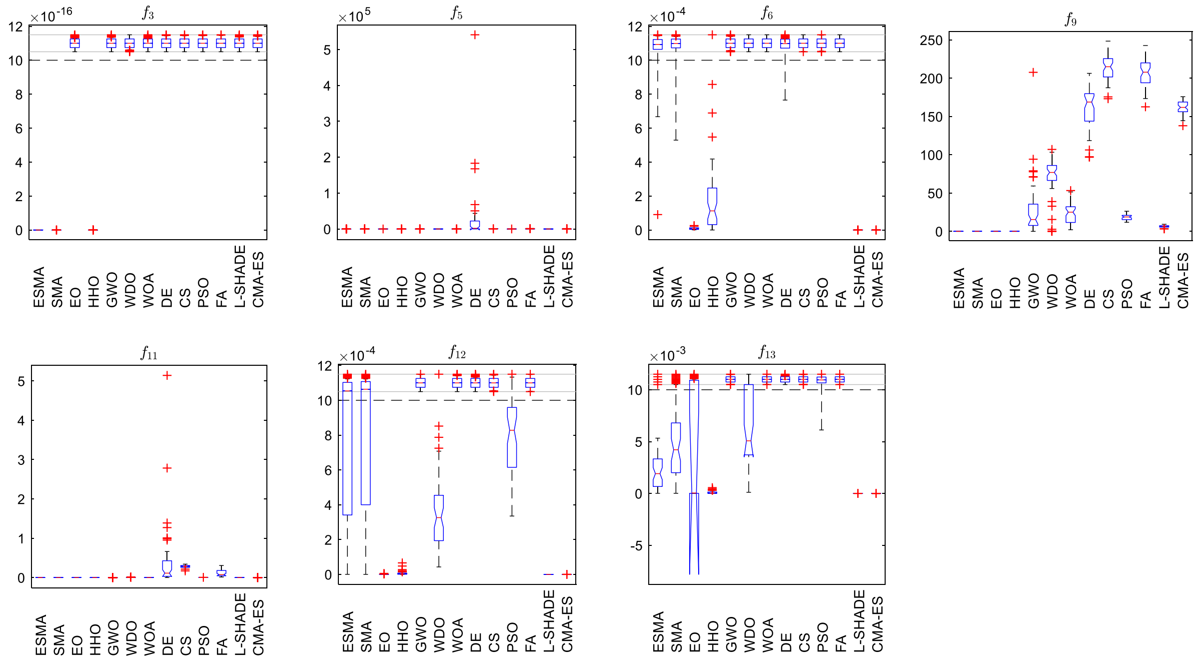

Fig. A.1. Boxplot of the test problems f_1, f_5, f_6, f_9, f_{11}, f_{12} and f_{13}.

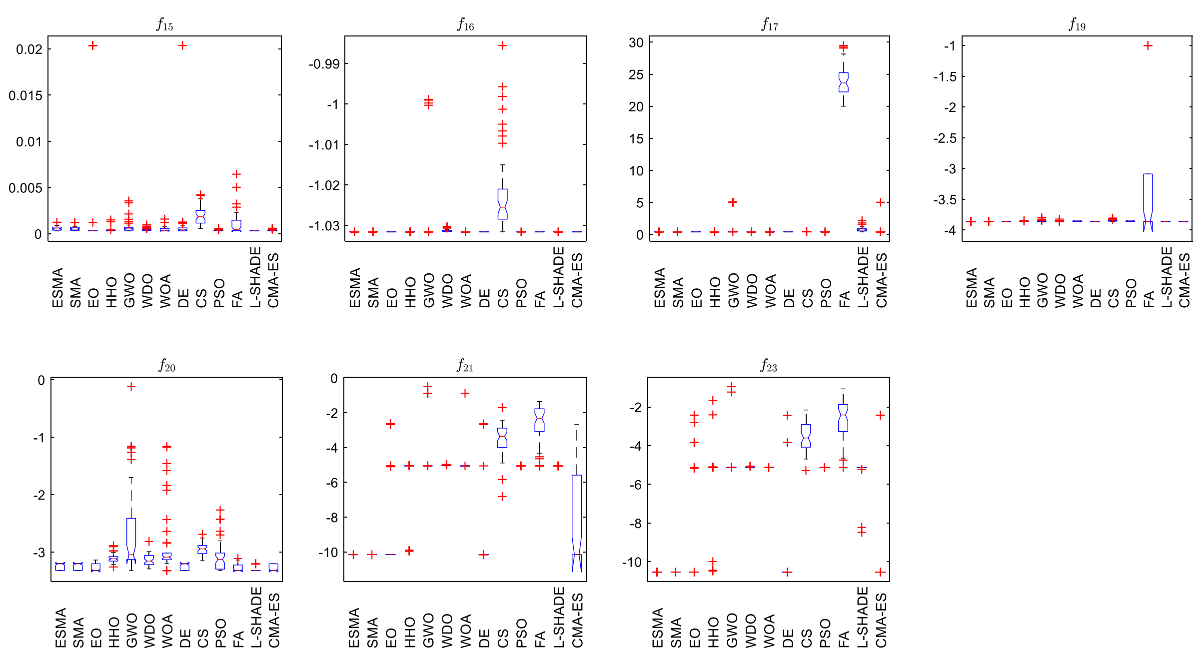

Fig. A.2. Boxplot of the test problems f_{15}, f_{16}, f_{17}, f_{19}, f_{20}, f_{21} and f_{23}.

multimodal test problems $f_{14} - f_{23}$ and thirty CEC 2014 test problems, when compared with state-of-the-art optimization algorithms including SMA, EO, HHO, GWO, WDO, WOA, DE, CS, PSO, FA, L-SHADE, and CMA-ES. From Table 9, it is observed that the ESMA obtains the first rank in the overall category and among the 30-dimensional problems of scalable test functions $f_1 - f_{13}$ and CEC 2014 test problems, however, it ranked third on fixed dimensional multimodal test functions $f_{14} - f_{23}$ among well-known state-of-the-art algorithms. From the Friedman mean rank statistical analysis of scalability shown in Fig. 12, the ESMA shows superiority in low dimensional problems and ranked first under 60 dimensions. However, the ESMA ranked second if the dimension increases. The equilibrium poll supplements the SMA in the exploration and the exploitation phases of the ESMA, to achieve optimal results. So, from the analysis of the results, the ESMA evolves as a notable optimization algorithm.

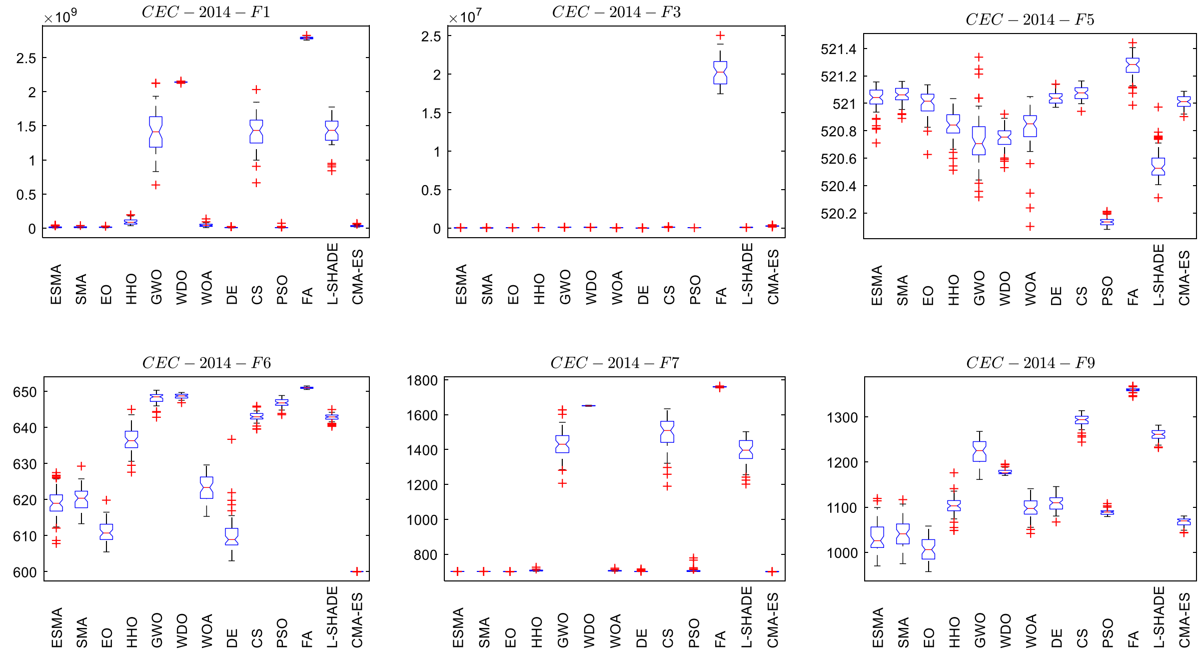

Fig. A.3. Boxplot of the test problems $CEC-2014-F1$, $CEC-2014-F3$, $CEC-2014-F5$, $CEC-2014-F6$, $CEC-2014-F7$, and $CEC-2014-F9$.

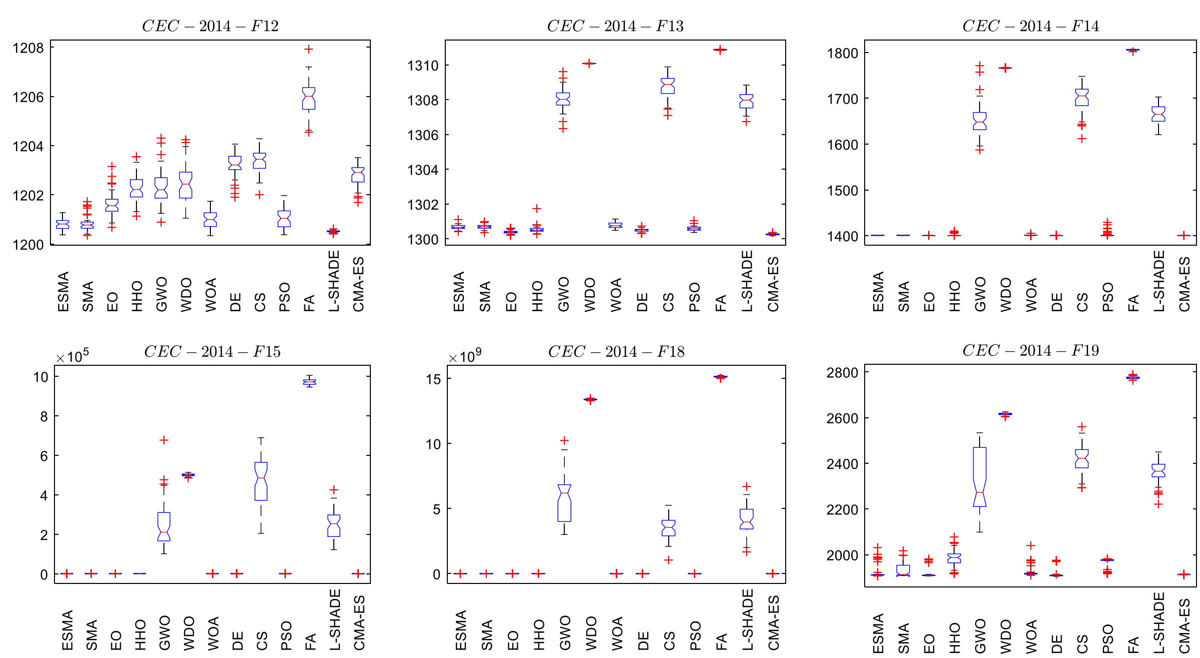

Fig. A.4. Boxplot of the test problems $CEC-2014-F12$, $CEC-2014-F13$, $CEC-2014-F14$, $CEC-2014-F15$, $CEC-2014-F18$ and $CEC-2014-F19$.

3. Multilevel colour image thresholding using entropy minimization based objective function

In this section, a method for multilevel colour thresholding for the analysis of breast thermograms is investigated. Here, the key ideas behind the development of this method are highlighted. The scheme is clearly explained to make the implementation simple. Attempts are made to make the method computationally quite efficient compared to the existing methods.

3.1. Multilevel colour image thresholding

The multilevel thresholding classifies the image into $K+1$ different classes based on a set of K threshold values $\{t_1, t_2, \ldots, t_K\}$ using the simple rules defined Eq. (14).

$$\begin{aligned} C_1 &\leftarrow s \qquad 0 \le s < t_1 \\ C_2 &\leftarrow s \qquad t_1 \le s < t_2 \\ C_i &\leftarrow s \qquad t_{i-1} \le s < t_i \\ C_{K+1} &\leftarrow s \qquad t_K \le s < L-1 \end{aligned} \tag{14}$$

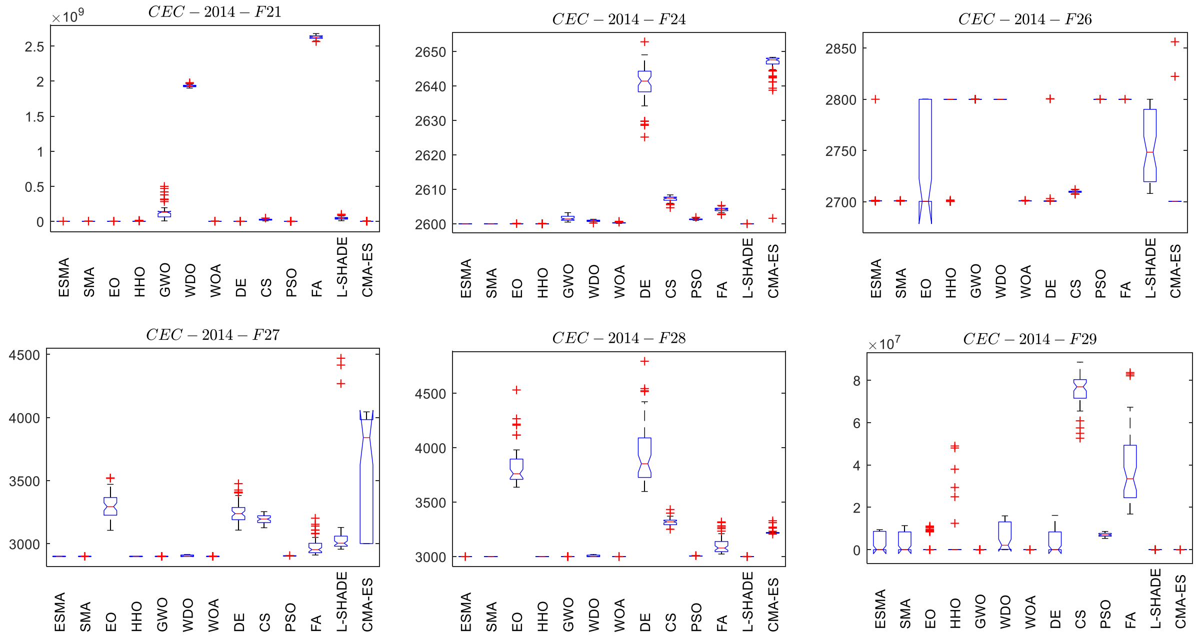

Fig. A.5. Boxplot of the test problems $CEC - 2014 - F21$, $CEC - 2014 - F24$, $CEC - 2014 - F26$, $CEC - 2014 - F27$, $CEC - 2014 - F28$ and $CEC - 2014 - F29$.

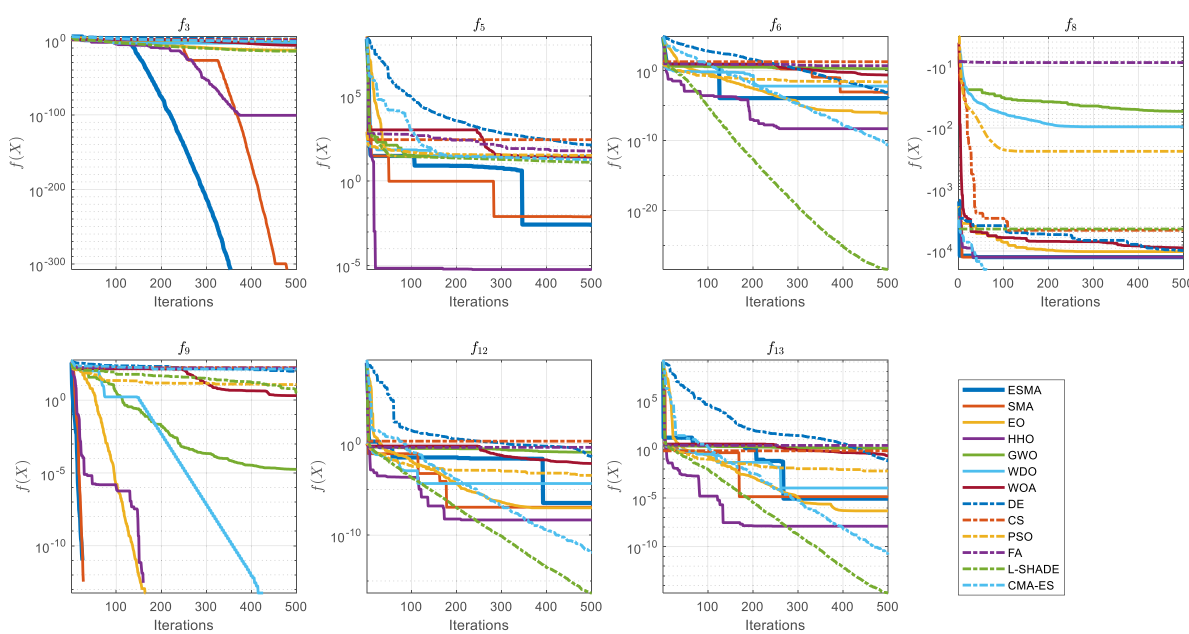

Fig. B.1. Convergence curve of test problems f_3, f_5, f_6, f_8, f_9, f_{12} and f_{13}.

where the s is a pixel in an image of size $M \times N$ and composed of L grey level. Eq. (14) holds for one component like greyscale image, whereas for a colour image, 3 sets of thresholds are obtained for red, green, and blue components individually using Eq. (14). The aim is to obtain the optimal threshold values, so that appropriately we can classify the different regions in an image.

3.2. The entropy minimization based objective function for image thresholding

A bi-level thresholding method using the information regarding the entropic dependence on different classes is described in [25]. A comprehensive report on the method is found in [26]. The idea is extended here to multilevel colour image thresholding.

Let us consider an image I with a grey level range $[0, L-1]$, then the probability of the ith grey level is calculated as

$$p_i = \frac{n_i}{M \times N}, \tag{15}$$

where n_i is the number of pixels with grey level values equal to i, M and N are numbers of rows and columns present in spatial dimensions of the image I, i is an index within the range of $[0, L-1]$, $\sum_{i=0}^{L-1} p_i = 1$ and $\sum_{i=0}^{L-1} n_i = M \times N$.

The optimal threshold t^* of bi-level thresholding is determined by the minimization of the information regarding the entropic dependence on each class, which is expressed in Eq. (16).

$$t^* = \arg \min_{0<t<L-1} [E_1 + E_2] \tag{16}$$

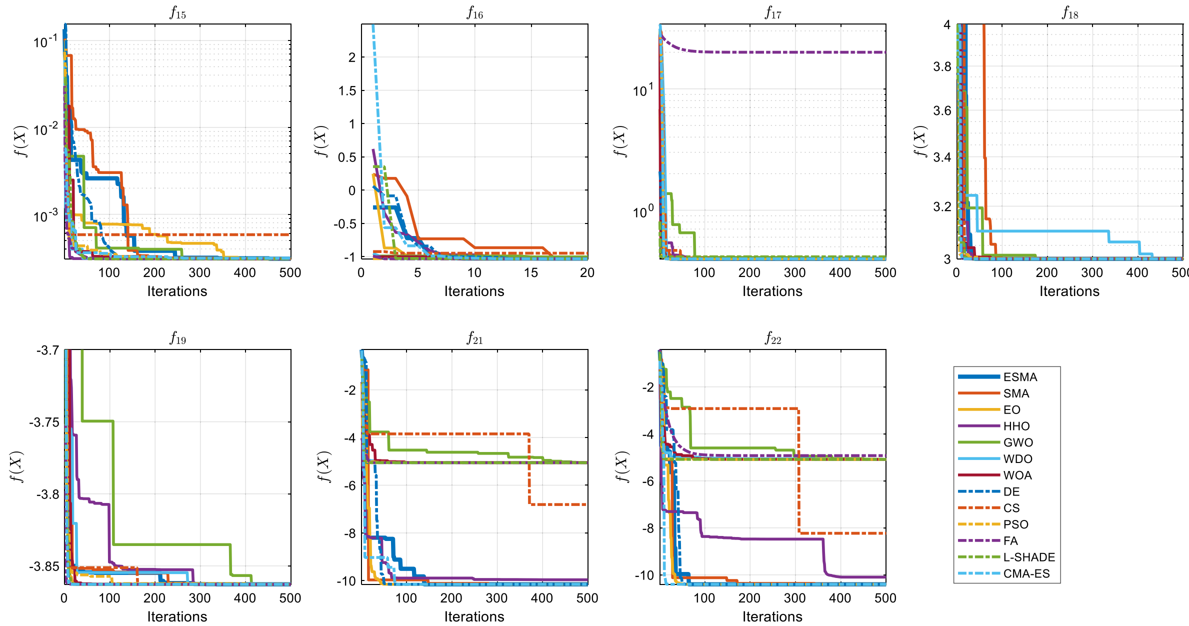

Fig. B.2. Convergence curve of test problems f_{15}, f_{16}, f_{17}, f_{18}, f_{19}, f_{21} and f_{22}.

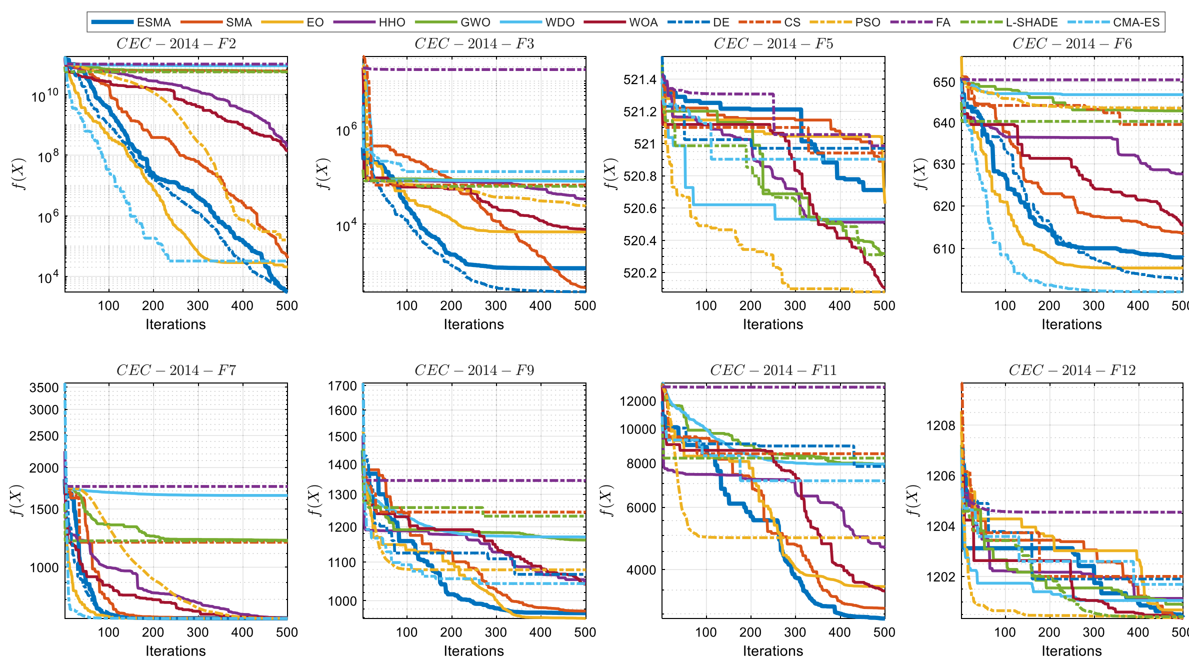

Fig. B.3. Convergence curve of test problems $CEC-2014-F2$, $CEC-2014-F3$, $CEC-2014-F5$, $CEC-2014-F6$, $CEC-2014-F7$, $CEC-2014-F9$, $CEC-2014-F11$, and $CEC-2014-F12$.

To be precise, the problem at hand is a minimization problem.

The E_1 and E_2 are the entropic information of the class C_1 and C_2 respectively, which are evaluated as

$$E_1 = \log_e\left(\sum_{i=0}^{t} p_i\right) - \frac{1}{\sum_{i=0}^{t} p_i} \times \left[p_t \log_e p_t + \left(\sum_{i=0}^{t-1} p_i\right) \log_e\left(\sum_{i=0}^{t-1} p_i\right)\right], \tag{17}$$

and

$$E_2 = \log_e\left(\sum_{i=t}^{L-1} p_i\right) - \frac{1}{\sum_{i=t}^{L-1} p_i} \times \left[p_t \log_e p_t + \left(\sum_{i=t+1}^{L-1} p_i\right) \log_e\left(\sum_{i=t+1}^{L-1} p_i\right)\right]. \tag{18}$$

The bi-level thresholding creation is extended to the multilevel thresholding creation using Eq. (19).

$$(t_1^*, t_2^*, \ldots, t_K^*) = \arg \min_{0<t_1^*<t_2^*<\cdots<t_K^*<L-1} \{E_1 + E_2 + \cdots + E_{K+1}\} \tag{19}$$

where E_i is the entropic information of the class C_i for $i = 1, 2, \ldots, K+1$ based on K number of the threshold value $\{t_1, t_2,$

Table 16
Wall clock average time (in sec) performance of ESMA and other optimization algorithms for test image Test1.

K		ESMA	SMA	EO	HHO	WOA	CMA-ES
2	Grey	1.3585	1.3618	1.2277	1.8366	1.2175	2.4419
	RGB	3.7661	3.7783	3.5402	5.2168	3.4006	6.8956
3	Grey	1.3386	1.3469	1.3272	1.8564	1.2282	2.7129
	RGB	4.0549	4.1904	4.2433	5.5441	3.6474	7.8834
4	Grey	1.4007	1.4048	1.3494	1.9520	1.2389	3.0863
	RGB	4.0756	4.1023	4.5436	5.7746	3.7366	8.9204
5	Grey	1.4560	1.4504	1.3321	2.0265	1.2763	3.4670
	RGB	4.3226	4.6414	4.0736	5.7770	3.8051	10.1154

$\ldots, t_K\}$, which are evaluated as

$$
\begin{aligned}
E_1 &= \log_e\left(\sum_{i=0}^{t_1} p_i\right) - \frac{1}{\sum_{i=0}^{t_1} p_i} \left[\left(\sum_{i=0}^{t_1-1} p_i\right)\log_e\left(\sum_{i=0}^{t_1-1} p_i\right) + p_{t_1}\log_e p_{t_1}\right] \\
E_i &= \log_e\left(\sum_{i=t_{i-1}}^{t_i} p_i\right) - \frac{1}{\sum_{i=t_{i-1}}^{t_i} p_i}\left[p_{t_{i-1}}\log_e p_{t_{i-1}} + \left(\sum_{i=t_{i-1}+1}^{t_i-1} p_i\right)\log_e\left(\sum_{i=t_{i-1}+1}^{t_i-1} p_i\right) + p_{t_i}\log_e p_{t_i}\right] \\
E_{K+1} &= \log_e\left(\sum_{i=t_K}^{L-1} p_i\right) - \frac{1}{\sum_{i=t_K}^{L-1} p_i}\left[p_{t_K}\log_e p_{t_K} + \left(\sum_{i=t_K+1}^{L-1} p_i\right)\log_e\left(\sum_{i=t_K+1}^{L-1} p_i\right)\right]
\end{aligned}
\tag{20}
$$

The multilevel thresholding creation, i.e., Eq. (19), needs to be minimized. This objective function can be used by an optimizer, to obtain the optimal threshold values. These values can be used for the multilevel thresholding of breast thermograms.

4. Results and discussions

The performance of our proposed optimizer ESMA and the multilevel thresholding creation is evaluated using a set of randomly selected 10 breast thermograms, which are retrieved from the Database for Breast Research with Infrared Images [40]. Here, 10 breast thermograms are taken as 4 of frontal orientations, 3 of 90° orientations, and 3 of 45° orientations. The retrieved images are in RGB coordinates with different sizes. Hence, for the experimental purpose, we resize the breast thermogram with 256 × 256 pixels, which are presented in Fig. 13 along with their histograms of red, green, blue, and grey components. The multilevel thresholding is performed with both the grey and the colour (RGB) coordinates, to visualize the advantages of the multilevel colour thresholding of breast thermograms. The experiments are carried out in the MATLAB environment using the Windows 10 operating system on the Intel Core i-3 processor with 8 GB RAM.

For a comparison of our proposed multilevel thresholding using the ESMA, other top-ranked optimizers SMA, EO, HHO, WOA, and CMA-ES, as validated from Section 2, are also used for the multilevel thresholding. The experimental parameters of ESMA, SMA, EO, HHO, WOA, and CMA-ES are taken the same as reported in Table 1. The performance metrics consist of the average value 'Avg', the standard deviation 'Std' of peak signal to noise ratio (PSNR) [41], the structured similarity (SSIM) [42], and the feature similarity (FSIM) [43]. The PSNR metric is used to analyse the quality of the thresholded image, a higher value indicates better thresholding. The FSIM and SSIM metrics are used to demonstrate how the feature and structure of the thresholded image are like the original image.

The performance of the proposed method for breast thermograms is evaluated. All algorithms go for 21 independent runs for threshold level = 2, 3, 4, 5, for a maximum iteration $T = 100$, to verify the consistency. The implementation of the proposed method is presented in a block diagram shown in Fig. 14. A flowchart is also presented in Fig. 15.

The performance of our proposed method in RGB and grey components is analysed here. A comparison of the average PSNR is presented in Table 11. The FSIM is presented in Table 12 and the SSIM is presented in Table 13. Note that the values are computed from 21 independent runs. Here, four threshold levels $K = 2, 3, 4, 5$ are considered for the experiment. Various state-of-the-art optimization algorithms are considered for comparison. The boldfaced letters indicate the best results. From Tables 11–13, it is seen that our proposed ESMA based multilevel thresholding provides superior results in both RGB and grey components. However, the ESMA based multilevel thresholding using RGB components proves to be a better thresholding approach to breast thermogram analysis. For instance, an improvement of the PSNR with 2.38%, FSIM with 6.06%; and SSIM with 26.10% of RGB components are achieved over the Grey components. This is also reflected in Fig. 16. Note that Fig. 16 shows a comparison of PSNR, FSIM, and SSIM for various optimization algorithms. Multilevel thresholding results considering both RGB and grey components are shown in Fig. 16. Based on Friedman's mean rank, a statistical analysis, it is noticed that the ESMA based multilevel thresholding using the RGB components ranked first over other methods, presented in Tables 11–13.

The optimal threshold values of 10 test images for threshold levels $K = 2, 3, 4, 5$ for grey components are presented in Table 14 and RGB components are displayed in Table 15. The threshold values of grey components presented in Table 14 are used to generate the thresholded images through pseudo colouring, which are shown in Fig. 17 corresponding to the threshold level = 5. Qualitative analysis is done using these results. Similarly, the threshold values of RGB components presented in Table 14 are used to generate the colour thresholded images, which are shown in Fig. 18 for the threshold level = 5. From the thresholded images, displayed in Figs. 17 and 18, it is observed that the RGB component-based approach could preserve more details, which can be helpful in pathological investigations.

A wall clock average time performance in connection with multilevel thresholding for test image Test1 is presented in Table 16. The wall clock average time reported in Table 16 is based on 21 independent runs of individual methods ESMA, SMA, EO, HHO, WOA, and CMA-ES based multilevel thresholding. The ESMA based multilevel thresholding shown better timing corresponding to HHO and CMA-ES based methods and similar time complexity to SMA and EO. Based on the performance metrics PSNR, FSIM, and SSIM, statistical analysis Friedman's mean rank and wall clock average time performance of ESMA based multilevel threshold shows significant improvement over other optimizer based multilevel thresholding methods.

5. Conclusions

Unlike early multilevel thresholding-based approaches reported in the breast thermogram analysis, which usually relied

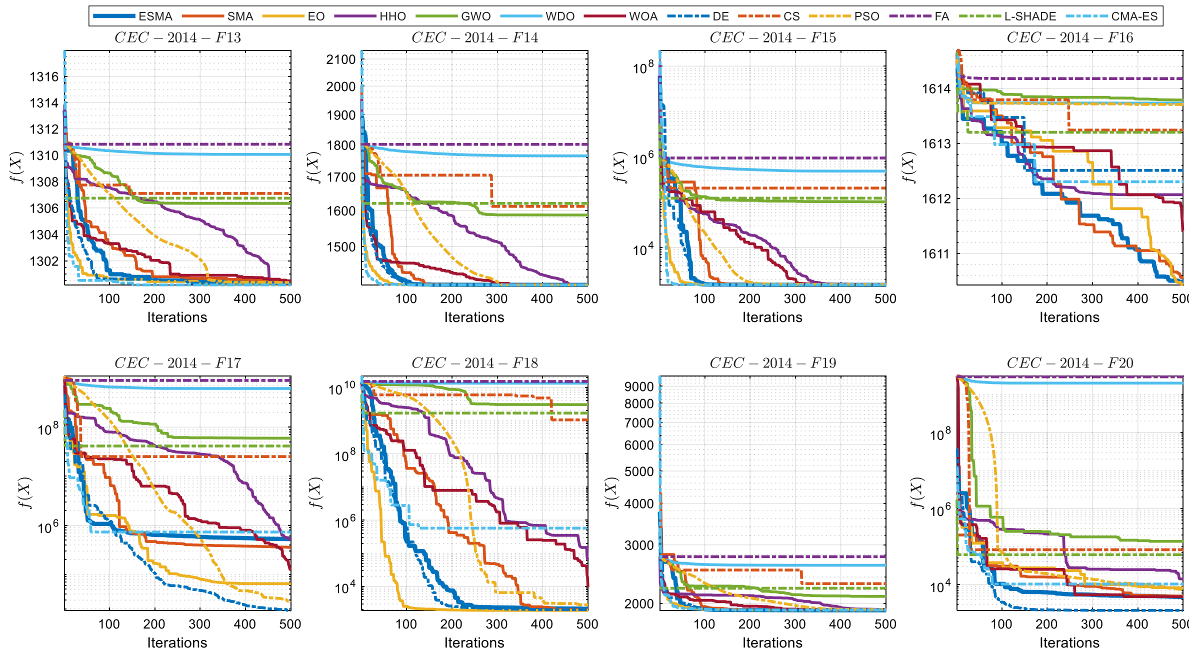

Fig. B.4. Convergence curve of test problems $CEC-2014-F13$, $CEC-2014-F14$, $CEC-2014-F15$, $CEC-2014-F16$, $CEC-2014-F17$, $CEC-2014-F18$, $CEC-2014-F19$ and $CEC-2014-F20$.

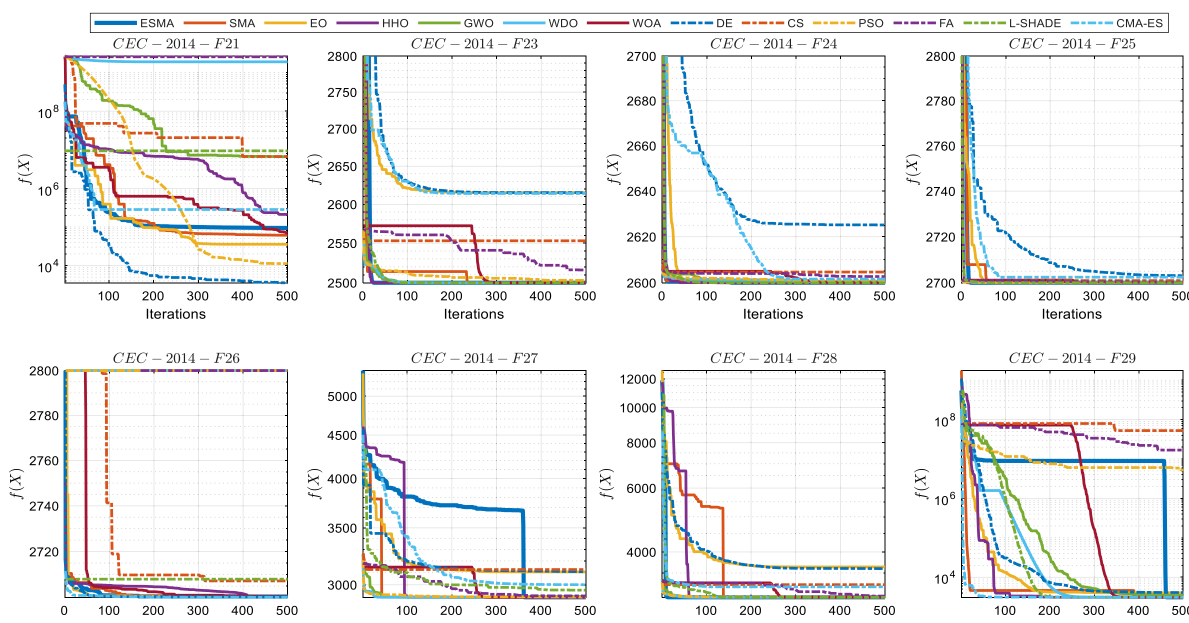

Fig. B.5. Convergence curve of test problems $CEC-2014-F21$, $CEC-2014-F23$, $CEC-2014-F24$, $CEC-2014-F25$, $CEC-2014-F26$, $CEC-2014-F27$, $CEC-2014-F28$ and $CEC-2014-F29$.

on the maximization of the objective functions, the suggested technique is created on the minimization of the entropic information. The proposal is well suited for breast thermogram analysis. Multilevel thresholded images may assist the clinicians, as an extra support, for the breast thermogram analysis. Minimization of dependency of entropy on various classes helps us to detect (visualize) clear boundaries between different regions. The method has shown its ability to extract low-resolution visual features, because the interdependencies of the entropy between various classes are minimized using a new hybrid equilibrium slime mould algorithm (ESMA). The exploration capability of the ESMA is enhanced, because the concept of equilibrium pool from the equilibrium optimizer (EO) algorithm is integrated into the system. Remarkable differences are observed while studying the convergence curves presented in the result section and Appendix B. The proposed ESMA performs better than state-of-the-art optimizers. The speed of convergence is implicit from the study (presented in Figs. 8–10 and Figs. B.1 to B.5). The quality of the visual results is explicitly shown to attract readers. From Tables 11–13, it is seen that the thresholding method using the RGB components ranked first over other methods, the reason is that it could preserve more details. Therefore, it is wise to recommend colour thresholding using the proposed method for pathological investigations. To figure out other merits, the proposal is stable and scalable (see Figs. 8–11). It is iterated that the suggested work may attract the use of low cost and portable infrared cameras to the diagnostic process. It means, realistically, one would be ready for the practical implementations. The future scope of the proposal would be the use of other databases containing infrared images together with a clinical study. Finally, it is believed that the ESMA would help function optimization.

CRediT authorship contribution statement

Manoj Kumar Naik: Methodology, Implementation, Data handling, Programming, Writing – original draft. **Rutuparna Panda:** Conceptualization, Methodology, Guidance, Data analysis, Writing – review & editing. **Ajith Abraham:** Supervision, Formal analysis.

Declaration of competing interest

The authors declare that they have no known competing financial interests or personal relationships that could have appeared to influencethe work reported in this paper.

Appendix A. Boxplot of the test problems

See Figs. A.1–A.5

Appendix B. Convergence curve of the test problems

See Figs. B.1–B.5

References

[1] A. Costa, Y. Kieffer, A. Scholer-Dahirel, F. Pelon, B. Bourachot, M. Cardon, P. Sirven, I. Magagna, L. Fuhrmann, C. Bernard, C. Bonneau, M. Kondratova, I. Kuperstein, A. Zinovyev, A.-M. Givel, M.-C. Parrini, V. Soumelis, A. Vincent-Salomon, F. Mechta-Grigoriou, Fibroblast heterogeneity and immunosuppressive environment in human breast cancer, Cancer Cell. 33 (2018) 463–479.e10, http://dx.doi.org/10.1016/j.ccell.2018.01.011.

[2] C. Desantis, J. Ma, M. Gaudet, L. Newman, K. Miller, A. Goding Sauer, A. Jemal, R. Siegel, Breast cancer statistics, 2019, CA, Cancer J. Clin. 69 (2019) http://dx.doi.org/10.3322/caac.21583.

[3] H. Lee, Y.-P.P. Chen, Image based computer aided diagnosis system for cancer detection, Expert Syst. Appl. 42 (2015) 5356–5365, http://dx.doi.org/10.1016/j.eswa.2015.02.005.

[4] M. Herranz, A. Ruibal, Optical imaging in breast cancer diagnosis: The next evolution, J. Oncol. 2012 (2012) 863747, http://dx.doi.org/10.1155/2012/863747.

[5] T.B. Borchartt, A. Conci, R.C.F. Lima, R. Resmini, A. Sanchez, Breast thermography from an image processing viewpoint: A survey, Signal Process. 93 (2013) 2785–2803, http://dx.doi.org/10.1016/j.sigpro.2012.08.012.

[6] S.J.S. Gardezi, A. Elazab, B. Lei, T. Wang, Breast cancer detection and diagnosis using mammographic data: Systematic review, J. Med. Internet Res. 21 (2019) e14464, http://dx.doi.org/10.2196/14464.

[7] Y. Okamura, N. Yoshizawa, M. Yamaguchi, I. Kashiwakura, Application of dual-energy computed tomography for breast cancer diagnosis, Int. J. Med. Phys. Clin. Eng. Radiat. Oncol. 05 (2016) 288–297, http://dx.doi.org/10.4236/ijmpcero.2016.54029.

[8] H.-B. Pan, The role of breast ultrasound in early cancer detection, J. Med. Ultrasound. 24 (2016) 138–141, http://dx.doi.org/10.1016/j.jmu.2016.10.001.

[9] G. Tsina, P. Simon, Breast magnetic resonance imaging and its impact on the surgical treatment of breast cancer, Obstet. Gynecol. Int. 2014 (2014) 632074, http://dx.doi.org/10.1155/2014/632074.

[10] R.M. Mann, C.K. Kuhl, L. Moy, Contrast-enhanced MRI for breast cancer screening, J. Magn. Reson. Imaging. 50 (2019) 377–390, http://dx.doi.org/10.1002/jmri.26654.

[11] I. Iakovou, E. Giannoula, A. Gkantaifi, S. Levva, S. Frangos, Positron emission tomography in breast cancer: 18F- FDG and other radiopharmaceuticals, Eur. J. Hybrid Imaging 2 (2018) 20, http://dx.doi.org/10.1186/s41824-018-0039-x.

[12] J.L. Vercher-Conejero, L. Pelegrí-Martinez, D. Lopez-Aznar, M.D.P. Cózar-Santiago, Positron emission tomography in breast cancer, Diagn. (Basel, Switzerland) 5 (2015) 61–83, http://dx.doi.org/10.3390/diagnostics5010061.

[13] N.K. Negied, Infrared thermography-based breast cancer detection — Comprehensive investigation, Int. J. Pattern Recognit. Artif. Intell. 33 (2018) 1957002, http://dx.doi.org/10.1142/S0218001419570027.

[14] R. Miles, F. Wan, T.L. Onega, A. Lenderink-Carpenter, E.S. O'Meara, W. Zhu, L.M. Henderson, J.S. Haas, D.A. Hill, A.N.A. Tosteson, K.J. Wernli, J. Alford-Teaster, J.M. Lee, C.D. Lehman, C.I. Lee, Underutilization of supplemental magnetic resonance imaging screening among patients at high breast cancer risk, J. Women's Heal. 27 (2018) 748–754, http://dx.doi.org/10.1089/jwh.2017.6623.

[15] T. Sarigoz, T. Ertan, O. Topuz, Y. Sevim, Y. Cihan, Role of digital infrared thermal imaging in the diagnosis of breast mass: A pilot study: Diagnosis of breast mass by thermography, Infrared Phys. Technol. 91 (2018) 214–219, http://dx.doi.org/10.1016/j.infrared.2018.04.019.

[16] S. Ekici, H. Jawzal, Breast cancer diagnosis using thermography and convolutional neural networks, Med. Hypotheses. 137 (2020) 109542, http://dx.doi.org/10.1016/j.mehy.2019.109542.

[17] S. Tello-Mijares, F. Woo, F. Flores, Breast cancer identification via thermography image segmentation with a gradient vector flow and a convolutional neural network, J. Healthc. Eng. 2019 (2019) 9807619, http://dx.doi.org/10.1155/2019/9807619.

[18] S. Kermani, N. Samadzadehaghdam, M. EtehadTavakol, Automatic color segmentation of breast infrared images using a Gaussian mixture model, Optik (Stuttg) 126 (2015) 3288–3294, http://dx.doi.org/10.1016/j.ijleo.2015.08.007.

[19] N.S.M. Raja, S.A. Sukanya, Y. Nikita, Improved PSO based multi-level thresholding for cancer infected breast thermal images using otsu, Procedia Comput. Sci. 48 (2015) 524–529, http://dx.doi.org/10.1016/j.procs.2015.04.130.

[20] M.-A. Díaz-Cortés, N. Ortega-Sánchez, S. Hinojosa, D. Oliva, E. Cuevas, R. Rojas, A. Demin, A multi-level thresholding method for breast thermograms analysis using dragonfly algorithm, Infrared Phys. Technol. 93 (2018) 346–361, http://dx.doi.org/10.1016/j.infrared.2018.08.007.

[21] X. Yue, H. Zhang, Modified hybrid bat algorithm with genetic crossover operation and smart inertia weight for multilevel image segmentation, Appl. Soft Comput. 90 (2020) 106157, http://dx.doi.org/10.1016/j.asoc.2020.106157.

[22] P. Upadhyay, J.K. Chhabra, Kapur's entropy based optimal multilevel image segmentation using crow search algorithm, Appl. Soft Comput. (2019) 105522, http://dx.doi.org/10.1016/j.asoc.2019.105522.

[23] N. Otsu, A threshold selection method from gray-level histograms, IEEE Trans. Syst. Man. Cybern. 9 (1979) 62–66, http://dx.doi.org/10.1109/TSMC.1979.4310076.

[24] J.N. Kapur, P.K. Sahoo, A.K.C. Wong, A new method for grey-level picture thresholding using the entropy of the histogram, Comput. Vision, Graph. Image Process. 29 (1985) 273–285, http://dx.doi.org/10.1016/0734-189X(85)90125-2.

[25] G. Johannsen, J. Bille, A threshold selection method using information measures, in: Proc. 6th Int. Conf. Pattern Recogn, Munich, 1982. (1982), https://ci.nii.ac.jp/naid/10020153254/en/.

[26] P.K. Sahoo, S. Soltani, A.K.C. Wong, A survey of thresholding techniques, Comput. Vision, Graph. Image Process. 41 (1988) 233–260, http://dx.doi.org/10.1016/0734-189X(88)90022-9.

[27] S. Mirjalili, S.M. Mirjalili, A. Lewis, Grey wolf optimizer, Adv. Eng. Softw. 69 (2014) 46–61, http://dx.doi.org/10.1016/j.advengsoft.2013.12.007.

[28] S. Mirjalili, A. Lewis, The whale optimization algorithm, Adv. Eng. Softw. 95 (2016) 51–67, http://dx.doi.org/10.1016/j.advengsoft.2016.01.008.

[29] D. Simon, Biogeography-based optimization, Evol. Comput. IEEE Trans. 12 (2009) 702–713, http://dx.doi.org/10.1109/TEVC.2008.919004.

[30] R. Tanabe, A.S. Fukunaga, Improving the search performance of SHADE using linear population size reduction, in: 2014 IEEE Congr. Evol. Comput, 2014, pp. 1658–1665, http://dx.doi.org/10.1109/CEC.2014.6900380.

[31] N. Hansen, S.D. Müller, P. Koumoutsakos, Reducing the time complexity of the derandomized evolution strategy with covariance matrix adaptation (CMA-ES), Evol. Comput. 11 (2003) 1–18, http://dx.doi.org/10.1162/106365603321828970.

[32] Z. Bayraktar, M. Komurcu, J.A. Bossard, D.H. Werner, The wind driven optimization technique and its application in electromagnetics, IEEE Trans. Antennas Propag. 61 (2013) 2745–2757, http://dx.doi.org/10.1109/TAP.2013.2238654.

[33] A. Faramarzi, M. Heidarinejad, B. Stephens, S. Mirjalili, Equilibrium optimizer: A novel optimization algorithm, Knowledge-Based Syst. 191 (2020) 105190, http://dx.doi.org/10.1016/j.knosys.2019.105190.

[34] X.-S. Yang, Cuckoo Search and Firefly Algorithm, Springer International Publishing, 2014, http://dx.doi.org/10.1007/978-3-319-02141-6.

[35] A.A. Heidari, S. Mirjalili, H. Faris, I. Aljarah, M. Mafarja, H. Chen, Harris hawks optimization: Algorithm and applications, Futur. Gener. Comput. Syst. 97 (2019) 849–872, http://dx.doi.org/10.1016/j.future.2019.02.028.

[36] S. Li, H. Chen, M. Wang, A.A. Heidari, S. Mirjalili, Slime mould algorithm: A new method for stochastic optimization, Futur. Gener. Comput. Syst. (2020) http://dx.doi.org/10.1016/j.future.2020.03.055.

[37] X. Yao, L. Yong, L. Guangming, Evolutionary programming made faster, Evol. Comput. IEEE Trans. 3 (1999) 82–102, http://dx.doi.org/10.1109/4235.771163.

[38] M.K. Naik, R. Panda, A novel adaptive cuckoo search algorithm for intrinsic discriminant analysis based face recognition, Appl. Soft Comput. 38 (2016) 661–675, http://dx.doi.org/10.1016/j.asoc.2015.10.039.
[39] J.J. Liang, B.Y. Qu, P.N. Suganthan, Problem definitions and evaluation criteria for the CEC 2014 special session and competition on single objective real-parameter numerical optimization, 2013.
[40] L.F. Silva, D.C.M. Saade, G.O. Sequeiros, A.C. Silva, A.C. Paiva, R.S. Bravo, A. Conci, G. Sequeiros Olivera, A.C. Silva, A.C. Paiva, R.S. Bravo, A. Conci, A new database for breast research with infrared image, J. Med. Imaging Heal. Inform. 4 (2014) 92–100, http://dx.doi.org/10.1166/jmihi.2014.1226.
[41] S. Agrawal, R. Panda, S. Bhuyan, B.K. Panigrahi, Tsallis entropy based optimal multilevel thresholding using cuckoo search algorithm, Swarm Evol. Comput. 11 (2013) 16–30, http://dx.doi.org/10.1016/j.swevo.2013.02.001.
[42] W. Zhou, A.C. Bovik, H.R. Sheikh, E.P. Simoncelli, Image quality assessment: from error visibility to structural similarity, IEEE Trans. Image Process. 13 (2004) 600–612, http://dx.doi.org/10.1109/TIP.2003.819861.
[43] L.Z. Lin Zhang, L. Zhang, L. Zhang, X. Mou, D. Zhang, L.Z. Lin Zhang, FSIM: A feature similarity index for image quality assessment, IEEE Trans. Image Process. 20 (2011) 2378–2386, http://dx.doi.org/10.1109/TIP.2011.2109730.
[44] M. Črepinšek, S. Liu, M. Mernik, Exploration and exploitation in evolutionary algorithms: A survey, ACM Comput. Surv. 45 (2013) http://dx.doi.org/10.1145/2480741.2480752, Article 35.